Technical Memorandum

No. 65

SUBHARMONIC GENERATION IN ACOUSTIC SYSTEMS
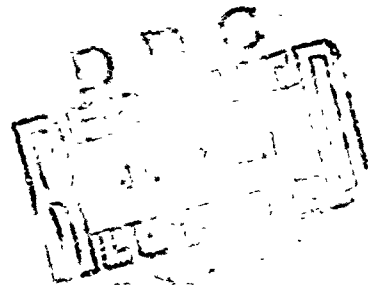
By

Nai-chyuan Yen

May 1971
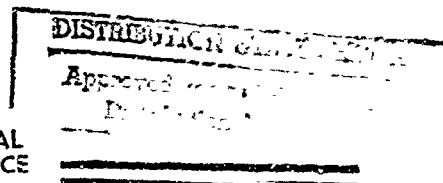
ACOUSTICS RESEARCH LABORATORY

Division of Engineering and Applied Physics

Harvard University • Cambridge, Massachusetts

138

SUBHARMONIC GENERATION IN ACOUSTIC SYSTEMS

by

Nai-chyuan Yen

May 1971

Abstract

This report is concerned with the theoretical and experimental study of subharmonic generation in acoustic systems. The generalized formulation for lumped systems is considered for the case of three oscillators coupled through a nonlinear element. The resulting analysis indicates that the high frequency oscillation is unstable and its energy can be diverted to low frequency oscillations; that is, subharmonics are generated. Based on this mathematical model, the conditions for sustaining subharmonics are deduced in terms of the system's parameters. For distributed systems, the quasilinear solution of the nonlinear wave equation, obtained by a two-variable (two-timing) perturbation method, shows that the nonlinear property of medium provides a coupling effect for signals of different frequencies. In a multi-resonant system, certain subharmonic modes, determined by a selection rule, can be excited by an external source. The present theory predicts the threshold for subharmonic generation as a function of the losses, nonlinearity, and detuning parameters of the system. Experimental measurements of such phenomena in an interferometer-type resonator, operated around 1.5 MHZ in water, are consistent with the analytic results, provided that cavitation in the medium is carefully avoided.

TABLE OF CONTENTS

LIST OF FIGURES

LIST OF TABLES

SYNOPSIS

Subharmonic generation is a phenomenon which has been observed in acoustic systems as a result of their response to intense signals. The purpose of this thesis is to develop a simple mathematical model for the basic mechanism of subharmonic generation and, under the conditions arranged in the laboratory, to investigate such a phenomenon experimentally for checking the adequacy of the theoretical analysis.

We introduce the subject with a study on the behavior of lumped systems with mass and spring elements. This particular problem is formulated by considering three coupled oscillators with a simple nonlinear element whose energy function is proportional to the product of the displacement amplitudes in these three oscillators. In a conservative system, the analysis results in three constraints for the response to the disturbance. That is, in addition to energy conservation, there are relations for the inbalance in energy exchange among the oscillators, and the amplitudes and phases of the response. These constraints can be used to reduce such a problem to quadrature. The phase diagram for describing the system's response indicates that the high frequency oscillation is unstable and its energy can be easily diverting to the low frequency oscillation. This tendency suggests that, for a nonconservative system, subharmonic

oscillation can be excited and sustained if the energy sup-
plied can balance out the energy losses in the system.
Based on this model, we derive the threshold for subharmonic
oscillation in relation to the nonlinear coupling, dissi-
pation, and detuning parameter of the system.

We then discuss subharmonic generation in distributed
systems by examining the solutions of the nonlinear wave
equation. We find that the nonlinear property of the medium
can provide a coupling effect for signals with distinct fre-
quencies. In free space, an intense acoustic wave will form
a shock wave and no subharmonic can be generated. But in a
closed system, such as a resonator, there is the possibility
for subharmonic modes to be excited. The mathematical analy-
sis for mode-coupling in a resonator shows some similarities
with the nonlinear coupling of the three oscillators in the
lumped system. Since a resonator generally possesses many
modes, the analysis has been extended to determine a selec-
tion rule for which modes will be excited at a given condi-
tion.

Experimental investigation of subharmonic generation
is carried out in an interferometer type resonator. Water
is used as the medium that supports the intense standing
wave for inducing the nonlinear coupling effect. Because
cavitation is carefully avoided by degassing and filtering
the liquid, we are able to obtain results that are consistent

with our theoretical model.

From the results of this research, we reach the con-
clusion that the subharmonic generation phenomenon is attrib-
uted to nonlinearity in the system and its sustenance also
depends on the loss factor and detuning parameter associated
with the particular subharmonic modes to be excited. In a
water-filled resonator whose linear dimension is larger than
serval wavelengths, we have found that, in the absence of
cavitation, the generation of subharmonics is mainly due to
the nonlinear property of the medium.

Chapter I

INTRODUCTION

The subharmonic phenomenon has been studied in this research, with particular emphasis on its existence in acoustical systems. We shall first discuss the nature of subharmonics and review some related work reported in the literature. We shall then define the purpose of doing such a study.

1. Subharmonics and superharmonics

In a nonlinear system, a response at other than the driving frequency is often observed. Most often, the frequencies of the response in such a system are related to the driving frequency by an interger multiplier, and these are known as harmonic responses. But under certain conditions, a response with a frequency less than the driving frequency can also appear. To distinguish between these two phenomena, the response with frequency less than driving frequency are known as subharmonics and the others as superharmonics.

Though both subharmonics and superharmonics are phenomena caused by nonlinearities in a system, they have a different character[1]*. Superharmonics are a stable response that

---

* Numerical superscripts correspond to references listed in the Bibliography.

will always occur when there is a driving source in the non-
linear system. Their frequency component is related to the
order of the nonlinearity of the system. On the other hand,
in order for subharmonics to be excited, a certain minimum
driving signal strength is required. The subharmonic oscil-
lation is due to an unstable property of the system and
their sustained excitation depends not only on the intensity
of the driving source but also on the proper phase relation
with the driving source. Except for the degenerate case of
subharmonics of one-half, subharmonics ordinarily exist in
pairs such that the sum of each frequency pair equals the
frequency of the driving signal.

The study of subharmonics and superharmonics in non-
linear mechanical and electrical systems has been carried
out in some detail by Hayashi[2] and Minorsky[1]. Stern's[3]
book on nonlinear systems analysis has extended the non-
linear phenomena into multidimension space vectors. Recent-
ly , Kronauer and Musa[4,5] have done some general analyses on
the synchronization of subharmonics with the excitation for
weakly coupled nonlinear systems.

Early studies of sub- and superharmonic phenomena were
pursued for the purpose of minimizing undersirable harmonic
effects in mechanical systems. These analyses generally end
up predicting the conditions for which the system will become
unstable and anharmonic oscillations will begin to grow.

Later, owing to the application of nonlinear elements in electrical circuits, it was found that harmonic generation can be used as a substitution for frequency multiplication when a direct means for obtaining such a source is not available. Since the recent development of high intensity laser beams, utilization of harmonic generation has even been extended to optics. The object of subharmonics studies has also been expanded from merely understanding their existence to research on the property of systems. From comparisons with the results of parametric amplifier studies[6], subharmonic generation seems to have features similiar to the down-conversion amplifier. According to the Manley-Rowe relation[6], high gains of such conversion should be easy to achieve through the subharmonic generation mechanism, but its unstable character and very narrow bandwidth have limited its practical application. Subharmonic generation can also be employed in frequency dividers if the proper synchronization can be adequately maintained. However, recent electronic digital techniques have provided a much simpler arrangement. This makes obsolete the idea of using the subharmonic generation mechanism as a alternate frequency source.

Tucker[7], in his study of nonlinear properties in underwater acoustics, has discussed some possible applications of subharmonics in forming narrow low frequency acoustic beams.

In the next section, we shall review some of the work related to subharmonic generation in the field of acoustics.

2. Work on Subharmonics in Acoustics

The earlist work related to subharmonics in acoustics is probably due to Helmholtz[8]. He described the phenomenon in which one can sense a fundamental pure tone when only two of its harmonics are present. This has been recognized later as the beating phenomenon whose real cause is not the inter- action of sound waves but rather the nonlinear response of the human ear. Lord Rayleigh[9] deduced solutions for a Duffing equation ($\ddot{u} + k\dot{u} + k'u^3 + n^2u = 0$) and indicated that, in the presence of a driving force, a response of less than the frequency of the driving source can be excited. Work of this kind has been studied extensively in the field of nonlinear mechanics ever since.

The extensive use of sound for underwater communica- tion, initiated in World War II, has provided a great deal of research into the generation, transmission, and reception of sound waves in a liquid. One of the major efforts is to maximize the range of acoustic information transmission. However, there are some limitations to such efforts. One of them is the cavitation problem. When the sound wave pressure reaches too great an intensity, foggy acoustic streamers form in front and on the surface of a transducer (this phe-

nomenon is what we now call "gaseous" cavitation). Such streamers produce noise detectable by hydrophones. This noise has a line spectrum containing subharmonics[10]. Subharmonics therefore become one of the interesting subjects in the study of cavitation phenomena. Some investigators[11,12] even suggest that the subharmonic can be regarded as an indication for the occurrence of cavitation.

Tucker[7] has pointed out some possibilities in underwater acoustics for the utilization of the nonlinear character of the med um. One such experimental investigation is the generation of subharmonics[13]. A focused standing wave system is employed during the investigation for building up a very strong acoustic field. When the acoustic pressure reaches a certain level, the subharmonic has been observed. Such a threshold appears to be correlated with the gas content of the liquid. When boiled water is used, those investigators reported that no subharmonics were observed.

Eller and Flynn[14] have focused their study on the nonlinear problem of subharmonics excited by gas bubble oscillations in the liquid. Their analytical results show that a bubble can be excited to its resonance when it is subjected to an acoustic field with twice the natural frequency of such a bubble. Neppiras[15] did some experimental work along this line by injecting bubbles of controlable size into a

liquid. The results indicate that subharmonics are easily excited and their intensity is strong when the condition of Eller and Flynn described above is established. They concluded that subharmonics are generated by bubbles through the cavitation process.

On a separate front, subharmonics have also been an interesting subject under discussion in the field of ultrasonics. While studying light diffraction patterns produced by standing waves in a liquid[16,17,18,19], it is observed that extra dots appear on the regular diffraction pattern when the sound pressure reaches a certain level. Those additional dots correspond to another imposed standing wave whose wavelength is larger than that of the original driving signal. Cook[20] has explained such a phenomenon by assuming possible wave interaction for subharmonic generation, but he did not obtain a complete description of the relation between the frequency of driving signal and the subharmonics observed. Adler and Breazeale[21] have interpreted this phenomenon differently. They concluded that the vibration of the boundary of the acoustical interferometer parametrically excites the subharmonics around the order of one-half of the original signal. However, such a hypothesis has ignored two observed experimental facts: that subharmonics of other order have also been observed[16,17,18,19] and that only at a certain length of the interfer-

ometer they can be excited[16].

Subharmonic phenomena have been detected in solids when an acoustic wave is applied to crystals[22,23,24]. Luukkala interprets these observations in terms of a phonon breakdown hypotnesis. The qualitative phenomenlogical arguments he uses seem to support the assumption that the general instability of subharmonic signals is caused by excessive energy going into an additionally accessible vibration mode. These arguments correctly predict the threshold for one-half subharmonics but are not comprehensive enough to include three-phonon interaction.

Dallos[25,26,27] reports observing subharmonics in auditory systems. That such subharmonics also occur in pairs and that sum of these frequency pairs equals the driving frequency seems to indicate a similarity with other physical systems.

3. Scope of This Thesis

The purpose of this thesis is to study the basic principles underlying subharmonic phenomena; no attempt is made to explain every aspect of the existing observations. We use a simplified mathematical model in hopes of obtaining some fundamental quantitative relations among the important parameters. In the accompanying experimental work, we not only try to confirm the theory but also intend to clarify

some inconsistencies among other reported experimental investigations. We are concerned with: What is the mechanism for subharmonic generation? What is the selection rule for the appearance of a given subharmonic mode? What is a systematic and practical way to excite subharmonics?

In Chapter II, we study, in a general sense, subharmonic generation in lumped systems. A model of three conservative oscillators coupled weakly through a nonlinear element is used for the analysis. Using a first order perturbation method, we have found that, besides the energy conservation law, such a system possesses two more invariants— enough to reduce the problem to quadrature. The analysis indicates that the high frequency mode can, under certain conditions, divert its energy to low frequency modes. By considering, then the effect of dissipation in the system, we have derived the threshold level of excitation for sustaining such subharmonic oscillation. The detuning problem, that is when the frequencies of subharmonics do not exactly match the driving signal frequency, has also been treated.

We discuss subharmonic generation in distributive systems in Chapter III. The response of the system has been examined for disturbances with a finite travelling speed. A wave equation is formulated for studying the effects of all pertinent parameters. We find that, due to the nonlinear property of the medium, there is a coupling relation among

signals with distinct frequencies. In a multiresonator, it
becomes mode-coupling which has features similar to the
coupling of oscillators described in Chapter II. The condi-
tion for forcing excitation of certain subharmonic modes is
then obtained analytically based on information about the
boundary conditions, detuning parameter, and the dissipation
factor of the system.

The detailed experimental set-up is described in
Chapter IV. The purpose of such an investigation is to seek
evidence in supporting of our hypothesis about subharmonic
generation. The liquid used in this experiment, water, has
been filtered and degassed in a controllable manner in order
to get consistent results. Data are collected in terms of
actual acoustical quantities so that an accurate physical
interpretation can be made.

Chapter V presents the conclusions of this research.
We compare our analysis and our experimental results, and
examine validity of our hypothesis in understanding the
mechanism of subharmonic generation. The direction for the
future work and some possible applications of the subharmonic
phenomenon are suggested.

Chapter II

SUBHARMONIC GENERATION IN LUMPED SYSTEMS

The problem under consideration in this chapter is the energy exchange among three oscillators. Gilchrist[28], in his investigation of conservative quasilinear systems with two degrees freedom, discovered an integral constraint on the amplitudes of the oscillators. This constraint actually is an energy conservation law of first order in a perturbation expansion. An additional constraint on phase and amplitude variations has been deduced by Kronauer and Musa[29] in their study of the exchange of energy between oscillations in weakly-nonlinear conservative systems.

In the model of three resonant tanks with a nonlinear element discussed here, we have derived a third constraint. This constraint gives an additional relation among the energy stored in each oscillator and, under a special circumstance, it can be reduced in the form of the Manley-Rowe relation[6]. With these three constraints, the behavior of three coupled oscillators can be reduced to a problem of quadrature.

We have also extended the analysis to the situation in which there are dissipation elements in the resonant tanks. In such a simplified model, the effect of damping imposes a similar influence on the energy exchange as that of detuning of the oscillation frequencies. If an external source is

provided, to make up for the energy loss in the system, a steady state will be reached. When the driving intensity exceeds a certain level, a response with an **oscillation frequency** less than that of the external source will appear.

1. Coupling of Three Matched Oscillators

In a linear system containing dissipationless elements only, there are in general some resonant modes and corresponding normal coordinates. Tranforming to these normal coordinates, the system may be described by a set of separated second order differential equations:

$$\frac{d^2 X_i}{dt^2} + \omega_i^2 X_i = 0 , \qquad (2-1)$$

where ω_i is the angular resonance frequency pertaining to the particular mode and X_i is the displacement in the corresponding normal coordinates. Any disturbances to the system may excite some of these modes. The resultant response of the system is the linear combination of these individual motions.

If the system possesses some nonlinear elements or the disturbance becomes so strong that elements lose their linear property, the system will act quite differently. The nonlinearity will cause interaction among modes, thereby negating the linear superposition principle. However, if the nonlinear effects are sufficiently weak, we can develop a perturbation expansion. The first order expansion theory is

known as the quasi-linear approximation.

In the following, we will discuss a system of three resonant modes with a single nonlinear element. Such a simplified model will illustrate the basic mechanism of non-linear coupling without involving too many mathematical complications and will provide a framework for understanding the phenomena which we shall pursue later.

We consider that the single nonlinear element is an energy storage device with the energy function given by:

$$V_n = \epsilon \sigma X_1 X_2 X_3 \, . \tag{2-2}$$

where ϵ is a nondimensional quantity with a magnitude of much less than one, and σ is a constant related to the non-linear element. This might be difficult to realize physically, but is, mathematically, an appropriative device. The total Lagrange of the three oscillators with such a non-linear element is:

$$L = \frac{a_1 \dot{X}_1^2}{2} + \frac{a_2 \dot{X}_2^2}{2} + \frac{a_3 \dot{X}_3^2}{2} - \frac{a_1 \omega_1^2 X_1^2}{2} - \frac{a_2 \omega_2^2 X_2^2}{2} - \frac{a_3 \omega_3^2 X_3^2}{2}$$

$$+ \epsilon \sigma X_1 X_2 X_3 \, , \tag{2-3}$$

where a's and ω's are parameters related to the system elements.

The response of such a system is governed by the following coupled equations:

$$\frac{d^2 X_1}{dt^2} + \omega_1^2 X_1 = \epsilon \sigma_1 X_2 X_3 ,$$

$$\frac{d^2 X_2}{dt^2} + \omega_2^2 X_2 = \epsilon \sigma_2 X_3 X_1 , \qquad (2\text{-}4)$$

$$\frac{d^2 X_3}{dt^2} + \omega_3^2 X_3 = \epsilon \sigma_3 X_1 X_2 ,$$

where σ_i's are constants derived by the relation $\sigma_i = \dfrac{\sigma}{a_i}$.

We will at first simplify things by assuming that the ω's obey the relation,

$$\omega_1 + \omega_2 = \omega_3 , \qquad (2\text{-}5)$$

In Eq. (2-4) σ's are a measure of the interaction among X_1, X_2, and X_3. Without such coupling, X_1, X_2, and X_3 will oscillate independently with angular frequencies ω_1, ω_2, and ω_3 respectively. We refer to the matched condition of Eq. (2-5) as the "sum rule" for angular frequencies of coupled oscillators.

Since $\epsilon \sigma_1$, $\epsilon \sigma_2$, $\epsilon \sigma_3$ are small quantities, we can linearize Eq. (2-4) by expanding the variables in terms of ϵ:

$$X_i = X_{i0} + \epsilon X_{i1} + \epsilon^2 X_{i2} + \cdots\cdots , \quad i = 1, 2, 3,$$

$$t_f = t(1 + b_1 \epsilon^2 + b_2 \epsilon^3 + \cdots\cdots) ,$$

$$t_s = t(\epsilon + d_1 \epsilon^2 + d_2 \epsilon^3 + \cdots\cdots) , \qquad (2\text{-}6)$$

where b's and d's are constants of expansion.

The dependent variable t is now expressed in two scales t_f and t_s. We choose that t_s is less than t_f by order of ϵ, thereby describing the response of the system in two time domains: a fast time scale t_f to indicate the immediate response, and a slow time scale t_s to show averaging effects due to the nonlinear terms in the equation. This mathematical approach has been adopted from the two-timing perturbation method.[30]

The differential operators then are changed to:

$$\frac{d}{dt} = \frac{\partial}{\partial t_f}\frac{dt_f}{dt} + \frac{\partial}{\partial t_s}\frac{dt_s}{dt} = \frac{\partial}{\partial t_f} + \epsilon\frac{\partial}{\partial t_s} + \cdots,$$

$$\frac{d^2}{dt^2} = \frac{\partial^2}{\partial t_f^2}(\frac{dt_f}{dt})^2 + \frac{2\partial^2}{\partial t_f \partial t_s}(\frac{dt_f}{dt}\frac{dt_s}{dt}) + \frac{\partial^2}{\partial t_s^2}(\frac{dt_s}{dt})^2$$

$$= \frac{\partial^2}{\partial t_f^2} + 2\epsilon\frac{\partial^2}{\partial t_f \partial t_s} + \cdots, \qquad (2\text{-}7)$$

and the X_i's are now a function of both t_f and t_s.

By substituting Eqs. (2-6) and (2-7) into Eq. (2-4), we can collect together terms of the same order as ϵ. The results are:

For ϵ^0 order:

$$\frac{\partial^2 X_{10}}{\partial t_f^2} + \omega_1^2 X_{10} = 0,$$

$$\frac{\partial^2 X_{20}}{\partial t_f^2} + \omega_2^2 \, X_{20} = 0,$$

$$\text{(2-8)}$$

$$\text{and} \quad \frac{\partial^2 X_{30}}{\partial t_f^2} + \omega_3^2 \, X_{30} = 0.$$

For ϵ^1 order:

$$\frac{\partial^2 X_{11}}{\partial t_f^2} + \omega_1^2 \, X_{11} = \sigma_1 X_{20} X_{30} - 2 \frac{\partial^2}{\partial t_f \partial t_s} X_{10},$$

$$\frac{\partial^2 X_{21}}{\partial t_f^2} + \omega_2^2 \, X_{21} = \sigma_2 X_{10} X_{30} - 2 \frac{\partial^2}{\partial t_f \partial t_s} X_{20}, \quad \text{(2-9)}$$

$$\text{and} \quad \frac{\partial^2 X_{31}}{\partial t_f^2} + \omega_3^2 \, X_{31} = \sigma_3 X_{10} X_{20} - 2 \frac{\partial^2}{\partial t_f \partial t_s} X_{30},$$

and so forth for higher order terms of ϵ.

The solutions of the differential equations (2-8) take the form:

$$X_{10} = R_1 \cos (\omega_1 t_f + \phi_1),$$

$$X_{20} = R_2 \cos (\omega_2 t_f + \phi_2), \quad \text{(2-10)}$$

$$\text{and} \quad X_{30} = R_3 \cos (\omega_3 t_f + \phi_3),$$

where the R's and ϕ's are functions of t_s and have to be determined. In seeking solutions for Eq. (2-9), we substitute the assumed solutions from Eq. (2-10) into the

right hand side of Eq. (2-9) as source terms. After expanding terms $X_{10}X_{30}$, $X_{10}X_{20}$, and $X_{20}X_{30}$, we find that they contain the same frequency components as the natural frequency of the first order equations. This means that the X_{il}'s would grow linearily with time, which would violate the assumption that the X_{il} terms remain smaller than X_{i0} terms. These terms, called secular terms, can be avoided if we set the excitation components equal to zero. The process of suppressing the secular terms gives the conditions for determining the R's and ϕ's. We then obtain the following relations from Eq. (2-9):

$$2\omega_1 \frac{\partial R_1}{\partial t_s} - \frac{\sigma_1}{2} R_2 R_3 \sin r = 0,$$

$$2\omega_2 \frac{\partial R_2}{\partial t_s} - \frac{\sigma_2}{2} R_1 R_3 \sin r = 0,$$

$$2\omega_3 \frac{\partial R_3}{\partial t_s} + \frac{\sigma_3}{2} R_1 R_2 \sin r = 0,$$

(2-11)

$$2\omega_1 R_1 \frac{\partial \phi_1}{\partial t_s} + \frac{\sigma_1}{2} R_2 R_3 \cos r = 0,$$

$$2\omega_2 R_2 \frac{\partial \phi_2}{\partial t_s} + \frac{\sigma_2}{2} R_1 R_3 \cos r = 0,$$

and $$2\omega_3 R_3 \frac{\partial \phi_3}{\partial t_s} + \frac{\sigma_3}{2} R_1 R_2 \cos r = 0,$$

where $r = \phi_3 - \phi_1 - \phi_2$.

Since the R's and ϕ's are now functions of t_s only, the partial differential operators can be changed to ordinary differential operators. By further combining the last three equations in Eq. (2-11), we have in this first order approximation four coupled equations to describe the response of the system.

$$\frac{dR_1}{dt_s} - \frac{\sigma_1}{4\omega_1} R_2 R_3 \sin r = 0,$$

$$\frac{dR_2}{dt_s} - \frac{\sigma_2}{4\omega_2} R_1 R_3 \sin r = 0,$$

$$\frac{dR_3}{dt_s} - \frac{\sigma_3}{4\omega_3} R_1 R_2 \sin r = 0, \qquad (2\text{-}12)$$

and $\quad \frac{dr}{dt_s} + \left\{ \frac{\sigma_3 R_1 R_2}{4\omega_3 R_3} - \frac{\sigma_1 R_2 R_3}{4\omega_1 R_1} - \frac{\sigma_2 R_1 R_3}{4\omega_2 R_2} \right\} \cos r = 0.$

Eq. (2-10) indicates that the response is mainly dominated by the oscillation of the system at its linear resonance frequencies, and Eq. (2-12) shows how the amplitudes and phases of such oscillations are modified slowly in time due to system's nonlinearities. If the initial conditions are known, the transient behavior at any instant can be determined by integrating Eq. (2-12).

From the first three equations of Eq. (2-12), we will obtain

$$\frac{(\omega_1 R_1)^2}{\sigma_1} + \frac{(\omega_2 R_2)^2}{\sigma_2} + \frac{(\omega_3 R_3)^2}{\sigma_3} = E, \qquad (2\text{-}13)$$

where E is a constant,

and
$$\frac{(\omega_1 R_1^2)}{\sigma_1} - \frac{(\omega_2 R_2^2)}{\sigma_2} = C, \qquad (2\text{-}14)$$

where C is also a constant.

A relation between phase and amplitudes can be also be deduced from Eq. (2-12):

$$R_1 R_2 R_3 \cos r = K, \qquad (2\text{-}15)$$

where K is a constant. With these constraints in Eqs. (2-13), (2-14), and (2-15), the response of the system can be integrated out in terms of slow time t_s.

There are some physical interpretations associated with the constraints of Eqs. (2-13), (2-14), and (2-15). Since the square of amplitude is a quantity for the energy, the constant E in Eq. (2-13) is related to the total energy initially stored in the system. Eq. (2-13) is just an expression for energy conservation and always exists for a conservative system.

Equation (2-14) indicates that a certain relation has to follow for energy exchange between two modes. It depends on the particular nonlinearity we have assumed for the system. If the R's are inversely proportional to the angular frequencies, the ω's and σ's are equal, and the initial condition makes the constant C equal to zero, Eq. (2-14) will have the form:

$$\frac{A_1^2}{\omega_1} = \frac{A_2^2}{\omega_2}, \quad \text{for } A_i = \omega_i R_i \quad i=1,2,3. \qquad (2\text{-}16)$$

Manley and Rowe[6] have derived this relation from the property
of a nonlinear capacitor. The constraint expressed by Eq.
(2-14) is, of course, implied to more general cases.

According to the analysis by Kronauer and Musa[29], the
amplitude and phase relation for a weakly-nonlinear, conser-
vative system is determined by the average value of the
incremental Lagrange of the system. As the incremental
Lagrange in the system discussed here is:

$$\ell = \epsilon \sigma X_1 X_2 X_3, \tag{2-17}$$

the average value of ℓ can be found by using the results of
Eq. (2-10):

$$\bar{\ell} = \frac{1}{T} \int_o^T \epsilon \sigma X_1 X_2 X_3 \, dt_f, \tag{2-18}$$

$$= \epsilon \sigma R_1 R_2 R_3.$$

Hence the constraint of Eq. (2-15) is due to the incremental
Lagrange of the system with $K = \dfrac{\bar{\ell}}{\epsilon \sigma}$, a general result of
first order approximation.

The transient behavior of such coupled oscillation can
be graphically illustrated by a topological approach as in
Fig. 2-1. The diagram uses three axes to express the mag-
nitude of $\omega_1 R_1$, $\omega_2 R_2$, and $\omega_3 R_3$. Any point in the space
represents a instantaneous state of the system's response.
A surface of constant E is an ellipsoid on this space. 0_1,
0_2, and 0_3 are singular points and they are stationary
states. However, 0_3 is an unstable stationary state. Any
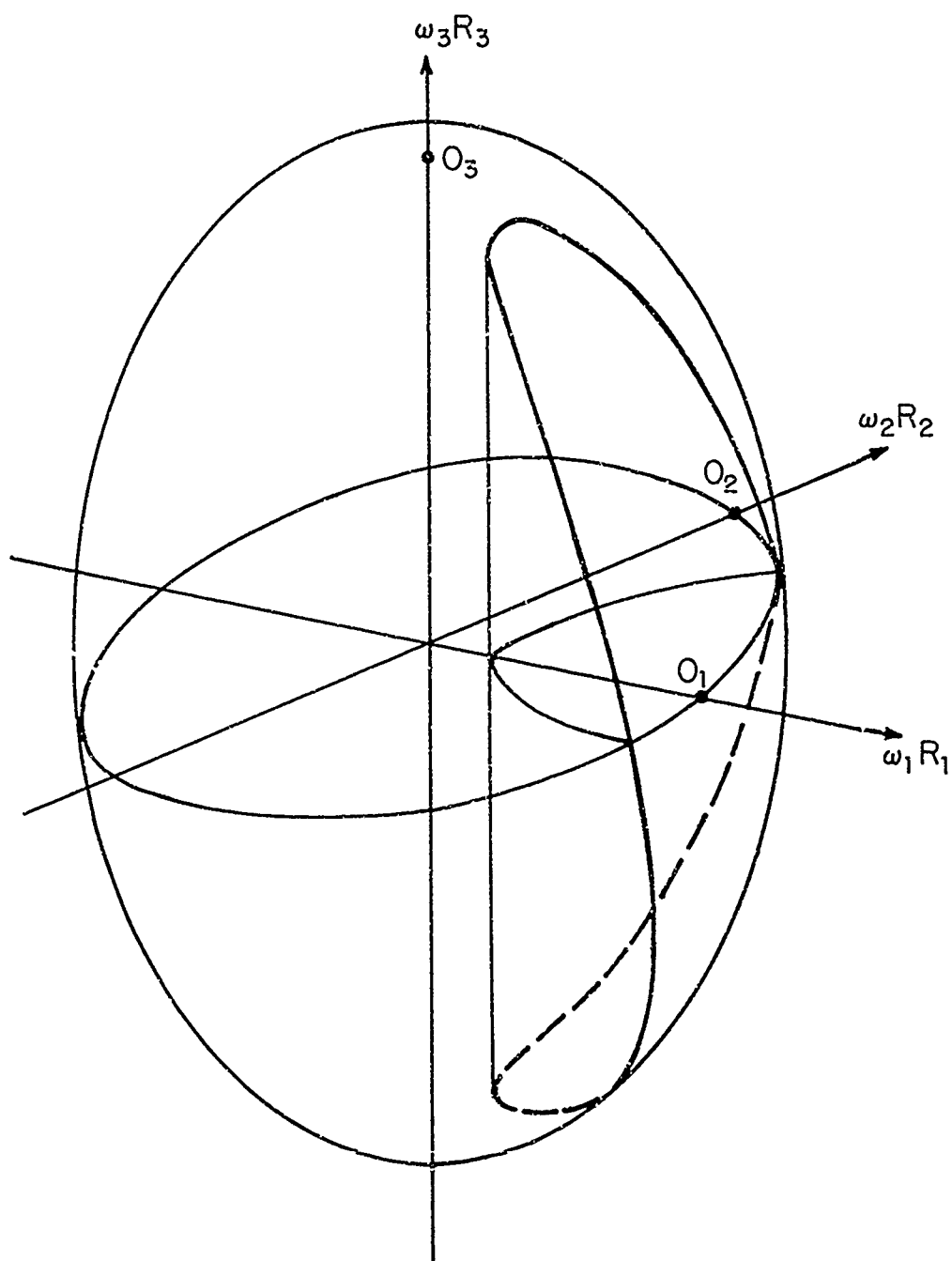
FIG. 2-1 TOPOLOGICAL CONFIGURATION FOR
COUPLED OSCILLATION

disturbance around O_3 will cause a response with a motion locus circling around the ellipsoid. This indicates that the energy associated with the high frequency mode is unstable and can easily be diverted to the energy in lower frequency modes. Systems exhibiting such features can be excited into subharmonic oscillation. We shall further explore such phenomenon later.

2. Effect of Detuning on Coupled Oscillation

We now consider the case when the frequencies of the three oscillators are not exactly matched. The deviation from Eq. (2-5) can be accounted for by solving a detuning problem. We can expand the unmatched relation in terms of the matched condition as follows:

as $\qquad \omega_1 + \omega_2 \neq \omega_3$,

we define $\quad \omega_1' = \omega_1 + \epsilon\delta_1$,

$$\omega_2' = \omega_2 + \epsilon\delta_2, \tag{2-19}$$

$$\omega_3' = \omega_3 + \epsilon\delta_3,$$

and let $\quad \omega_1' + \omega_2' = \omega_3'$,

where δ's are detuning parameters from their corresponding modes.

The original coupling equations can be rewritten as:

$$\frac{d^2 X_1}{dt^2} + \omega_1'^2 X_1 = \epsilon\sigma X_2 X_3 + 2\epsilon\delta_1\omega_1' X_1 \ ,$$

$$\frac{d^2 X_2}{dt^2} + \omega_2'^2 X_2 = \epsilon\sigma X_1 X_3 + 2\epsilon\delta_2\omega_2' X_2 \ , \qquad (2\text{-}20)$$

and $\qquad \dfrac{d^2 X_3}{dt^2} + \omega_3'^2 X_3 = \epsilon\sigma X_1 X_2 + 2\epsilon\delta_3\omega_3' X_3 \ ,$

where we let all σ's be the same to simplify the analysis. Using again the two-timing perturbation method, we obtain the first order solution:

$$X_{10} = R_1 \cos (\omega_1' t_f + \phi_1) \ ,$$

$$X_{20} = R_2 \cos (\omega_2' t_f + \phi_2) \ , \qquad (2\text{-}21)$$

and $\qquad X_{30} = R_3 \cos (\omega_3' t_f + \phi_3) \ .$

with the auxiliary relations:

$$\frac{dR_1}{dt_s} - \frac{\sigma R_2 R_3}{4\omega_1'} \sin r = 0 \ ,$$

$$\frac{dR_2}{dt_s} - \frac{\sigma R_1 R_3}{4\omega_2'} \sin r = 0 \ ,$$

$$\qquad\qquad\qquad\qquad\qquad\qquad (2\text{-}22)$$

$$\frac{dR_3}{dt_s} + \frac{\sigma R_1 R_2}{4\omega_3'} \sin r = 0 \ ,$$

and $\qquad \dfrac{dr}{dt_s} + \left(\dfrac{R_1 R_2}{4\omega_3' R_3} - \dfrac{R_2 R_3}{4\omega_1' R_1} - \dfrac{R_1 R_3}{4\omega_2' R_2} \right) \sigma \cos r + \delta = 0 \ ,$

where $\delta = \delta_1 + \delta_2 + \delta_3$.

Comparing with Eqs. (2-10) and (2-12), we find that the

total detuning factor δ appears in the phase equation only.
We shall analyze its effect through the motion locus in the
phase diagrams.

Changing R's into new variables, we get:

$$A_1 = \omega_1' R_1, \quad A_2 = \omega_2' R_2, \quad A_3 = \omega_3' R_3. \quad (2-23)$$

The corresponding constraints become:

$$A_1^2 + A_2^2 + A_3^2 = E = e^2. \quad (2-24)$$

$$\frac{A_1^2}{\omega_1'} - \frac{A_2^2}{\omega_2'} = C = 2 \, \epsilon^2 K. \quad (2-25)$$

$$A_1 A_2 A_3 \cos r + 2\delta \omega_1' \omega_2' A_3^2 = K, \quad (2-26)$$

where we have defined new constants e and K.
Since these three constraints are directly derived from
Eq. (2-22), the original four variables A_1, A_2, A_3, and r
for describing the state of the system in four-dimension
space can be reduced to quadrature and the time variable can
be found by integrating out such a relation.

The ellipsoid diagram of Fig. 2-1 is still appropriate
to represent the response of the system, but, because of
detuning, it is no longer possible to deduce the phase, r,
unambiguously from that diagram. That is, detuning makes
possible monotonic phase change (while with $\delta = 0$ phase
oscillates periodically). To observe the phase, we make
a transformation based on the first two constraints, Eqs.

(2-24) and (2-25), introducing a new variable χ defined by:

$$A_1 = e \left(\frac{\omega_1'}{\omega_3'} \sin^2 \chi + K \right)^{\frac{1}{2}},$$

$$A_2 = e \left(\frac{\omega_2'}{\omega_3'} \sin^2 \chi - K \right)^{\frac{1}{2}}, \qquad (2\text{-}27)$$

and $\qquad A_3 = e \cos \chi$.

The variable χ is a measure of the extent of energy exchange from A_3 to the A_1 and A_2 set. The third constraint now becomes:

$$e^3 \left(\frac{\omega_1' \omega_2'}{\omega_3'^2} \sin^4 \chi - \frac{\omega_1' \omega_2'}{\omega_3'} K \sin^2 \chi - K^2 \right) \cos \chi \cos r$$

$$+ 2e^2 \delta \omega_1' \omega_2' \cos^2 \chi = K . \qquad (2\text{-}28)$$

The properties described by Eq. (2-28) can best be understood by considering four cases. First, we observe that the parameter K represents a fixed energy imbalance between oscillators 1 and 2 and is unaltered by an exchange of energy between this pair and oscillator 3. The parameter δ of course represents detuning. Fig. 2-2 shows the solution trajectories (plots of Eq. (2-28) for various fixed values of K)for the four interesting cases.

Case I. (Fig. 2-2a). With no detuning, the trajectories remain in a cell of width π. Since the imbalance is zero, the full range of χ is accessible.

Case II. (Fig. 2-2b). With detuning, same trajectories
can exhibit steady phase change. Since the
imbalance is zero, the full range of χ is
still accessible, although there is no single
trajectory which makes the swing from $\chi=0$ to
$\chi=\pi/2$. Thus we can say that the presence of
detuning acts to reduce the extent of energy
exchange between oscillators 3 and the 1, 2
set.

Case III.(Fig. 2-2c). With imbalance, the accessible
range of χ is reduced. The absence of de-
tuning permits trajectories with maximum ex-
change (subject to the imbalance reduction).
As in Case I, the trajectories are confined
to a cell of width π.

Case IV. (Fig. 2-2d). With both detuning and imbal-
ance, two effects are seen to reduce the
extent of energy exchange throughout the
field. Steady phase change is also common.
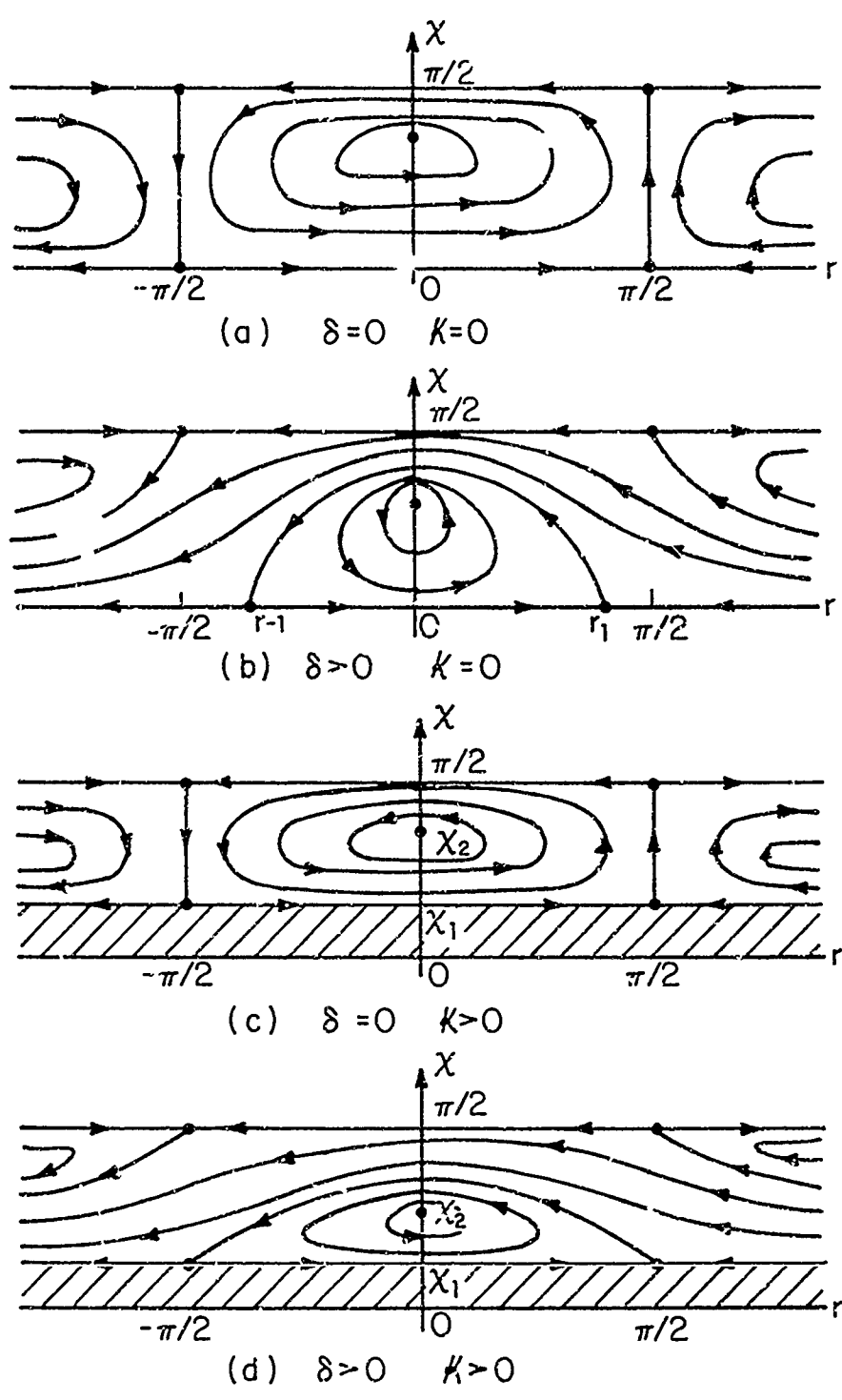
FIG. 2-2 PHASE PLANE FOR COUPLED OSCILLATIONS

3. Forced Excitation for Subharmonic Oscillation

For systems containing damping elements, a transient
disturbance will not excite and sustain subharmonic oscil-
lation, because the signal's limited energy will be quickly
dissipated. In general, in order to sustain a steady re-
sponse, a constant energy source should be provided to com-
pensate for the energy loss in the system.

From our study of the transient behavior of a conser-
vative system, we have learned that the energy in the high
frequency mode can be easily converted into the energy in
lower frequency modes by some disturbance. We shall now
investigate the criteria for sustaining subharmonic oscil-
lation when a constant energy source is applied to the system.

We use the same model for three coupled oscillators but
include a damping element in each oscillator. The original
three oscillation frequencies, ω_1, ω_2, ω_3, are not exactly
matched, that is $\omega_1 + \omega_2 \neq \omega_3$. The external source with
angular frequency ω_0 has excited two subharmonics of angular
frequencies ω_1' and ω_2' with the following relation:

$$\omega_0 = \omega_1' + \omega_2' = \omega_3 + \epsilon\delta_3 ,$$

$$\omega_1' = \omega_1 + \epsilon\delta_1 ,$$

$$\omega_2' = \omega_2 + \epsilon\delta_2 , \qquad\qquad (2\text{-}29)$$

where δ's are detuning factors for each oscillation mode and

ϵ is a small constant of magnitude less than one.

The mathematical formulation of this problem is expressed in Eq. (2-30):

$$\frac{d^2X_3}{dt^2} + \epsilon\eta_3\frac{dX_3}{dt} + \omega_0^2X_3 = \epsilon\sigma_3X_1X_2 + 2\epsilon\omega_0\delta_3X_3$$
$$-\epsilon F\sin\omega_0 t ,$$

$$\frac{d^2X_1}{dt^2} + \epsilon\eta_1\frac{dX_1}{dt} + \omega_1^{'2}X_1 = \epsilon\sigma_1X_2X_3 + 2\epsilon\omega_1'\delta_1X_1 ,$$

and $\dfrac{d^2X_2}{dt^2} + \epsilon\eta_2\dfrac{dX_2}{dt} + \omega_2^{'2}X_2 = \epsilon\sigma_2X_1X_3 + 2\epsilon\omega_2'\delta_2X_2 ,$

$$(2-30)$$

where we have considered that the dissipation factors, η's, coupling coefficients, σ's, and the forcing term due to the external source, F, are small order terms.

We again use the two-timing perturbation method, expanding the dependent variable t in a fast scale, t_f, and a slow one, t_s. After summing up functions of same order, we have; for ϵ^0 order:

$$\frac{\partial^2}{\partial t_f^2}X_{30} + \omega_0^2X_{30} = 0 ,$$

$$\frac{\partial^2}{\partial t_f^2}X_{10} + \omega_1^{'2}X_{10} = 0 ,$$

$$(2-31)$$

and $\dfrac{\partial^2}{\partial t_f^2}X_{20} + \omega_2^{'2}X_{20} = 0 ;$

for ϵ^1 order:

$$\frac{\partial^2}{\partial t_f^2}X_{31} + \omega_0^2 X_{31} = -2\frac{\partial^2}{\partial t_f \partial t_s}X_{30} + \sigma_3 X_{10}X_{20} + 2\omega_0 \delta_3 X_{30}$$

$$-\eta_3\frac{\partial}{\partial t_f}X_{30} - F \sin \omega_0 t \ ,$$

$$\frac{\partial^2}{\partial t_f^2}X_{11} + \omega_1'^2 X_{11} = -2\frac{\partial^2}{\partial t_f \partial t_s}X_{10} + \sigma_1 X_{20}X_{30} + 2\omega_1' \delta_1 X_{10}$$

$$-\eta_1\frac{\partial}{\partial t_f}X_{10} \ ,$$

and $$\frac{\partial^2}{\partial t_f^2}X_{21} + \omega_2'^2 X_{21} = -2\frac{\partial^2}{\partial t_f \partial t_s}X_{20} + \sigma_2 X_{10}X_{30} + 2\omega_2' \delta_2 X_{20}$$

$$-\eta_2\frac{\partial}{\partial t_f}X_{20} \ .$$

$$(2\text{-}32)$$

The solutions of Eq. (2-31) are:

$$X_{30} = R_3 \cos (\omega_0 t_f + \phi_3) \ ,$$

$$X_{10} = R_1 \cos (\omega_1' t_f + \phi_1) \ , \qquad (2\text{-}33)$$

and $$X_{20} = R_2 \cos (\omega_2' t_f + \phi_2) \ .$$

After eliminating the secular terms in Eq. (2-32), we find the supplemental equations for solutions in Eq. (2-33).

$$2\omega_0\frac{\partial R_3}{\partial t_s} + \eta_3\omega_0 R_3 + \frac{\sigma_3}{2}R_1 R_2 \sin r - F \cos \phi_3 = 0 \ ,$$

$$2\omega_1'\frac{\partial R_1}{\partial t_s} + \eta_1\omega_1' R_1 - \frac{\sigma_1}{2}R_2 R_3 \sin r = 0 \ ,$$

$$2\omega_2'\frac{\partial R_2}{\partial t_s} + \eta_2\omega_2' R_2 - \frac{\sigma_2}{2}R_1 R_3 \sin r = 0 \ ,$$

$$2\omega_0 R_3\frac{\partial \phi_3}{\partial t_s} + \frac{\sigma_3}{2}R_1 R_2 \cos r + 2\omega_0 \delta_3 R_3 + F \sin \phi_3 = 0 \ ,$$

$$2\omega_1' R_1\frac{\partial \phi_1}{\partial t_s} + \frac{\sigma_1}{2}R_2 R_3 \cos r + 2\omega_1' \delta_1 R_1 = 0 \ , \quad (2\text{-}34)$$

$$\text{and} \quad 2\omega_2' R_2\frac{\partial \phi_2}{\partial t_s} + \frac{\sigma_2}{2}R_1 R_3 \cos r + 2\omega_2' \delta_2 R_2 = 0.$$

For transient behavior, we let $F = 0$. The total energy of the system to zeroth order is:

$$E = \frac{(\omega_1' R_1)^2}{\sigma_1} + \frac{(\omega_2' R_2)^2}{\sigma_2} + \frac{(\omega_0 R_3)^2}{\sigma_3} \ . \quad (2\text{-}35)$$

By the relations in Eq. (2-34), we have:

$$\frac{dE}{dt_s} = - \frac{\eta_1}{\sigma_1}(\omega'_1 R_1)^2 - \frac{\eta_2}{\sigma_2}(\omega'_2 R_2)^2 - \frac{\eta_3}{\sigma_3}(\omega_0 R_3)^2 \ .$$

$$(2\text{-}36)$$

It is convenient to let $\eta_1 = \eta_2 = \eta_3 = \eta$, then Eq. (2-36) becomes:

$$\frac{dE}{dt_s} = - \eta E \quad \text{or} \quad E = E_0 e^{-\eta t_s} \ . \quad (2\text{-}37)$$

This indicates that the total energy will eventually be dissipated. The ellipsoid of Fig. 2-1 will shrink to zero in the limit of long time.

The forced response can also be expressed in terms of the system's energy by keeping the F term in Eq. (2-36). The result is:

$$\frac{dE}{dt_s} = - \eta E + \frac{F\omega_0 R_3}{\sigma_3} \cos \phi_3 \quad (2\text{-}38)$$

There is a competition between the energy dissipated in the system and the energy supplied from external source, and a sustained driven oscillation will correspond to a balance of this effect.

Another interesting feature of this nonconservative system is that the previous constraint,

$$C = \frac{\omega_1' R_1^2}{\sigma_1} - \frac{\omega_2' R_2^2}{\sigma_2} , \qquad (2\text{-}39)$$

is no longer a constant. By the relations in Eq. (2-34), we can determine its variation as:

$$\frac{dC}{dt_s} = - \frac{\eta_1 \omega_1' R_1^2}{\sigma_1} + \frac{\eta_2 \omega_2' R_2^2}{\sigma_2} . \qquad (2\text{-}40)$$

For $\eta_1 = \eta_2 = \eta_3 = \eta$, it can be further simplified to

$$\frac{dC}{dt_s} = -\eta C \qquad \text{or} \qquad C = C_0 e^{-\eta t_s} . \qquad (2\text{-}41)$$

For the steady state ($t_s \rightarrow \infty$), C will become zero in this case of balanced dissipation. Hence Eq. (2-41) gives the exact condition for the Manley-Rowe relation[6].

The response of each frequency component after the system reaches a steady state can be worked out by letting all the time variable terms in Eq. (2-34) go to zero. A condition for detuning factor δ's is obtained as:

$$\frac{\delta_1}{\delta_2} = \frac{\eta_1}{\eta_2} \qquad (2\text{-}42)$$

or we can define a new constant Δ as the ratio of δ to η

in the following way:

$$\Delta = \frac{\delta_1}{\eta_1} = \frac{\delta_2}{\eta_2} \qquad (2\text{-}43)$$

Eq. (2-43) shows that the detuning is proportional to the dissipation factor and it shifts in same direction according to whether the driving signal frequency is larger or less than the sum of two original subharmonic frequencies. The amplitude of each frequency component is given by:

$$R_1^2 = \frac{4\omega_2'^2\omega_0\eta_2}{\sigma_2\sigma_3}\left[\left\{(\eta_3 - 4\Delta\delta_3)^2 + (1 + 4\Delta^2)\right.\right.$$

$$\left.\left.\times\left[\frac{F^2\sigma_1\sigma_2}{4\omega_0^2\omega_1'\omega_2'\eta_1\eta_2(1+4\Delta^2)} - (\eta_3^2+4\delta_3^2)\right]\right\}^{\frac{1}{2}} - (\eta_3 - 4\Delta\delta_3)\right] \ .$$

$$R_2^2 = \frac{4\omega_1'^2\omega_0\eta_1}{\sigma_1\sigma_3}\left[\left\{(\eta_3 - 4\Delta\delta_3)^2 + (1 + 4\Delta^2)\right.\right.$$

$$\left.\left.\times\left[\frac{F^2\sigma_1\sigma_2}{4\omega_0^2\omega_1'\omega_2'\eta_1\eta_2(1+4\Delta^2)} - (\eta_3^2+4\delta_3^2)\right]\right\}^{\frac{1}{2}} - (\eta_3 - 4\Delta\delta_3)\right] \ .$$

and $\quad R_3^2 = \dfrac{4\omega_1'\omega_2'\eta_1\eta_2}{\sigma_1\sigma_2}(\ 1 + 4\Delta^2) \ .$

$$(2\text{-}44)$$

Since all R's are physical quantities, they have to be real values. The minimum intensity of F for R_1 and R_2 to appear, or, in other words, the threshold for generating the subharmonic components, is determined by:

$$F_{th}^2 = \frac{4\omega_1'\omega_2'\omega_0^2\eta_1\eta_2}{\sigma_1\sigma_2}(\eta_3^2 + 4\delta_3^2)(1 + 4\Delta^2) \ . \quad (2\text{-}45)$$

Below this threshold, the only significiant response is R_3, which is described by :

$$R_3 = \frac{F}{\omega_0(\eta_3^2 + 4\delta^2)^{\frac{1}{2}}} \quad . \tag{2-46}$$

We see that R_3 exhibits a very interesting behavior: it increases linearly with the external driving force and then stays at a constant value after the threshold for subharmonic generation is reached. Fig. 2-3a is a typical graphical display of the change in R_1, R_2, and R_3, with respect to the increase in the intensity of F. Fig. 2-3b shows the experimental data collected by Y. Tsuzuki and M. Kakuishi[31] in their observation of the excitation of contour modes of vibration in AT-cut quartz. The responses of the subharmonics have been squared in that diagram, so they appear to be linear past the threshold. They fit our mathematical model and analysis very well.
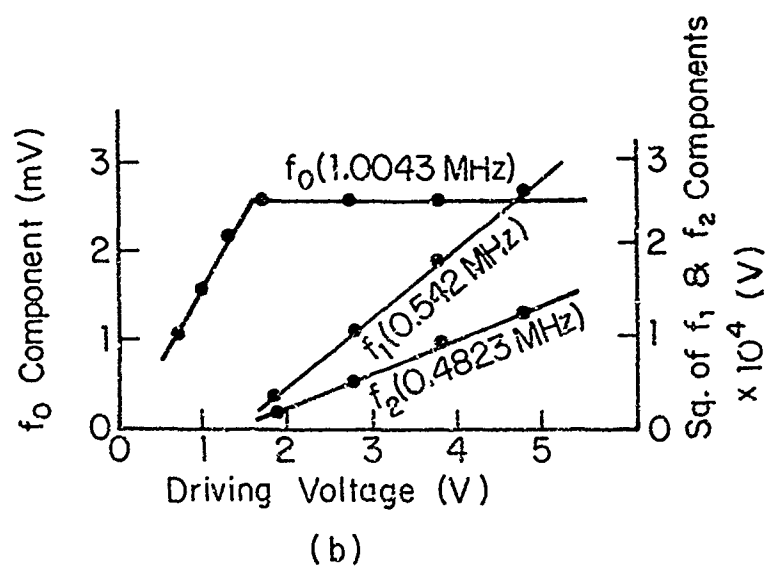
$$2\left[\frac{\omega_1\omega_2\eta_1\eta_2}{\sigma_1\sigma_2}(1+4\Delta^2)\right]^{\frac{1}{2}}$$

(a)

(b)
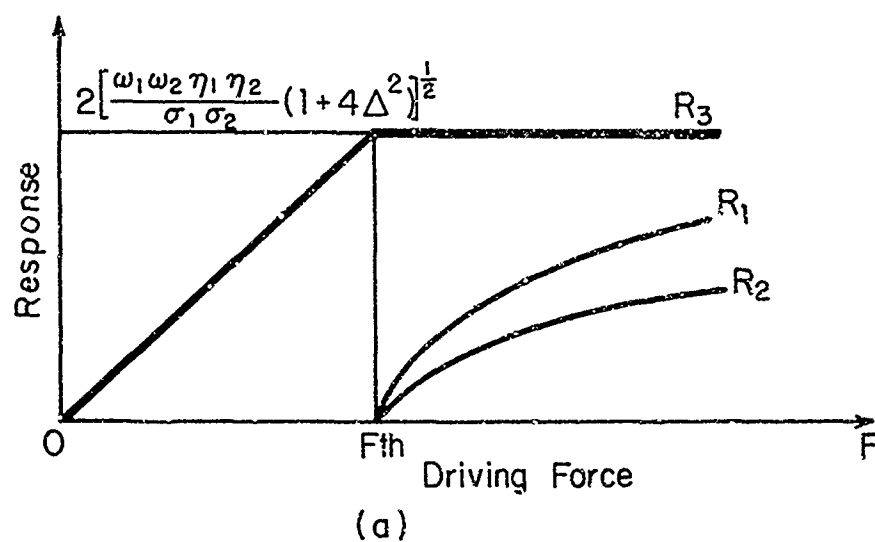
FIG. 2-3 RESPONSE OF FORCED EXCITATION

Chapter III

SUBHARMONIC GENERATION IN DISTRIBUTED SYSTEMS

The effect of intense acoustic waves has been studied by various authors, for example: Ghiron[32], Hunt[33], and Andreev[34]. They indicated that the nonlinear properties of the medium as well as convection of the disturbance usually cause wave distortion during propagation and the generation of superharmonics of the original signal. Experimental observations[35] have confirmed these analytic predictions. However such a theoretical approach has failed to supply an explanation for the phenomenon of subharmonics. We shall provide a detailed study of this aspect of the problem.

In order to simplify the mathematical operations, the entire analysis throughout this chapter is based on a one-dimensional model. Eulerian coordinates are employed in all derivations to facilitate comparison of the theoretical results with the laboratory data from the experimental work that is described in the next chapter.

We review the formulation of the acoustic wave equation from the basic conservation laws in the beginning of this chapter. As the primary interest of this study is to look for the essential contribution to the subharmonic generation for an intense acoustic wave, the order of magnitude of all pertinent parameters in the system considered is examined.

The two-variable method is adopted to fir' an approximate solution for the nonlinear wave equation. We obtain the energy exchange relations among three signals when their frequencies follow a sum rule.

This analysis is then extended to a multiresonator, and the threshold of exciting a subharmonic pair is deduced. We also discuss the effects of detuning and energy dissipation on subharmonic generation.

1. Formulation of Finite Amplitude Acoustic Wave Motion

The basic laws describing acoustic wave motion can be derived from the hydrodynamic equations. In one-dimensional Eulerian form, they are[*]:

Conservation of mass

$$\frac{\partial \rho'}{\partial t'} + \frac{\partial \rho'u'}{\partial x'} = 0 \qquad (3-1)$$

Conservation of momentum

$$\frac{\partial \rho'u'}{\partial t'} + u'\frac{\partial \rho'}{\partial x'} + \frac{\partial p'}{\partial x'} - \mu'\frac{\partial^2 u'}{\partial x'^2} = 0, \qquad (3-2)$$

where ρ' and u' are the density and the particle velocity respectively and μ' is the coefficient of viscosity which consists of the coefficient of shear viscosity ν' and the coefficient of dilatation viscosity λ', as defined by the

---

[*] The primes are used to denote dimensional quantities. We will shortly reduce them to nondimensional variables and the primes will be dropped.

relation:

$$\mu' = 2\nu' + \lambda'.\qquad\qquad(3\text{-}3)$$

The losses due to viscosity are small, and so are the losses due to heat conduction. Under these conditions, the process can be assumed to be adiabatic as far as wave speed is concerned since the losses affect the speed only quadratically. The state variable p', the pressure, can be expressed by expanding around the equilibrium state as follows:

$$p' = P'(\rho'),$$

$$= P_0' + \left(\frac{\partial p'}{\partial \rho'}\right)_q (\Delta\rho') + \frac{1}{2}\left(\frac{\partial^2 p'}{\partial \rho'^2}\right)_q (\Delta\rho')^2 + \cdots\cdots ,$$

$$= P_0' + c_0'^2(\Delta\rho') + \frac{1}{2}\Gamma'(\Delta\rho')^2 + \cdots\cdots\cdots,\qquad(3\text{-}4)$$

c_0' is so called the small signal sound speed, Γ' is a non-linear parameter and $\Delta\rho' = \rho' - \rho_0'$ is the deviation of the density from the equilibrium state. The subscript q denotes that the expansion is assumed adiabatic.

Some authors[36,37], in discussing the nonlinear behavior of a fluid, write Eq. (3-4) in the form

$$p' = P_0' + A\,\frac{\rho'-\rho_0'}{\rho_0'} + \frac{B}{2}\left(\frac{\rho'-\rho_0'}{\rho_0'}\right)^2 + \cdots\cdots\cdots ,\qquad(3\text{-}5)$$

These coefficients are related by

$$A = \rho_0' c_0'^2, \qquad B = \rho_0'^2 \Gamma', \qquad \text{and} \quad \frac{B}{A} = \frac{\rho_0'\Gamma'}{c_0'^2} \cdots\cdots\cdots .$$

$$(3\text{-}6)$$

In the case of an ideal gas, these coefficients can be re-
lated to the ratio of specific heat γ :

$$A = \gamma P_0', \quad B = \gamma(\gamma-1)p_0', \quad \text{and} \quad \frac{B}{A} = \gamma-1. \quad (3-7)$$

By using the approximate relation of Eq. (3-4), Eqs.
(3-1) and (3-2) then can be written in terms of ρ' and u' as
follows:

$$\frac{\partial \rho''}{\partial t'} + \frac{\partial \rho' u'}{\partial x'} = 0,$$

$$\frac{\partial \rho' u'}{\partial t'} + u' \frac{\partial \rho' u'}{\partial x'} + c_0'^2 \frac{\partial(\Delta\rho')}{\partial x'} + \frac{1}{2}\Gamma' \frac{\partial(\Delta\rho')^2}{\partial x'} - \mu' \frac{\partial^2 u'}{\partial x'^2} = 0. \quad (3-8)$$

In order to make an approximation with regard to the
order of magnitude of various terms in Eq. (3-8), we put
Eq. (3-8) in nondimensional form by adopting the following
scaling parameters:

Independent variables:

Length .... X cm

Time .... T sec

Dependent variables: (3-9)

Partical velocity .... U cm/sec

Density .... ρ_0 gm/cm^3

Then Eq. (3-8) has the form:

$$\frac{\partial \varrho}{\partial t} + \frac{UT}{X}\frac{\partial \varrho u}{\partial x} = 0,$$

$$\frac{UT}{X}\frac{\partial \varrho u}{\partial t} + \frac{U^2T^2}{X^2}u\frac{\partial \varrho u}{\partial x} + \frac{c_0^2 T^3}{X^2}\frac{\partial(\Delta \varrho)}{\partial x} + \frac{1}{2}\frac{\Gamma' T^2 P}{X^2}\frac{\partial(\Delta \varrho)^2}{\partial x}$$

$$- \frac{\mu' U T^2}{X^2 \varrho_0}\frac{\partial^2 u}{\partial x^2} = 0. \qquad (3\text{-}10)$$

We denote the nondimensional constants by:

$$M = \frac{UT}{X},$$

$$\Gamma = \frac{\Gamma_0' T^2 \varrho_0}{X^2}, \qquad (3\text{-}11)$$

$$c^2 = \frac{c_0'^2 T^2}{X^2},$$

$$\mu = \frac{\mu'}{\varrho_0 XU}.$$

Eq. (3-10) then becomes:

$$\frac{\partial \varrho}{\partial t} + M\frac{\partial \varrho u}{\partial x} = 0,$$

$$M\frac{\partial \varrho u}{\partial t} + M^2 u\frac{\partial \varrho u}{\partial x} + c^2\frac{\partial(\Delta \varrho)}{\partial x} + \frac{1}{2}\Gamma\frac{\partial(\Delta \varrho)^2}{\partial x} - M^2\mu\frac{\partial^2 u}{\partial x^2} = 0.$$

$$(3\text{-}12)$$

For the case of a propagating harmonic wave where both losses and nonlinear effects are small, the natural scaling parameters to use are:

$$T = \frac{1}{\omega_r'}$$

$$X = \frac{1}{k_r'} \qquad (3\text{-}13)$$

where ω_r' and k_r' are the dimensional angular frequency and

wave number of the wave, respectively, and $\frac{\omega_r'}{k_r'} = c_0'$. Then

$M = \frac{UK_r'}{\omega_r'} = \frac{U}{c_0'}$ is seen to be the particle velocity Mach

number and $c = c_0'(\frac{k_r'}{\omega_r'}) = 1$. The problem of interest here is

when M is small, but not negligibly so. Therefore we intro-
duce the symbol

$$\epsilon = M = \frac{U}{c_0'} \qquad (3\text{-}14)$$

and Eq. (3-12) becomes

$$\frac{\partial \varrho}{\partial t} + \epsilon \frac{\partial \varrho u}{\partial x} = 0,$$

$$\frac{\partial \varrho u}{\partial \tau} + \epsilon^2 u \frac{\partial u}{\partial x} + \frac{\partial (\Delta \varrho)}{\partial x} + \frac{1}{2}\Gamma^2 \frac{\partial (\Delta \varrho)^2}{\partial x} - \epsilon^2 \mu \frac{\partial^2 u}{\partial x^2} = 0,$$

$$\epsilon = M = \frac{U_r}{c_0} \ll 1. \qquad (3\text{-}15)$$

2. Wave Equations in Terms of Slow and Fast Variables

To get the explicit expression for ϱ and u as a func-
tion of x and t by solving Eq. (3-15) is a rather difficult
mathematical task. An approximate method can be developed
for the case of a small Mach number. First, consider the
linearized inviscid form of Eq. (3-15). (Remember, density
is nondimensionalized so $\varrho = 1$ at equilibrium).

$$\frac{\partial \mathcal{C}}{\partial t} + \epsilon \frac{\partial u}{\partial x} = 0,$$

$$\epsilon \frac{\partial u}{\partial t} + \frac{\partial \mathcal{C}}{\partial x} = 0,$$

(3-16)

which further reduces to the form of a wave equation,

$$\frac{\partial^2 u}{\partial x^2} - \frac{\partial^2 u}{\partial t^2} = 0.$$

(3-17)

The corresponding solution of Eq. (3-17) has the form

$$u = f(x-t) + g(x+t),$$

(3-18)

where f represents tne wave travelling to the right, a forward wave, and g represents the wave travelling to the left, a backward wave.

For a simple sinusoidal excitation with an angular frequency ω,

$$u = A \sin(\omega t - kx + \phi) + B \sin(\omega t + kx + \Phi),$$

(3-19)

where A, B, ϕ, and Φ are constants which depend on the initial condition of excitation.

Eq. (3-19) describes a wave propagating with a constant amplitude. For finite amplitude wave motion, if ϵ is much less than one, the physical picture of Eq. (3-15) should not be very different from Eq. (3-16). The convection, nonlinear parameter and viscosity may just modify slightly the propagating wave form. Since their effect is small, it may be considered that the original wave form has a slow variation in the amplitude and phase, with respect to time and space, as it propagates through the medium. With

this physical argument, it is possible to divide the independent variables into fast and slow components. That is, we describe the phenomenon in two different domains, fast and slow, by defining:

$$t_f = t,$$
$$t_s = \epsilon t,$$
$$x_f = x,$$
$$x_s = \epsilon x.$$

$$(3-20)$$

The dependent variables, ρ and u are now consider to be functions of t_f, t_s, x_f, and x_s.

According to our method of nondimensionalization, ρ' was normalized by ρ_0 and therefore its variation from ρ_0 will be small (order ϵ or higher). On the other hand, u was nondimensionalized by U_r which is a reference velocity small compared to c_0'. Therefore the leading variation in u is of order ϵ^0. Then we write the expansions of the dependent variables as:

$$\rho = 1 + \epsilon\rho_1 + \epsilon^2\rho_2 + \cdots\cdots ,$$
$$u = \quad u_1 + \epsilon u_2 + \cdots\cdots .$$

$$(3-21)$$

Note that there is no term u_0. This signifies that at equilibrium, the fluid is at rest.

The differential operators in term of the new variables are:

$$\frac{\partial}{\partial t} = \frac{\partial}{\partial t_f} + \epsilon \frac{\partial}{\partial t_s} \ ,$$

$$\frac{\partial}{\partial x} = \frac{\partial}{\partial x_f} + \epsilon \frac{\partial}{\partial x_s} \ , \qquad\qquad (3\text{-}22)$$

and $\qquad \dfrac{\partial^2}{\partial x^2} = \dfrac{\partial^2}{\partial x_f^2} + 2\epsilon \dfrac{\partial^2}{\partial x_f \partial x_s} + \epsilon^2 \dfrac{\partial^2}{\partial x_s^2} \ .$

Substituting Eqs. (3-21) and (3-22) into Eq. (3-15)
we have:

$$(\frac{\partial}{\partial t_f} + \epsilon \frac{\partial}{\partial t_s})(1 + \epsilon \rho_1 + \epsilon^2 \rho_2 + \dots) + \epsilon(\frac{\partial}{\partial x_f} + \epsilon \frac{\partial}{\partial x_s})$$

$$\cdot (1 + \epsilon \rho_1 + \epsilon^2 \rho_2 + \dots)(u_1 + \epsilon u_2 + \dots) = 0,$$

$$\epsilon(\frac{\partial}{\partial t_f} + \epsilon \frac{\partial}{\partial t_s})(1 + \epsilon \rho_1 + \epsilon^2 \rho_2 + \dots)(u_1 + \epsilon u_2 + \dots)$$

$$+ \epsilon^2(u_1 + \epsilon u_2 + \dots)(\frac{\partial}{\partial x_f} + \epsilon \frac{\partial}{\partial x_s})(1 + \epsilon \rho_1 + \epsilon^2 \rho_2 + \dots)$$

$$\cdot (u_1 + \epsilon u_2 + \dots) + (\frac{\partial}{\partial x_f} + \epsilon \frac{\partial}{\partial x_s})(\epsilon \rho_1 + \epsilon^2 \rho_2 + \dots)$$

$$+ \frac{\Gamma}{2}(\frac{\partial}{\partial x_f} + \epsilon \frac{\partial}{\partial x_s})(\epsilon \rho_1 + \epsilon^2 \rho_2 + \dots)^2$$

$$- \epsilon^2 \mu(\frac{\partial^2}{\partial x_f^2} + 2\epsilon \frac{\partial^2}{\partial x_f \partial x_s} + \epsilon^2 \frac{\partial^2}{\partial x_s^2})(u_1 + \epsilon u_2 + \dots) = 0.$$

$$(3\text{-}23)$$

In Eq. (3-23), the order ϵ^1 yields

$$\frac{\partial}{\partial t_f} \rho_1 + \frac{\partial}{\partial x_f} u_1 = 0,$$

$$(3\text{-}24)$$

$$\frac{\partial}{\partial t_f} u_1 + \frac{\partial}{\partial x_f} \rho_1 = 0,$$

which can be reduced to a first order wave equation by eliminating c_1.

$$\frac{\partial^2}{\partial x_f^2} u_1 - \frac{\partial^2}{\partial t_f^2} u_1 = 0. \qquad (3\text{-}25)$$

For order ϵ^2, we have the following equations:

$$\frac{\partial}{\partial t_f} c_2 + \frac{\partial}{\partial t_s} c_1 + \frac{\partial}{\partial x_f} u_2 + \frac{\partial}{\partial x_f} c_1 u_1 + \frac{\partial}{\partial x_s} u_2 = 0,$$

$$\frac{\partial}{\partial t_f} u_2 + \frac{\partial}{\partial t_f} c_1 u_1 + \frac{\partial}{\partial t_s} u_1 + u_1 \frac{\partial}{\partial x_f} u_1 + \frac{\partial}{\partial x_f} c_2$$

$$+ \frac{\partial}{\partial x_s} c_1 + \frac{\Gamma}{2} \frac{\partial}{\partial x_f} c_1^2 - \mu \frac{\partial^2}{\partial x_f^2} u_1 = 0.$$

$$(3\text{-}26)$$

The corresponding second order wave equation is:

$$\frac{\partial^2}{\partial x_f^2} u_2 - \frac{\partial^2}{\partial t_f^2} u_2 = \frac{\partial^2}{\partial t_f^2} c_1 u_1 - \frac{\partial^2}{\partial x_f^2} c_1 u_1 + \frac{\partial}{\partial t_f}\left(u_1 \frac{\partial}{\partial x_f} u_1\right)$$

$$+ \frac{\Gamma}{2} \frac{\partial^2}{\partial t_f \partial x_f} c_1^2 - \frac{\mu}{2} \frac{\partial^3}{\partial x_f^2 \partial t_f} u_1 + \frac{\partial^2}{\partial t_f \partial t_s} u_1$$

$$- \frac{\partial^2}{\partial x_f \partial x_s} u_1 + \frac{\partial^2}{\partial t_f \partial x_s} c_1 - \frac{\partial^2}{\partial x_f \partial t_s} c_1.$$

$$(3\text{-}27)$$

The first order solution can be found from Eq. (3-25). It is then used to generate source terms in the right hand side of Eq. (3-27). The higher order solutions can be found in a similar way. However, this only gives the general form

of the solution. For a particular problem, the initial and the boundary conditions are required to select the meaningful solution. In the following sections, particular cases of subharmonic generation will be studied in some detail.

3. Interaction of Waves

For certain initial disturbances, the response, in terms of the particle velocity of the medium, according to Eq. (3-25), has the general form:

$$u_n = \sum_{n=1}^{\infty} \left[A_n \cos\xi_n + B_n \cos\zeta_n \right] , \quad (3\text{-}28)$$

where

$$\begin{aligned}
A_n &= A_n(x_s, t_s), \\
B_n &= B_n(x_s, t_s), \\
\xi_n &= \omega_n t_f - k_n x_f + \phi_n(x_s, t_s), \\
\zeta_n &= \omega_n t_f + k_n x_f + \Phi_n(x_s, t_s).
\end{aligned} \quad (3\text{-}29)$$

Suppose the disturbance at $x = 0$ is mainly dominated by three distinct signals with angular frequencies ω_1, ω_2, and ω_3 related by:

$$\omega_1 + \omega_2 = \omega_3 . \quad (3\text{-}30)$$

Then Eq. (3-28) can be rewritten as

$$u_n = \sum_{n=1}^{3} \left[A_n \cos\xi_n + B_n \cos\zeta_n \right], \quad (3\text{-}31)$$

with a corresponding density:

$$\rho_n = \sum_{n=1}^{?} \left[A_n \cos \xi_n - B_n \cos \zeta_n \right] . \quad (3\text{-}32)$$

For nondispersive media, the wave number k's will follow the same sum rule as that of angular frequency from Eq. (3-30):

$$k_1 + k_2 = k_3 . \quad (3\text{-}33)$$

A_n, B_n, ϕ_n, and Φ_n are only given for the initial condition $x_s = 0$, $t_s = 0$. To determine how they change with respect to time and space (in slow scale) depends on further information from the second order wave equation in Eq. (3-27).

When we substitute Eqs. (3-31) and (3-32) into the second order wave equation, Eq. (3-27), to solve for the second order term of u, we find that the source terms on the right hand side of that equation contain the same frequencies as the natural frequencies on the left hand side. This means that the solution will have terms increasing linearly with time and space. Such solutions will ultimately violate the original requirement of $\epsilon u_2 \ll u_1$ in the perturbation expansion. Those terms which cause such limitations on perturbation expansion are called the secular terms. Since the amplitude and phase are assumed to be functions of the slow variables in the case discussed here, the problem can be avoided by choosing the slowly varying amplitude and phases in order to make the secular terms vanish. This choice leads to the relation showing how amplitude and phase change with time and space (in slow scale) after the initial disturbance.

After some tedious algebraic operations, we achieve
the following results:

$$\frac{\partial A_1}{\partial t_s} + \frac{\partial A_1}{\partial x_s} + \mu\omega_1^2 A_1 - \sigma\omega_1 A_2 A_3 \sin r = 0,$$

$$\frac{\partial A_2}{\partial t_s} + \frac{\partial A_2}{\partial x_s} + \mu\omega_2^2 A_2 - \sigma\omega_2 A_1 A_3 \sin r = 0,$$

$$\frac{\partial A_3}{\partial t_s} + \frac{\partial A_3}{\partial x_s} + \mu\omega_3^2 A_3 + \sigma\omega_3 A_1 A_2 \sin r = 0,$$

$$A_1 \frac{\partial \phi_1}{\partial t_s} + A_1 \frac{\partial \phi_1}{\partial x_s} + \sigma\omega_1 A_2 A_3 \cos r = 0,$$

$$A_2 \frac{\partial \phi_2}{\partial t_s} + A_2 \frac{\partial \phi_2}{\partial x_s} + \sigma\omega_2 A_1 A_3 \cos r = 0,$$

$$A_3 \frac{\partial \phi_3}{\partial t_s} + A_3 \frac{\partial \phi_3}{\partial x_s} + \sigma\omega_3 A_1 A_2 \cos r = 0, \qquad (3\text{-}34)$$

$$\frac{\partial B_1}{\partial t_s} - \frac{\partial B_1}{\partial x_s} + \mu\omega_1^2 B_1 - \sigma\omega_1 B_2 B_3 \sin s = 0,$$

$$\frac{\partial B_2}{\partial t_s} - \frac{\partial B_2}{\partial x_s} + \mu\omega_2^2 B_2 - \sigma\omega_2 B_1 B_3 \sin s = 0,$$

$$\frac{\partial B_3}{\partial t_s} - \frac{\partial B_3}{\partial x_s} + \mu\omega_3^2 B_3 + \sigma\omega_3 B_1 B_2 \sin s = 0,$$

$$B_1 \frac{\partial \Phi_1}{\partial t_s} - B_1 \frac{\partial \Phi_1}{\partial x_s} + \sigma\omega_1 B_2 B_3 \cos s = 0,$$

$$B_2 \frac{\partial \Phi_2}{\partial t_s} - B_2 \frac{\partial \Phi_2}{\partial x_s} + \sigma\omega_2 B_1 B_3 \cos s = 0,$$

$$B_3 \frac{\partial \Phi_3}{\partial t_s} - B_3 \frac{\partial \Phi_3}{\partial x_s} + \sigma\omega_3 B_1 B_2 \cos s = 0,$$

where

$$\sigma = \frac{1}{4}\,(1 + \Gamma)\;,$$

$$r = \phi_3 - \phi_1 - \phi_2\;,\qquad\qquad (3\text{-}35)$$

$$s = \Phi_3 - \Phi_1 - \Phi_2\;.$$

In Eq. (3-34), the first six equations are independent of the last six equations. This indicates that there is no coupling between A_n, ϕ_n, and B_n, Φ_n. Since, from Eq. (3-29), A_n and ϕ_n are amplitudes and phases respectively of the forward travelling waves and B_n and Φ_n are amplitudes and phases respectively of the backward travelling waves, the results expressed in Eq. (3-34) show that these two types of wave propagate independently without interaction.

We now further examine the character of the forward wave to understand the mechanics of wave interaction (the conclusion will also apply to the case of backward wave).

The first six equations in (3-34) have a single set of characteristics in slow space and time with slope unity. Therefore if we introduce the variable

$$\tau = t_s - x_s\;,\qquad\qquad (3\text{-}36)$$

these equations may be written as:

$$\frac{dA_1}{d\tau} + \mu\omega_1^2 A_1 - \sigma\,\omega_1 A_2 A_3 \sin r = 0,$$

$$\frac{dA_2}{d\tau} + \mu\omega_2^2 A_2 - \sigma\omega_2 A_1 A_3 \sin r = 0,$$

$$\frac{dA_3}{d\tau} + \mu\omega_3^2 A_3 + \sigma\omega_3 A_1 A_2 \sin r = 0,$$

$$A_1 \frac{d\phi_1}{d\tau} + \sigma\omega_1 A_2 A_3 \cos r = 0,$$

$$A_2 \frac{d\phi_2}{d\tau} + \sigma\omega_2 A_1 A_3 \cos r = 0, \qquad (3\text{-}37)$$

$$A_3 \frac{d\phi_3}{d\tau} + \sigma\omega_3 A_1 A_2 \cos r = 0.$$

Although amplitudes and phases change slowly, it is interesting to see that the slow behavior propagates at the same speed as the waves themselves. Eq. (3-37) can be further reduced to

$$\frac{dA_1}{d\tau} + \mu\omega_1^2 A_1 - \sigma\omega_1 A_2 A_3 \sin r = 0,$$

$$\frac{dA_2}{d\tau} + \mu\omega_2^2 A_2 - \sigma\omega_2 A_1 A_3 \sin r = 0,$$

$$\frac{dA_3}{d\tau} + \mu\omega_3^2 A_3 + \sigma\omega_3 A_1 A_2 \sin r = 0, \qquad (3\text{-}38)$$

$$\frac{dr}{d\tau} + \left[\frac{\omega_3 A_1 A_2}{A_3} - \frac{\omega_1 A_2 A_3}{A_1} - \frac{\omega_2 A_1 A_3}{A_2}\right]\sigma \cos r = 0.$$

For a nonviscous medium, these coupling equations can be even simplified to:

$$\frac{dA_1}{d\tau} - \sigma\omega_1 A_2 A_3 \sin r = 0,$$

$$\frac{dA_2}{d\tau} - \sigma\omega_2 A_1 A_3 \sin r = 0,$$

where

$$\sigma = \frac{1}{4}(1 + \Gamma) ,$$

$$r = \phi_3 - \phi_1 - \phi_2 , \tag{3-35}$$

$$s = \Phi_3 - \Phi_1 - \Phi_2 .$$

In Eq. (3-34), the first six equations are independent of the last six equations. This indicates that there is no coupling between A_n, ϕ_n, and B_n, Φ_n. Since, from Eq. (3-29), A_n and ϕ_n are amplitudes and phases respectively of the forward travelling waves and B_n and Φ_n are amplitudes and phases respectively of the backward travelling waves, the results expressed in Eq. (3-34) show that these two types of wave propagate independently without interaction.

We now further examine the character of the forward wave to understand the mechanics of wave interaction (the conclusion will also apply to the case of backward wave).

The first six equations in (3-34) have a single set of characteristics in slow space and time with slope unity. Therefore if we introduce the variable

$$\tau = t_s - x_s , \tag{3-36}$$

these equations may be written as:

$$\frac{dA_1}{d\tau} + \mu\omega_1^2 A_1 - \sigma\omega_1 A_2 A_3 \sin r = 0,$$

$$\frac{dA_2}{d\tau} + \mu\omega_2^2 A_2 - \sigma\omega_2 A_1 A_3 \sin r = 0,$$

$$\frac{dA_3}{d\tau} + \mu\omega_3^2 A_3 + \sigma\omega_3 A_1 A_2 \sin r = 0,$$

$$A_1 \frac{d\phi_1}{d\tau} + \sigma\omega_1 A_2 A_3 \cos r = 0,$$

$$A_2 \frac{d\phi_2}{d\tau} + \sigma\omega_2 A_1 A_3 \cos r = 0,$$

$$A_3 \frac{d\phi_3}{d\tau} + \sigma\omega_3 A_1 A_2 \cos r = 0.$$

(3-37)

Although amplitudes and phases change slowly, it is interesting to see that the slow behavior propagates at the same speed as the waves themselves. Eq. (3-37) can be further reduced to

$$\frac{dA_1}{d\tau} + \mu\omega_1^2 A_1 - \sigma\omega_1 A_2 A_3 \sin r = 0,$$

$$\frac{dA_2}{d\tau} + \mu\omega_2^2 A_2 - \sigma\omega_2 A_1 A_3 \sin r = 0,$$

$$\frac{dA_3}{d\tau} + \mu\omega_3^2 A_3 + \sigma\omega_3 A_1 A_2 \sin r = 0,$$

$$\frac{dr}{d\tau} + \left[\frac{\omega_3 A_1 A_2}{A_3} - \frac{\omega_1 A_2 A_3}{A_1} - \frac{\omega_2 A_1 A_3}{A_2}\right]\sigma \cos r = 0.$$

(3-38)

For a nonviscous medium, these coupling equations can be even simplified to:

$$\frac{dA_1}{d\tau} - \sigma\omega_1 A_2 A_3 \sin r = 0,$$

$$\frac{dA_2}{d\tau} - \sigma\omega_2 A_1 A_3 \sin r = 0,$$

$$\frac{dA_3}{d\tau} + \sigma\omega_3 A_1 A_2 \sin r = 0, \qquad (3\text{-}39)$$

$$\frac{dr}{d\tau} + \left[\frac{\omega_3 A_1 A_2}{A_3} - \frac{\omega_1 A_2 A_3}{A_1} - \frac{\omega_2 A_1 A_3}{A_2}\right] \sigma \cos r = 0.$$

There are then three constraints, as we have discussed in Chapter II for three oscillators:

$$A_1^2 + A_2^2 + A_3^2 = E,$$

$$\frac{A_1^2}{\omega_1} - \frac{A_2^2}{\omega_2} = C, \qquad (3\text{-}40)$$

$$A_1 A_2 A_3 \cos r = K.$$

The mathematical similarility between wave interaction and coupled oscillators suggests the possibility of using such a mechanism for subharmonic generation. If we could find a way to supply power to the ω_3 signal to keep amplitude A_3 constant, the condition to excite ω_1 and ω_2 signal would be governed by :

$$\frac{dA_1}{d\tau} + \mu\omega_1^2 A_1 - \sigma\omega_1 A_2 A_3 = 0,$$

$$\frac{dA_2}{d\tau} + \mu\omega_2^2 A_2 - \sigma\omega_2 A_1 A_3 = 0, \qquad (3\text{-}41)$$

where r is properly adjusted to be $\pi/2$.

Then the threshold of a stable subharmonic pair with angular frequencies ω_1 and ω_2 is determined by :

$$A_3 = \frac{\mu\sqrt{\omega_1\omega_2}}{\sigma} \qquad (3\text{-}42)$$

or in original nondimensionalized notations :

$$A_3 = \frac{2\mu'/\omega_1'\omega_2'}{e_0'c_0'\left[1+\dfrac{\Gamma'e_0'}{c_0'^2}\right]} \quad .\qquad (3-43)$$

The correspon.'ng pressure will be :

$$p_3' = \frac{2\mu'/\omega_1'\omega_2'}{\left[1+\dfrac{\Gamma'e_0'}{c_0'^2}\right]} \quad .\qquad (3-44)$$

For water, $\dfrac{\Gamma'e_0'}{c_0'^2} = 6.5$ [36,37] and $\mu' = 0.01$ poise, the minimum

pressure threshold to excite the subharmonic pair with a

1 MHZ signal, according to Eq. (3-44), should be 0.0017 bar.

However, there are two factors to prevent subharmonics from

occurring in real physical situations: the formation of shock

wave and energy spreading into free space. The former is

also caused by convection and the nonlinearity of the medium,

as well as the accumulated effect of superharmonic generation.

The latter is due to the fact that since the size of the

energy source is finite and in real situations is, of course,

three dimensional, the wave will spread out in part as a

spherical wave. Under those conditions, energy is dispersed

faster than it is converted to subharmonis, Thus, the phe-

nomenon of subharmonic generation will not be observed. To

avoid such limitations, we will analyze in the next section

the situation for an intense wave in a closed boundary which

confines the energy spreading. Because only certain modes will be allowable in a closed boundary, we can also eliminate superharmonic generation.

4. Mode-Coupling in a Simple Resonator

In a closed homogeneous region with energy reflection, there exist resonance modes which are easily excited. We will now analyze the mode-coupling induced by the nonlinearity of the medium in such a closed region.

If the dimension of the bounded region is small (say, about 100 wavelength) and the dissipation and the nonlinearity of the medium do not make large changes in wave energy in a single pass. Then we can consider any disturbance, however distributed, as causing the build-up of a standing wave in this closed bounded region. The amplitude and the phase of such standing waves will change gradually due to the effect of the nonlinearity of the medium*. To examine their behavior, we rewrite the two-variable wave equation derived in Section 1 by considering slow time as the only slow variable.

$$\frac{\partial^2 u_1}{\partial x_f^2} - \frac{\partial^2 u_1}{\partial t_f^2} = 0,$$

$$\frac{\partial^2 u_2}{\partial x_f^2} - \frac{\partial^2 u_2}{\partial t_f^2} = \frac{\partial^2}{\partial t_f^2}\rho_1 u_1 - \frac{\partial^2}{\partial x_f^2}\rho_1 u_1 + \frac{\partial}{\partial t_f}\left(u_1\frac{\partial}{\partial x_f}u_1\right)$$

$$+ \frac{\Gamma}{2} \frac{\partial^2}{\partial t_f \partial x_f} \wp_1^2 + \frac{\partial^2}{\partial t_f \partial t_s} u_1 - \frac{\partial^2}{\partial x_f \partial t_s} \wp_1$$

$$- \mu \frac{\partial^3}{\partial x_f^2 \partial t_f} u_1 = 0 \ . \qquad (3\text{-}46)$$

General solutions of Eq. (3-45) are :

$$u_1 = \sum_{n=1}^{\infty} \left\{ A_n'(t_s) \cos\left[\omega_n t_f - k_n x_f + \phi_n(t_s)\right] \right.$$
$$\left. + B_n'(t_s) \cos\left[\omega_n t_f + k_n x_f + \Phi_n(t_s)\right] \right\} \ ,$$
$$(3\text{-}47)$$

where by our previous nondimensionalization,

$$\omega_n = k_n \qquad (3\text{-}48)$$

If u_1 vanishes at boundary $x_f = 0$, then

$$A_n'(t_s) = - B_n'(t_s) \ ,$$
$$\phi_n(t_s) = \Phi_n(t_s) \ . \qquad (3\text{-}49)$$

Eq. (3-47) will be in a form of a standing wave :

$$u_1 = \sum_{n=1}^{\infty} A_n(t_s) \sin\left[\omega_n t_f + \phi_n(t_s)\right] \sin k_n x_f \ .$$
$$(3\text{-}50)$$

The particular values of k_n are determined by the end condition at $x_f = L$; thus, if u vanishes at $x_f = L$, then $k_n = n\pi/L$. If the end termination is taken to be some frequency dependent complex impedance, the modal frequencies will not be in-

---

*The effect of moving boundary is discussed in Appendix A.

tegrally related.

We now suppose that, in a particular case, there are only three resonant modes of angular frequencies ω_1, ω_2, and ω_3, which have significant amplitude and that these modes obey the forgoing sum rule :

$$\omega_1 + \omega_2 = \omega_3 \; . \tag{3-51}$$

Considering these basic modes, we can rewrite solutions for u_1 in the form :

$$u_1 = \sum_{n=1}^{3} A_n(t_s) \sin \left[\omega_n t_f + \phi_n(t_s) \right] \sin k_n x_f \; , \tag{3-52}$$

with the corresponding density variation:

$$\varrho_1 = \sum_{n=1}^{3} A_n(t_s) \cos \left[\omega_n t_f + \phi_n(t_s) \right] \cos k_n x_f \; . \tag{3-53}$$

We use the same argument discussed in Section 2 to find the second order function from Eq. (3-46). By setting the secular terms equal to zero, we obtain the results :

$$\frac{\partial A_1}{\partial t_s} + \mu \omega_1^2 A_1 - \sigma \omega_1 A_2 A_3 \sin r = 0 \; ,$$

$$\frac{\partial A_2}{\partial t_s} + \mu \omega_2^2 A_2 - \sigma \omega_2 A_1 A_3 \sin r = 0 \; ,$$

$$\frac{\partial A_3}{\partial t_s} + \mu \omega_3^2 A_3 - \sigma \omega_3 A_1 A_2 \sin r = 0 \; ,$$

$$A_1\frac{\partial \phi_1}{\partial t_s} - \sigma \omega_1 A_2 A_3 \cos r = 0 , \qquad (3-54)$$

$$A_2\frac{\partial \phi_2}{\partial t_s} - \sigma \omega_2 A_1 A_3 \cos r = 0 ,$$

$$A_3\frac{\partial \phi_3}{\partial t_s} - \sigma \omega_3 A_1 A_2 \cos r = 0,$$

where

$$\sigma = \frac{1}{8} (1 + \Gamma) ,$$

$$r = \phi_3 - \phi_1 - \phi_2 .$$

Since the A's and the ϕ's are functions of slow time t_s only, those partial differential operators can be replaced by total differential operators. After combining the last three equations in Eq. (3-54), we have mode-coupling equations for a closed region (resonator).

$$\frac{dA_1}{dt_s} + \mu \omega_1^2 A_1 - \sigma \omega_1 A_2 A_3 \sin r = 0,$$

$$\frac{dA_2}{dt_s} + \mu \omega_2^2 A_2 - \sigma \omega_2 A_1 A_3 \sin r = 0,$$

$$\frac{dA_3}{dt_s} + \mu \omega_3^2 A_3 + \sigma \omega_3 A_1 A_2 \sin r = 0, \qquad (3-55)$$

$$\frac{dr}{dt_s} + (\frac{\omega_3 A_1 A_2}{A_3} - \frac{\omega_1 A_2 A_3}{A_1} - \frac{\omega_2 A_1 A_3}{A_2}) \, \sigma \cos r = 0 .$$

Eq. (3-55) shows that mode-coupling in a resonator is similar to that of oscillators described in Chapter II provided the

coupling parameters in Eq. (2-12) are made equal in all equations. Since the oscillators are resonance modes of the same medium, as in the resonator, the result is less general than that of separate mechanical oscillators which may have different impedances and different dissipation.

For a nonviscous medium, we can obtain, analogous to Chapter II, the three constraints for the resonator :

$$A_1^2 + A_2^2 + A_3^2 = E.$$

$$\frac{A_1^2}{\omega_1} - \frac{A_2^2}{\omega_2} = C, \qquad (3-56)$$

$$A_1 A_2 A_3 \cos r = K.$$

Since the system is assumed to be lossless, once the disturbance is excited, the energy will keep exchanging among the modes. If we take the dissipation into consideration, the terms $\omega_n^2 A_n$ in Eq. (3-55) will cause the disturbances to decay and so, also, the exchange rate among the modes. Eventually, the response will vanish.

The constraints of Eq. (3-56) can be used to illustrate the response of a lossless resonator. We do this by using a three dimension phase space shown in Fig. 3-1 which is similar to Fig. 2-2 but with A_1, A_2, and A_3 as axes. Since all the modes have the same impedance, the motion is confined to a spherical surface while in Fig. 2-2 the surface is ellipsoidal. The locus in the phase space suggests that, in a resonator,
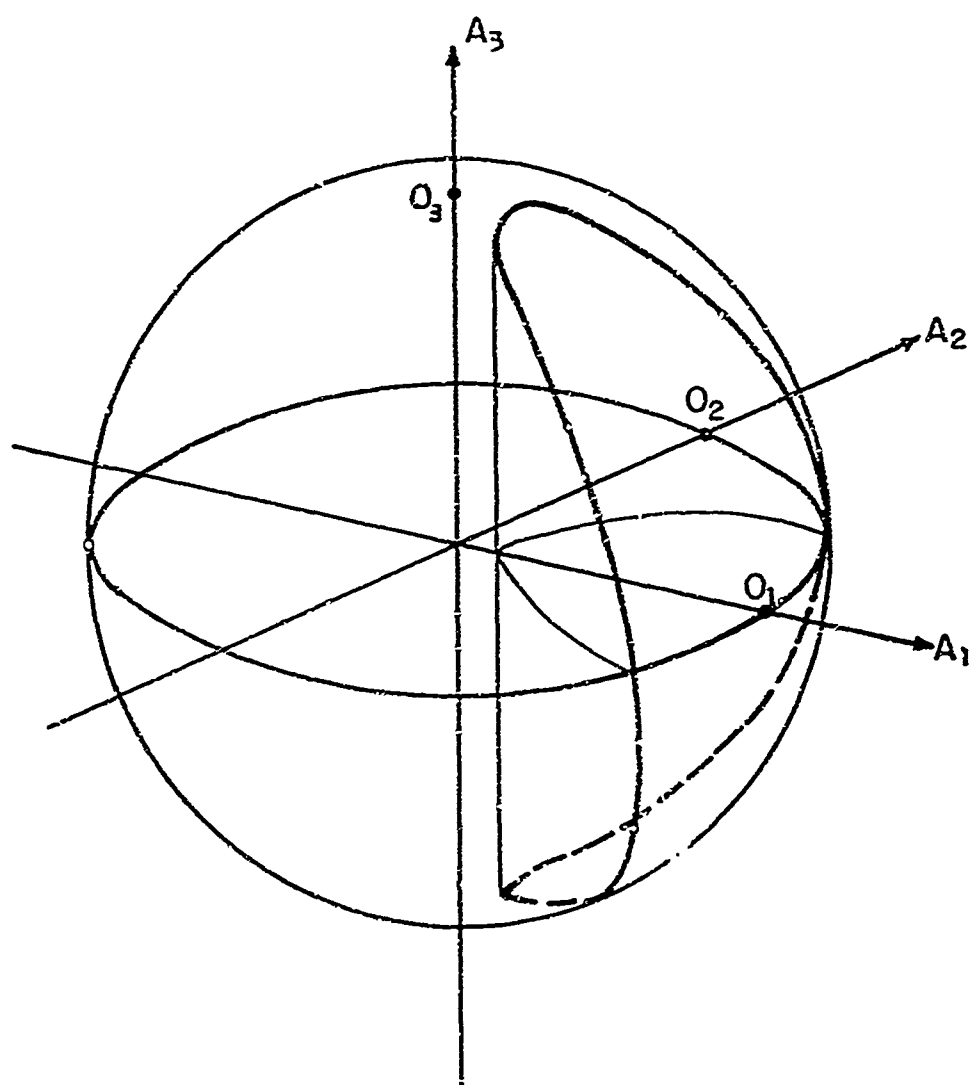
FIG. 3-1 PHASE SPACE FOR MODE-COUPLING IN A
RESONATOR

the high frequency mode is quite unstable and its energy
can be easily converted to low frequency modes. With dis-
sipation elements in the resonator, there exists a thresh-
old for exciting such subharmonic components.

In general, there are, in addition to viscous losses,
less mechanisms such as dissipation at the reflecting ends or
radiation losses along the sides of the active interferometer
volume. As long as these losses are sufficiently small, they
may be considered equivalent to an effective loss. Thus in
Eq. (3-55), we replace $\mu\omega_n^2 A_n$ by $\eta_n A_n$. These coefficients
can be determined directly by small amplitude measurements
of modal decay rate, since under such condition

$$\frac{dA_n}{dt_s} = -\eta_n A_n \ .$$
(3-57)

Then, for subharmonics to be excited, we require:

$$\frac{1}{A_1}\frac{dA_1}{dt_s} \gg 0, \quad \text{or} \quad \eta_1 < \sigma\omega_1\frac{A_2 A_3}{A_1} \ ,$$
(3-58)

and $$\frac{1}{A_2}\frac{dA_2}{dt_s} \gg 0, \quad \text{or} \quad \eta_2 < \sigma\omega_2\frac{A_1 A_3}{A_2} \ ,$$
(3-59)

with $\sin r = 1$.

We, therefore, arrive at a condition of the minimum thresh-
old for subharmonic excitation:

$$A_3 = \frac{\sqrt{\eta_1\eta_2}}{\sigma\sqrt{\omega_1\omega_2}} \ .$$
(3-60)

Eq. (3-60) indicates that the threshold is inversely propor-

the high frequency mode is quite unstable and its energy
can be easily converted to low frequency modes. With dis-
sipation elements in the resonator, there exists a thresh-
old for exciting such subharmonic components.

In general, there are, in addition to viscous losses,
less mechanisms such as dissipation at the reflecting ends or
radiation losses along the sides of the active interferometer
volume. As long as these losses are sufficiently small, they
may be considered equivalent to an effective loss. Thus in
Eq. (3-55), we replace $\mu\omega_n^2 A_n$ by $\eta_n A_n$. These coefficients
can be determined directly by small amplitude measurements
of modal decay rate, since under such condition

$$\frac{dA_n}{dt_s} = -\eta_n A_n \, .$$ (3-57)

Then, for subharmonics to be excited, we require:

$$\frac{1}{A_1}\frac{dA_1}{dt_s} \gg 0, \quad \text{or} \quad \eta_1 < \sigma\omega_1\frac{A_2 A_3}{A_1} \, ,$$ (3-58)

and $$\frac{1}{A_2}\frac{dA_2}{dt_s} \gg 0, \quad \text{or} \quad \eta_2 < \sigma\omega_2\frac{A_1 A_3}{A_2} \, ,$$ (3-59)

with sin r = 1.

We, therefore, arrive at a condition of the minimum thresh-
old for subharmonic excitation:

$$A_3 = \frac{\sqrt{\eta_1 \eta_2}}{\sigma\sqrt{\omega_1\omega_2}} \, .$$ (3-60)

Eq. (3-60) indicates that the threshold is inversely propor-

tional to the square root of the product of the subharmonic paired frequencies. Hence, when the paired subharmonic frequencies are equal, the required threshold will be minimum. Therefore subharmonics of one-half can be observed relatively easier provided that the one-half frequency is indeed close to the resonance mode of the system.

5. Modes of a Composite Resonator and the Selection Rule for Subharmonic Generation

The results of the previous analysis indicate that a resonator containing a nonlinear medium can provide a mechanism for subharmonic generation. We have shown that if a resonator has three resonance modes ω_1', ω_2', ω_3', and initially there is a strong signal in the mode with angular frequency ω_3', then some transient disturbance may cause other modes ω_1' or ω_2' to appear suddenly. Such a disturbance may be weak, but the energy in mode ω_3' will provide a source for modes ω_1' and ω_2' through the nonlinear coupling effect provided the $\omega_3' = \omega_1' + \omega_2'$ condition is approximately met.

For a simple one-dimensional resonator of Length L with the boundary conditions $p' = 0$ or $u' = 0$ at both ends, the angular frequency of the fundamental mode is

$$\omega_0' = \frac{\pi c_0'}{L} \qquad (3\text{-}61)$$

and any integer multiple of ω_0' will still be a resonance mode of such a system. Therefore, there are many possibilities for modes that satisfy the condition $\omega_3' = \omega_1' + \omega_2'$. However, in practical situations, some means must be provided for a driving source. The actual construction of a resonator is very complicated. Fig. 3-2 illustrates one simplified arrangement.

To find the resonance modes of this composite resonator, we not only have to know the boundary conditions on both ends but we also have to match the acoustic impedance at the interface due to two different media to provide the continuity of pressure and particle velocity. Such requirements result in a characteristic equation for modes of this composite resonator[*]:

$$R(\tan k_w'D + \tan k_w'H) + \tan k'S$$

$$- R^2 \tan k_w'D \tan k_w'H \tan k'S = 0 \qquad (3\text{-}62)$$

where R is the ratio of wall impedance to medium impedance, the k's are wave numbers in the corresponding region, and D, H, and S are the thickness of the two end walls and the length of the actual resonator, respectively. Eq. (3-62) can be rewritten in nondimensional form:

---

[*] Eq. (3-62) is derived in detail in Appendix B.
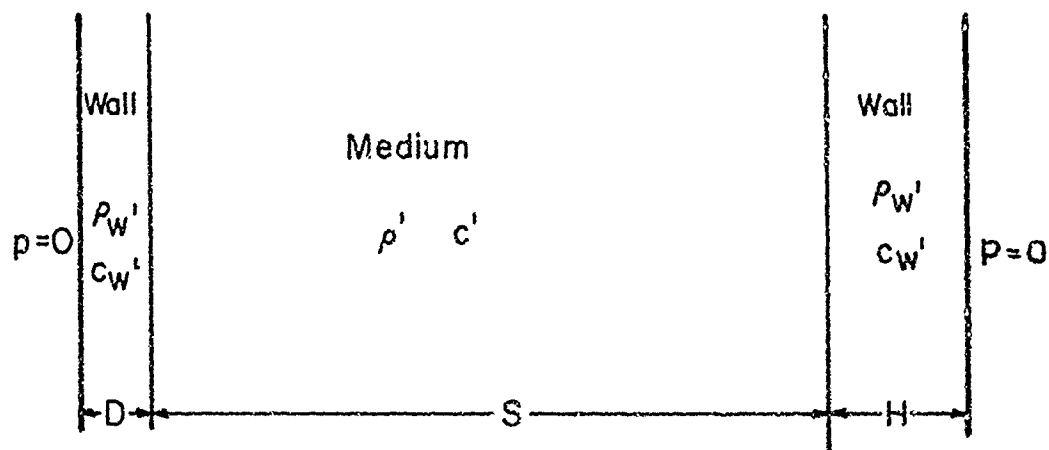
Characteristic Equation for Modes f'

$$R \left(\tan \frac{f'}{f'_D} \pi + \tan \frac{f'}{f'_H} \pi \right) + \tan \frac{f'}{f'_S} \pi$$

$$- R^2 \tan \frac{f'}{f'_D} \pi \cdot \tan \frac{f'}{f'_H} \pi \cdot \tan \frac{f'}{f'_S} = 0$$

where

$$R = \frac{\rho'_W c'_W}{\rho' c'}$$

$$f'_D = \frac{c'_W}{2D}$$

$$f'_H = \frac{c'_W}{2H}$$

$$f'_S = \frac{c'}{2S}$$

FIG. 3-2 A THREE-SECTION COMPOSITE RESONATOR

$$R(\tan \frac{f'}{f'_d} \pi + \tan \frac{f'}{f'_h} \pi) + \tan \frac{f'}{f'_s} \pi$$

$$- R^2(\tan \frac{f'}{f'_d} \pi)(\tan \frac{f'}{f'_h} \pi)(\tan \frac{f'}{f'_s} \pi) = 0, \quad (3-63)$$

where
$$f'_d = \frac{c'_w}{2D} ,$$

$$f'_h = \frac{c'_w}{2H} ,$$

and
$$f'_s = \frac{c'}{2S}$$

correspond to the fundamental resonance frequency of each individual region, respectively. Exact analytical solution for the roots in Eq. (3-63) are impossible to obtain. However, such a transcendantal function does show that the modes of this type resonator are not necessarily integrally related, as in the case of the simple resonator. Hence, there may be only a limited number of modes that will meet the $\omega'_3 = \omega'_1 + \omega'_2$ condition.

After the modes of a resonator are determined either by numerical methods or from experimental measurements, a graphical method can be used as selection rule for modes which can be excited as subharmonics. Fig. 3-3 shows ω'_1 and ω'_2 used as vertical and horizontal axes respectively. The vertical and the horizontal parallel lines are drawn from resonance frequency points on the ω'_1 and ω'_2 axes. An inclined line connects the point on the vertical axis at $\omega'_1 = \omega'_3$ and the point on the horizontal axis at $\omega'_2 = \omega'_3$.
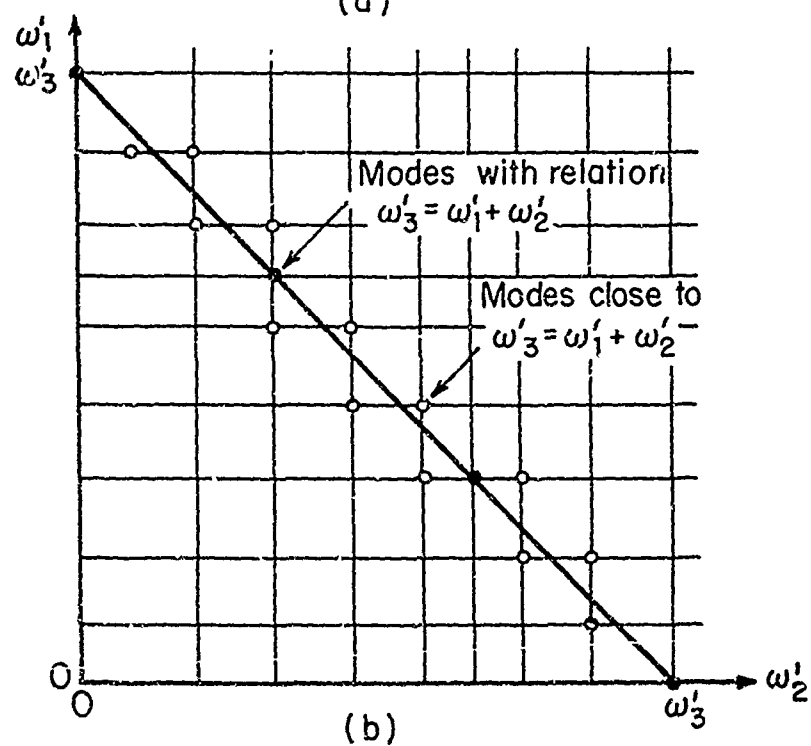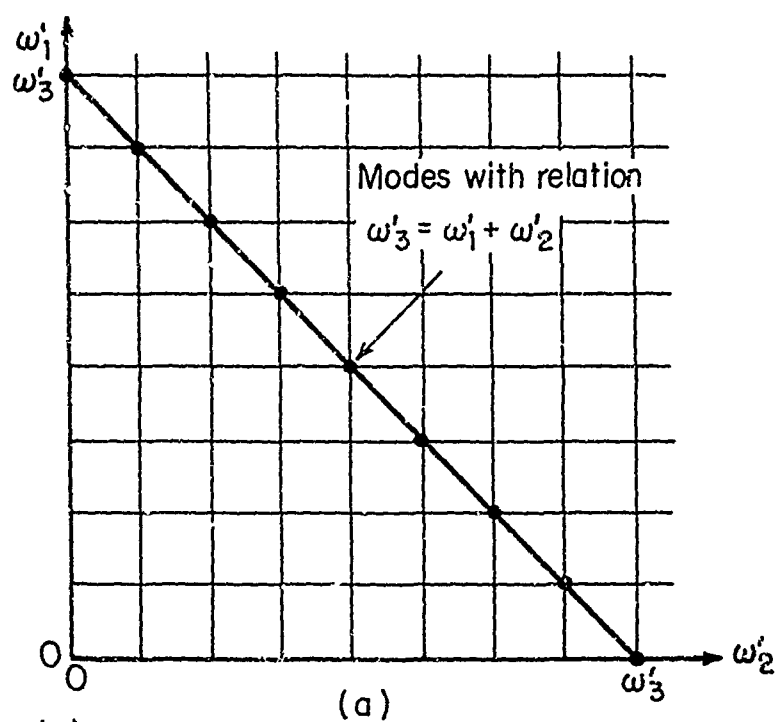
FIG. 3-3 SELECTION RULE FOR SUBHARMONIC
GENERATION MODES BY GRAPHICAL
METHOD

Any intersection point of three lines gives the modes with the condition $\omega_3' = \omega_1' + \omega_2'$. Fig 3-3a is the case for a simple resonator. It indicates that all the modes have the integer relation and there are many intersection points which will satify the condition $\omega_3' = \omega_1' + \omega_2'$. Fig. 3-3b is an example for the composite resonator described in Fig. 3-2. As the figure shows, there are only limited number of modes meeting the condition $\omega_3' = \omega_1' + \omega_2'$.

This graphical method can be extended to more complicated situations. Modes of a given resonator can be determined either through numerical solution or by actual experimental measurement. This information can be plotted on a graph. The closeness of intersection will be one of the important factors determining the possibility of generating subharmonics in the system. Any intersection point close to the inclined line may also be a mode that can be excited if the driving source is intense enough (the detuning problem will be further discussed in next section). Another effect, associated with dissipation, is that there will be some dispersion. That is, at high frequencies the sound speed in the medium will vary with frequency. Condition $\omega_3' = \omega_1' + \omega_2'$ does not necessarily mean $k_3 = k_1 + k_2$. This makes it more difficult to excite high frequency subharmonics.

6. Detuning for Forcing Excitation of Subharmonics in a Resonator

If three modes with angular frequencies ω_1, ω_2, and ω_3 in a resonator do not exactly match according to the sum rule of Eq. (3-51), we then define a detunig factor δ's as:

$$\omega_{01} = \omega_1 + \epsilon\delta_1,$$

$$\omega_{02} = \omega_2 + \epsilon\delta_2,$$

$$\omega_{03} = \omega_3 + \epsilon\delta_3, \qquad (3\text{-}64)$$

$$\omega_3 \neq \omega_1 + \omega_2,$$

but $\qquad \omega_{03} = \omega_{01} + \omega_{02}.$

The solution of the first order wave equation of Eq. (3-45) is assumed to be:

$$u = \sum_{n=1}^{3} A_n(t_s) \sin\left[\omega_{0n}t_f + \phi_n(t_s)\right] \sin k_{0n}x_f. \qquad (3\text{-}65)$$

for the standing wave in the resonator.

The A's and ϕ's are functions of slow variable t_s and can be determined by eliminating the secular terms in the second order equation of Eq. (3-46). The following is the result for a dissipationless resonator:

$$\frac{dA_3}{dt_s} + \sigma A_1 A_2 \omega_{03} \sin r = 0,$$

$$\frac{dA_1}{dt_s} - \sigma A_2 A_3 \omega_{01} \sin r = 0,$$

$$\frac{dA_2}{d\tau_s} - \sigma A_1 A_3 \omega_{02} \sin r = 0,$$

$$A_3 \frac{d\phi_3}{dt_s} + \delta_3 A_3 + \sigma A_1 A_2 \omega_{03} \cos r = 0, \qquad (3\text{-}66)$$

$$A_1 \frac{d\phi_1}{dt_s} + \delta_1 A_1 + \sigma A_2 A_3 \omega_{01} \cos r = 0,$$

$$A_2 \frac{d\phi_2}{dt_s} + \delta_2 A_2 + \sigma A_1 A_3 \omega_{02} \cos r = 0.$$

where all notations are defined as previously.
Eq. (3-66) indicates that the detuning factors δ's only
appear in the phase equation. According to the analysis in
Section 2, Chapter II, the effect of the detuning factors
δ's is to impose a limitation on the range of energy ex-
change among the modes.

For a dissipative resonator, we have to provide an
external source for compensating the losses. Suppose such
a source is supplying energy at one end of the resonator
by displacing the boundary at $x = 0$ with a particle velocity
of $U_0^\bullet \cos (\omega_{03} t)$. As the standing wave in a resonator is
the combination of forward and backward travelling waves,
the propagation of the particle velocity $U_0^\bullet$ by reflecting
back and forth inside the resonator will build up the ampli-
tude of a standing wave. If the frequency of the driving
source ω_{03} happens to be one of the resonance modes of the

resonator, for each round trip the travelling wave propa-
gates, the amplitude of the standing wave will increase by
$2U_0'$. In mathematical expression, we have:

$$\frac{\Delta A_3'}{\Delta T'} = \frac{2U_0'}{2\frac{L'}{c_0'}} \, , \qquad (3\text{-}67)$$

where L' is the length of the resonator, c_0' is the sound
speed and L'/c_0' corresponds to the time taken for a wave
travelling across the resonator.

If the frequency of the driving source is only near
the resonance mode of the resonator, then there will be some
phase shift for the standing wave during the building up
process. We can consider that the travelling wave contains
in-phase and out-phase components with respect to the origi-
nal standing wave. Fig. 3-4 is a vector diagram showing
such relations. The in-phase component increases the ampli-
tude for the resulting standing wave while out-phase compo-
nent shifts their phase relation. That is, for each round
trip,

$$\frac{\Delta A_3'}{\Delta T'} = \frac{2U_0'}{2\frac{L'}{c_0'}} \cos \phi_3' \, ,$$

$$(3\text{-}68)$$

$$\frac{\Delta \phi_3'}{\Delta T'} = - \frac{2 \, U_0'/A_3'}{2 \, L'/c_0'} \sin \phi_3' \, .$$
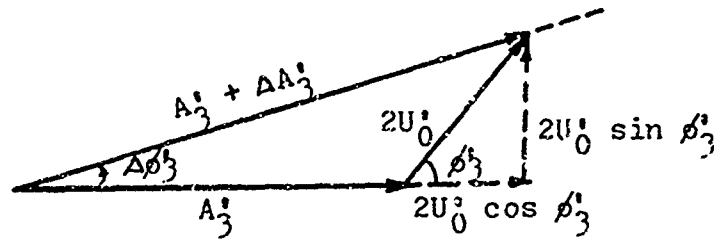
Fig. 3-4 Build up the Standing
Wave in the Resonator

By changing to the nondimensional notation in slow
time scale, we can incorporate the relation in Eq. (3-68)
into Eq. (3-66) to describe the response of the forcing
excitation of subharmonic modes in a dissipative resonator.
The results are:

$$\frac{dA_3}{dt_s} + \eta_3 A_3 + \sigma A_1 A_2 \omega_{03} \sin r - GU_0 \cos \phi_3 = 0.$$

$$\frac{dA_1}{dt_s} + \eta_1 A_1 - \sigma A_2 A_3 \omega_{01} \sin r = 0,$$

$$\frac{dA_2}{dt_s} + \eta_2 A_2 - \sigma A_1 A_3 \omega_{02} \sin r = 0,$$

$$A_3 \frac{d\phi_3}{dt_s} + \delta_3 A_3 + \sigma A_1 A_2 \omega_{03} \cos r + GU_0 \sin \phi_3 = 0,$$

$$A_1 \frac{d\phi_1}{dt_s} + \delta_1 A_1 + \sigma A_2 A_3 \omega_{01} \cos r = 0,$$

$$A_2 \frac{d\phi_2}{dt_s} + \delta_2 A_2 + \sigma A_1 A_3 \omega_{02} \cos r = 0, \qquad (3\text{-}69)$$

where
$$G = \frac{\omega_r c_0'}{L} .$$

For steady state, when the intensity of waves in the resonator is not strong enough to cause the nonlinear effect ($\sigma = 0$), the amplitude of the standing wave in the resonator can be deduced from Eq. (3-69),

$$A_3 = \frac{GU_0}{\sqrt{\eta_3^2 + \delta_3^2}} ,$$

$$A_1 = 0,$$

$$A_2 = 0. \qquad (3\text{-}70)$$

For a strong external exitation, the coupling caused by the nonlinearity of medium will result in a different set of steady-state amplitudes of modes in the resonator:

$$A_3^2 = \frac{(\eta_1 \eta_2 + \delta_2 \delta_2)}{\sigma^2 \omega_{01} \omega_{02}} ,$$

$$A_1^2 = \eta_2 a,$$

and
$$A_2^2 = \bar{\eta}_1 a,$$

where $\quad a = \frac{1}{\sigma^2 \omega_{01} \omega_{02}} \left\{ \left[(\eta_3 - \delta_3 \Delta)^2 + (1 + \Delta^2) \right. \right.$

$$x\left(\frac{G^2 U_0 \sigma^2 \omega_{01}\omega_{02}}{\eta_1 \eta_1 (1 + \Delta^2)} - \eta_3^2 - \delta_3^2\right)^{\frac{1}{2}} - (\eta_3 - \delta_3\Delta)\Bigg\} , \qquad (3-71)$$

$$\Delta = \frac{\delta_1}{\eta_1} = \frac{\delta_2}{\eta_2} = \frac{\delta_1 + \delta_2}{\eta_1 + \eta_2} .$$

Since amplitudes are real quantities, a minimum value of U_0 is required for A_1 and A_2 to appear. That threshold for subharmonic generation is given by:

$$U_{TH}^2 = \frac{\eta_1 \eta_2 (\eta_3^2 + \delta_3^2)(1 + \Delta^2)}{G^2 \sigma^2 \omega_{01}\omega_{02}} . \qquad (3-72)$$

As the threshold is inversely proportional to the square root of the product of subharmonic frequency pairs, it will be a minimum when they are equal ($\omega_{01} = \omega_{02}$).

In general, only the acoustic pressure is accessible for actual measurement. If ω_{03} component is taken as a reference for monitoring the occurrence of subharmonics, we can modify A_3 in Eq. (3-71) in term of pressure and express it as a function of the original parameters as:

$$P_{3TH} = \frac{8 \rho_0' c'^2_0}{1 + \frac{\Gamma' \rho_0'}{c'^2_0}} \left(\frac{1}{Q_1'} \frac{1}{Q_2} + \frac{\delta_1'}{\omega_{01}'} \frac{\delta_2'}{\omega_{02}'}\right)^{\frac{1}{2}} \qquad (3-73)$$

where Q_1, and Q_2 are the quality factor associated with modes ω_1', and ω_2' respectively.

Chapter IV

EXPERIMENTAL INVESTIGATION ON SUBHARMONIC GENERATION

IN AN ACOUSTIC RESONATOR

In this chapter, we describe the experimental set up,
procedure and results of an investigation on subharmonic
generation in an acoustic resonator.

The acoustic resonator used in this experiment is con-
structed in the form of an interferometer with two quartz
crystals as the resonator boundaries. One of the crystals
is also used as a transmitting transducer to supply the
driving signal into the resonator and the other serves as a
detector in monitoring the response of the system. A cali-
brated acoustic probe smaller than the acoustic wavelength
of the signal in the medium has been employed for absolute
acoustic pressure measurements during the experimental inves-
tigation.

Throughout the entire experiment, distilled water has
served as a medium. It has been filtered and degassed
before use. The whole acoustic resonator is enclosed in a
sealed container so that contamination of water during the
experimental process can be reduced to a minimum.

The experimental system can be operated in the frequen-
cy range from 1 MHZ to 5 MHZ, although detailed studies in
observing subharmonics are only carried out around the re-

gion of 1.5 MHZ, which is the natural resonance frequency of
the transmitting quartz crystal. As the validity of using
the acoustic probe is limited in measuring of absolute
acoustic pressures at high frequency, the subharmonic pheno-
menon is only considered for qualitative reference when the
crystal is driven around 4.5 MHZ, the third harmonic of its
natural frequency.

Data concerned with actual modes of the resonator, the
loss factor associated with each mode, and the signal thresh-
old for exciting subharmonics at various resonator lengths
and at different signal frequencies are recorded. Such 'rfor-
mation has been compared with the theoretical analysis dis-
cussed in the previous chapters.

1. Conditions for the Experimental Investigation of Sub-
   harmonic Generation

According to the previous analysis, there are two
necessary conditions for subharmonics to be excited. One
is that the system should contain the subharmonic modes and
the other is that the high intensity acoustic wave should be
built up to provide the necessary nonlinear coupling mech-
anism.

With this consideration, an interferometer type reso-
nator is adopted for our experimental investigation of sub-
harmonic generation. In general, the interferometer pos-

sesses many resonance modes. If one such resonance mode is excited by a external source, a high intensity standing wave can easily be achieved. Any modes whose frequencies are below the external driving signal can ther be considered subharmonic modes. Another advantage for using an interferometer as a resonator is that the end reflectors can be utilized as transducers to provide a means of supplying the driving signal or detecting the system's response. Since there is no side boundary to enclose the interferometer, only one type of mode exists in such a resonator. In the case that the wavelength of the acoustic wave in the medium is much smaller than the dimension of the end reflectors, the interferometer will act almost as a one-dimensional resonator.

The design of interferometer depends very much on its operating frequency. Most interferometers used for experimental observation of subharmonics are in the frequency range 3 MHZ to 5 MHZ[16,17,18,19,38]. The advantage of applying high frequency signal for subharmonic generation is that the threshold for exciting subharmonics is lower according to the inverse relation between the signal frequency and the threshold derived in our previous analysis, Eq. (3-60) Chapter III. An additional reason for working in this frequency range is that a ham radio transmitter can be easily modified for the driving signal power source. But there are some disadvantages to using high frequency signals. The

important one is that the absolute instantaneous acoustic pressure will be difficult to measure without causing scattering effects. (The wavelength in that frequency range will be less than 0.03 cm in water.) The laser beam diffraction method, employed by previous experimenters as a means of detecting the acoustic wave, does not directly give the absolute acoustic pressure and it involves elaborate equipment and alignment. A second handicap for driving the interferometer at high frequencies is that a thinner quartz crystal plate has to be used for the transmitting transducer. This presents the difficulty of mounting the crystal for direct coupling with the medium. A common practice is to cement the crystal on a metal plate for making a composite transducer[39]. Our preliminary tests of such an arrangement shows that when an intense signal is applied to the composite transducer, the cement between crystal and metal plate seems to change its adhesive force, and a nonlinear response begins to appear. In some cases, even subharmonics are presented. They are very stable and can not be affected by just changing the length of the interferometer.

Surveying the current literatures, we found that it is possible to make an acoustic probe of size about 0.03 cm[40,41]. This corresponds to the wavelength of a 5 MHZ acoustic wave in water. Then the proper highest frequency that should be used without causing seriously scattering effects will be

around 1.5 MHZ, which requires a 0.19 cm thick quartz plate
for the transmitting transducer in the interferometer.
Quartz of such thickness is strong enough to be used as the
reflecting wall in the interferometer. This solves the prob-
lem by avoiding the complication of using a composite trans-
ducer. A much lower frequency quartz is chosen for the
other reflecting wall of the interferometer for two reasons:
first, it will have better sensitivity in detecting the sub-
harmonic components; second, its thickness will allow for a
knife edge mounting for the crystal, thereby reducing me-
chanic losses.

In our first pilot interferometer composed of 1.5 MHZ
and 600 KHZ quartz crystal plates as the reflecting walls of
the interferometer, the Q (quality factor) of such a reso-
nator measured during preliminary test was about 10^3. Ac-
cording to the relation derived in Chapter III, Eq. (3-73),
an acoustic pressure amplitude of at least 15 bars is needed
for exciting subharmonics for this Q.

An acoustic standing wave with this intensity will also
cause cavitation in ordinary water[42]. To avoid the compli-
cation of the cavitation phenomenon during the observation
of subharmonics, we decided to process the liquid before
using it in the interferometer. The threshold for cavitation
will increase after the liquid has been purified through a
degassing and filtering process. Hence, the subharmonic

threshold will be less than the cavitation threshold.

We also designed a system to enclose the interferometer
so that the treated liquid would not be subsequently contami-
nated. This involves the elaborate construction of a sealed
system. As we do not find that previous experimenters speci-
fied how they have treated the liquid used in their investi-
gation of subharmonics, we hoped that our effort to make the
whole test system a closed one would provide some new and
interesting information.

There are other advantages to using a low driving
signal frequency in the resonator. Since the wavelength of
acoustic wave in the water is longer, the mechanical align-
ment for parallelism of the two reflecting plates is easier
and there are less appreciable detuning drifts due to temper-
ature changes in the interferometer.

Based on the above considerations, our final design
of the test system for observing subharmonic generation
phenomena possesses the following special features:

(a)   The acoustic transducers which also serve as
reflecting walls for the interferometer are directly coupled
to the medium in the resonator.

(b)   The medium used in the resonator has been care-
fully filtered and degassed to a high purity. Cavitation is
avoided in the range of tests used for observing the subhar-
monic phenomenon.

(c)   An acoustic probe smaller than half a wavelength
of the acoustic wave in water can be calibrated for record-
ing the instantaneous acoustic pressure.

(d)   The system can be operated in a pulsed mode
for studying the translent behavior of subharmonic genera-
tion.

Fig. 4-1 is the block diagram of whole testing system.
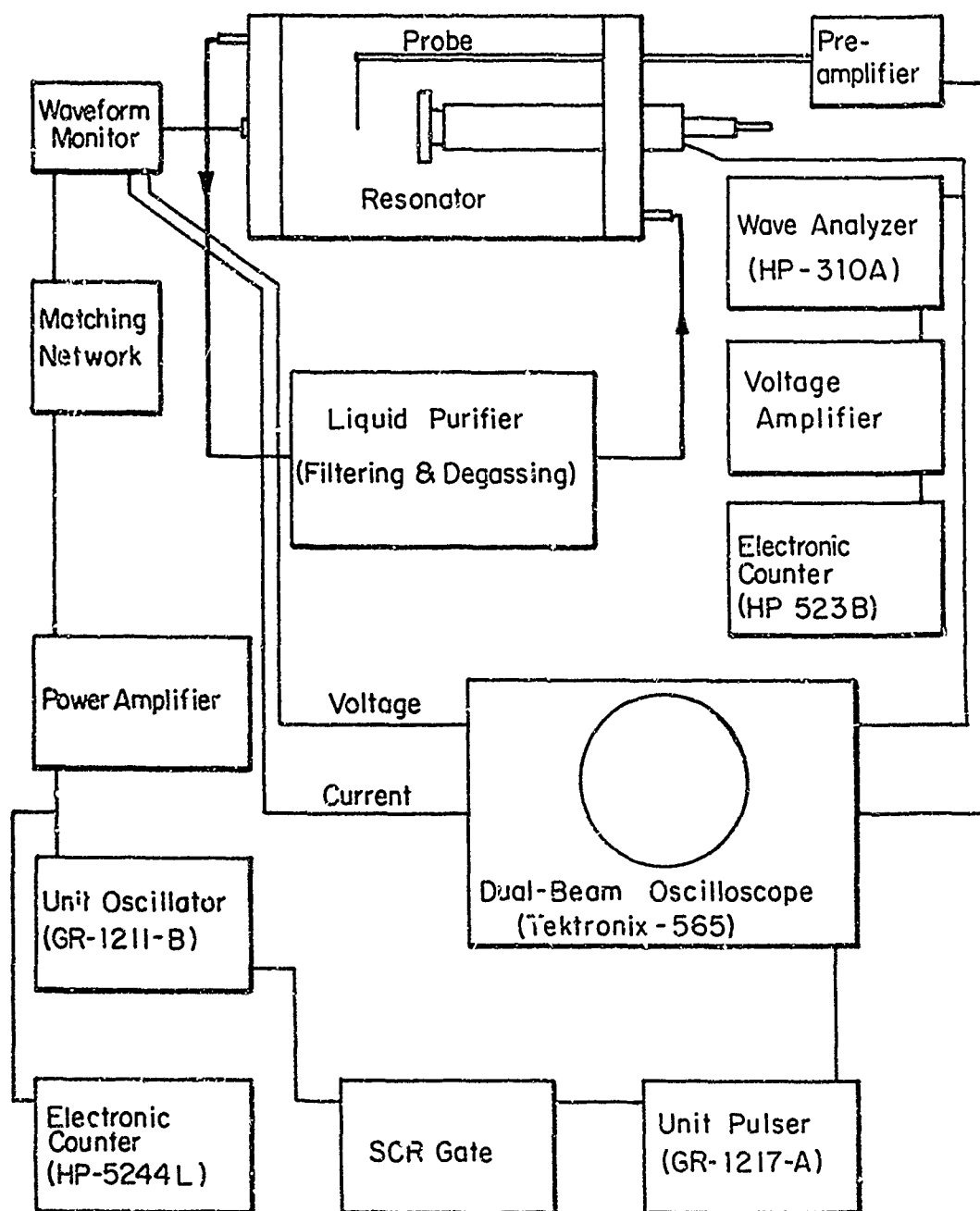In next section, each component will be described in detail.

FIG. 4-1 BLOCK DIAGRAM FOR EXPERIMENTAL INVESTIGATION
OF SUBHARMONICS

2. Apparatus

The actual apparatus used in this experiment for the investigation of subharmonic generation can be seen in the photograph of Fig. 4-2. According to function, we can divide the apparatus into three subsystems: resonator, the liquid purification equipment, and electronic instruments. Some items are adopted from available commercial products but most equipment is designed and constructed only for our special purpose in this experiment. Each subsystem's function and construction is described below:

(a) The Resonator

The construction of the resonator is shown by the sketch in Fig. 4-3. It mainly contains an interferometer with two x-cut quartz crystal plates as its boundary walls. The space between these two walls can be adjusted from 0 to 13 cm. The fine adjustment is controlled by a micrometer which only can cover a range of 2.5000 cm. An additional coarse adjustment is provided for larger space changes.

One of the quartz plates, which we use as a transmitting transducer to supply the acoustic signal to the resonator, is a disc of 2.54 cm in diameter and 0.19 cm in thickness whose natural resonance frequency in air is 1.5 MHZ. One side of this disc is plated with gold on chrome and the other side is plated with the same material but is left with a 0.0625 cm wide blank annulus on the edge. This disc
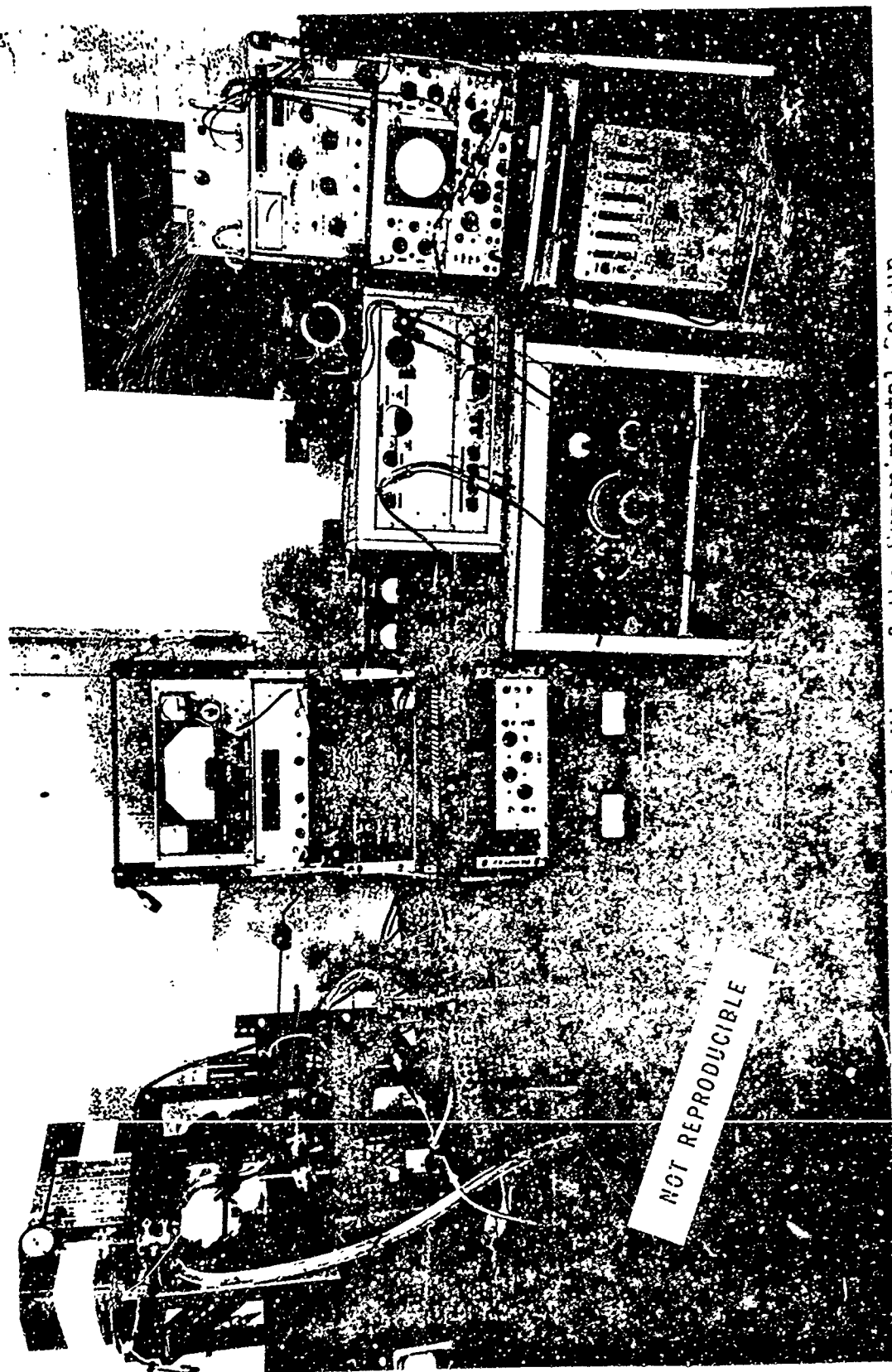
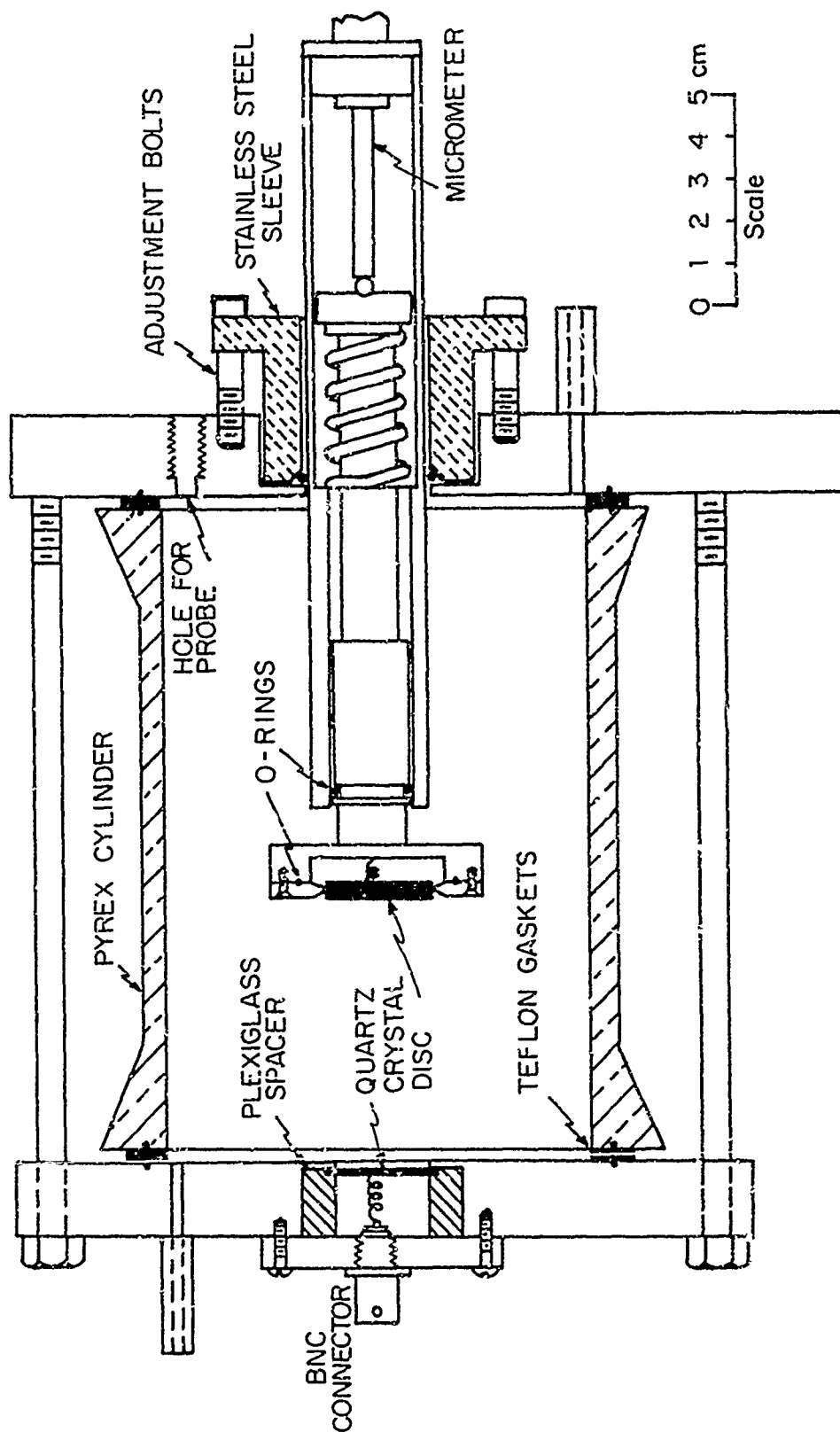Fig. 4-2 Photographic View of the Experimental Set-up

FIG. 4-3 THE RESONATOR

ADJUSTMENT BOLTS

STAINLESS STEEL SLEEVE

MICROMETER

HOLE FOR PROBE

O-RINGS

PYREX CYLINDER

PLEXIGLASS SPACER

QUARTZ CRYSTAL DISC

TEFLON GASKETS

BNC CONNECTOR

Scale

0 1 2 3 4 5 cm

is mounted on a brass housing with an open hole of 2.2 cm in diameter so that the large part of the plated surface will be in direct contact with the liquid in the resonator. A plexglass ring is used on the other side of the quartz disc for pressing it against the brass housing. Silicon grease is applied around the edge of the quartz disc before instal- lation so that there is a good seal between disc and brass housing to prevent a leak. Electrical contact with the back face of the quartz disc is made with a soft spring which is soldered to a BNC connector. During operation, the signal is introduced through the BNC connector and the brass housing and the front surface of the quartz disc are at ground poten- tial.

A much thicker quartz disc is used for the other boundary wall of the interferometer and acts as a detector for the system's response. This disc also has a diameter of 2.54 cm and is clamped on the knife edge of a brass ring which can be mounted on an another brass housing. Between the knife edge and the circumference of the quartz disc, stycast 2850 FT (manufactured by Emerson and Cuming, Inc.) is used to avoid possible leakage. One side of this unit is vacuum deposited with silver as the front surface of the boundary wall. The other side of the quartz disc is plated with gold on chrome and touches a soft spring which serves as one of the electrodes after this unit is mounted on a

brass housing. An O ring is inserted between the brass
housing and the detecting quartz unit for leakage prevention.
We have made several such units with various natural reso-
nance frequency quartz discs: 1 MHZ, 600 KHZ, and 360 KHZ.
They are easily interchangeable. The housing of the de-
tecting unit is a part of a brass telescope which has a mi-
crometer to adjust its length.

Both transmitting transducer and detecting unit are
mounted separately on 2 cm thick brass plates. A pyrex
cylinder, 10 cm inside diameter and 15 cm in length, with
two teflon gaskets is inserted between these two brass
plates to form a container. The whole unit is fixed on a
steel frame. There are three adjustment bolts for the
alignment of the parallelism between the transmitting
transducer and the detecting unit. An inlet and an outlet
are provided for this container for filling and circulating
the liquid. Fig. 4-4 is the photographical close view of
the actual arrangement.

An acoustic probe is also placed inside the pyrex con-
tainer for absolute acoustic pressure measurement. The
active tip of this probe is about 0.05 cm in diameter and
has a microdot connector on its end   (Microdot Inc., part
No. 032 0015 0001). This unit is then attached to a 0.5 cm
diameter brass tubing going through the mounting plate with
an O ring as a sealing element. The probe tip is detachable;
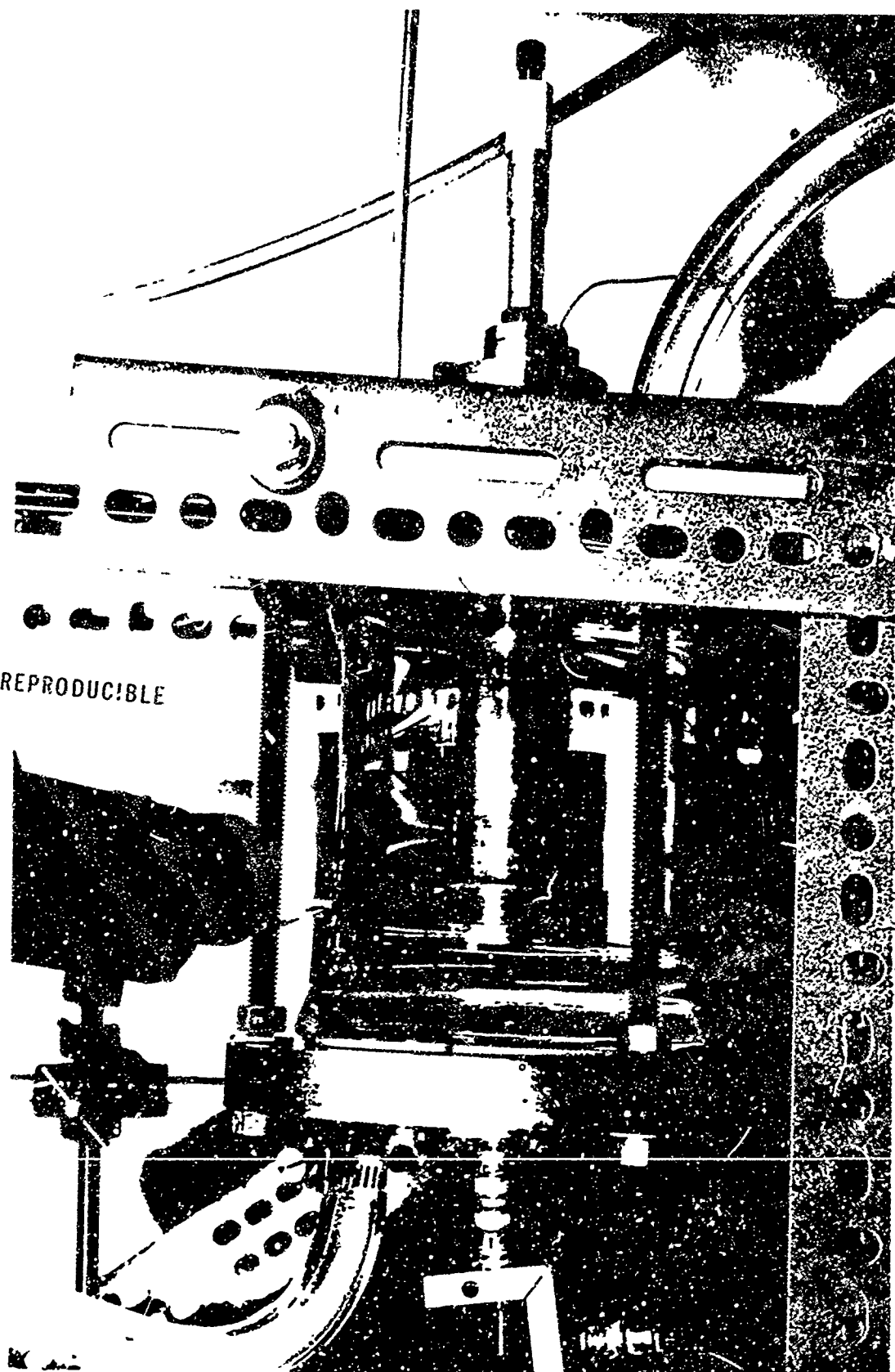
NOT REPRODUCIBLE

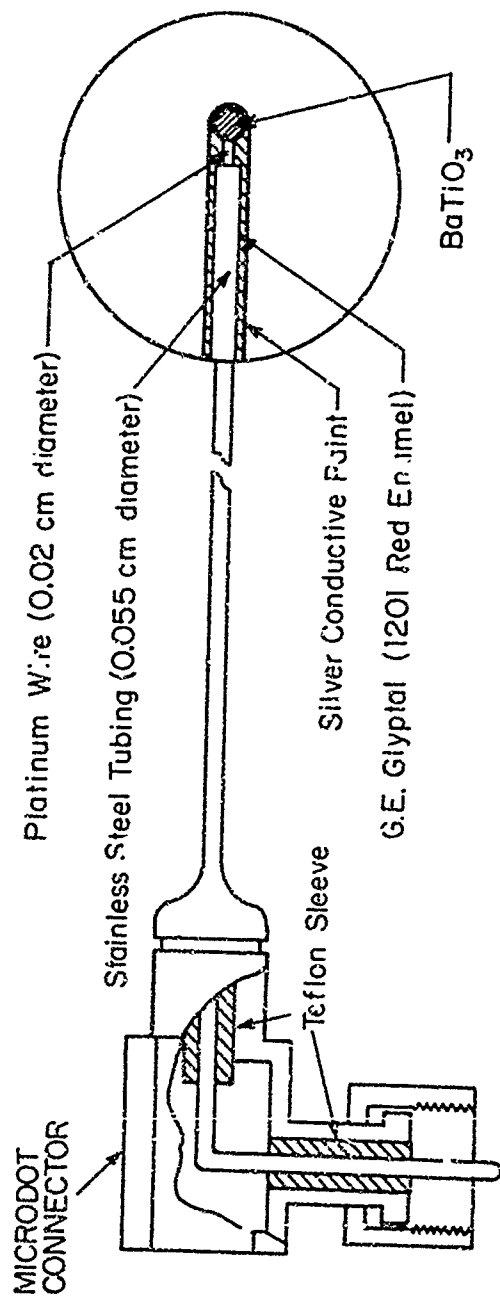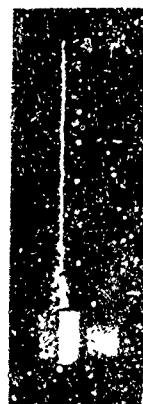Platinum Wire (0.02 cm diameter)

Stainless Steel Tubing (0.055 cm diameter)

Silver Conductive Paint

Teflon Sleeve

G.E. Glyptal (1201 Red Enamel)

MICRODOT CONNECTOR

$BaTiO_3$

(a)

CENTIMETERS

0 1 2 3 4 5

(b)

FIG. 4-5 THE ACOUSTIC PROBE

j

the picture in Fig. 4-5b shows its actual size.

The construction of the acoustic probe is shown in the detailed sketch in Fig. 4-5a. The tip is $BaTiO_3$ powder melted on a 0.02 cm diameter platinum wire by a microflame torch (manufactured by Microflame Inc.). The main frame of the probe is 0.055 cm diameter stainless tubing covered with a layer of C.E. Glyptal (1201 Red Enamel). The external surface of the probe's main frame is coated with E-Kote 40 silver paint (manufactured by Epoxy Products Co.) to serve as an electrode for the probe. The $BaTiO_3$ tip is polarized with 30 V DC at $130^{O}C$.

The sensitivity of such a probe with the preamplifier is about 23 mV per bar. The calibration procedure for the probe will be described later.

(b) The Liquid Purification Equipment

To control the purity of the liquid under experimental investigation, the container with its interferometer is connected through Tygon Vacuum Tubing, 3/8" in inside diameter (made by Norton Plastics and Synthetics Division), to the accessories for the liquid cleaning process. Fig. 4-6 shows the detailed arrangement.

Two Millipore Filters (manufactured by Millipore Filter Co.) of 5.0 micron pore size are used in the cleaning system. One is for trapping the contaminant before the liquid gets into the system the other is inserted in the

Platinum Wire (0.02 cm diameter)

Stainless Steel Tubing (0.055 cm diameter)

Silver Conductive Paint

G.E. Glyptal (1201 Red Enamel)

BaTiO₃

Teflon Sleeve

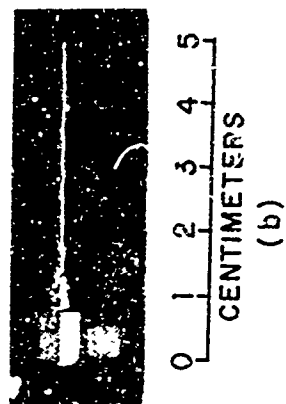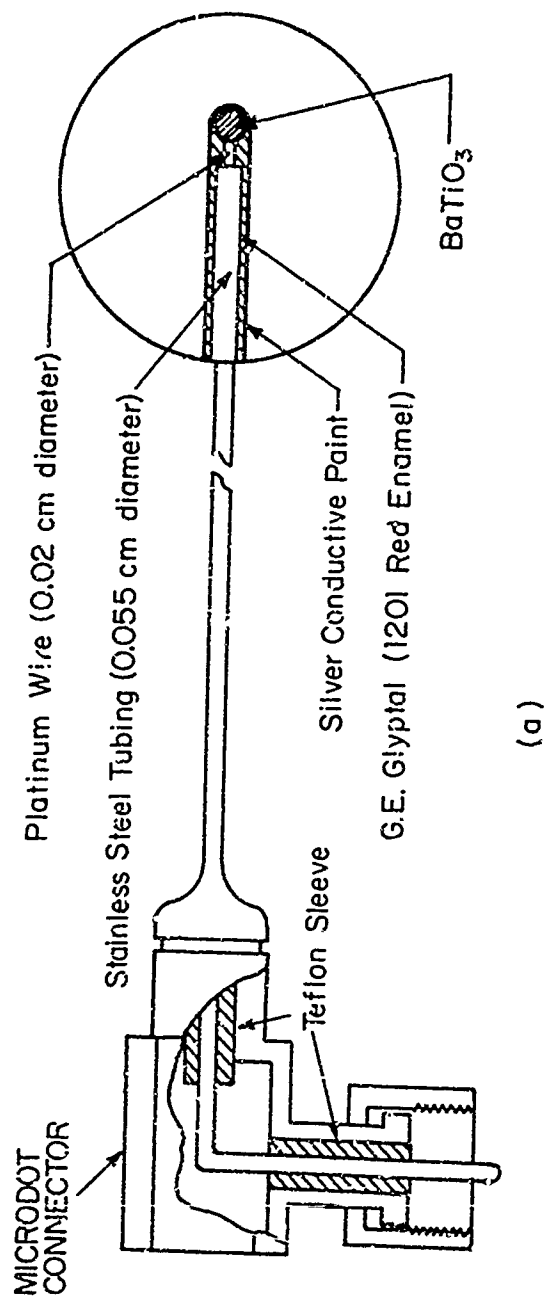MICRODOT CONNECTOR

(a)

CENTIMETERS
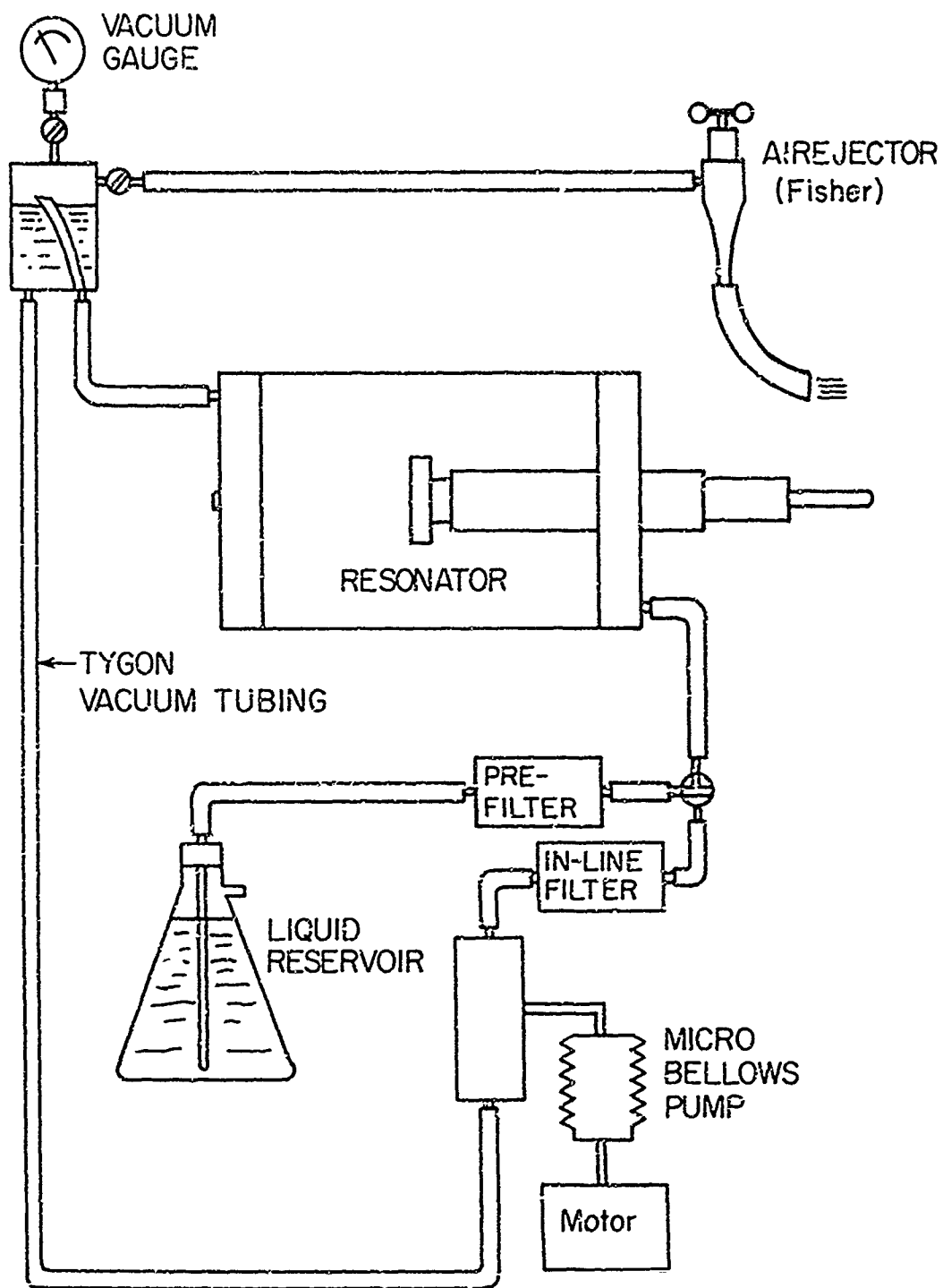(b)

FIG. 4-5 THE ACOUSTIC PROBE

FIG. 4-6 ARRANGEMENT AND EQUIPMENT FOR
FILTERING AND DEGASSING

system for closed-loop filtering.

A Fisher Airejector is adopted as a vacuum pump for degassing the liquid in the system. Such a simple arrangement can easily reach a vacuum less than 30 mm Hg. The vacuum is monitored by a pressure gauge (made by Marshalltown MFG. Co.).

Circulation of the liquid around the system is provided by a micro-bellows pump (manufactured by Research Appliance Co. serial No. 619616 4648). During the actual experimental investigation of subharmonics, the operation of the pump is stopped in order to avoid the possible interference caused by the vibration.

(c) Electronic Instruments

We have two signal generators for use as the signal sources in this experiment. The General Radio 1001-A, which covers a range from 5 KHZ to 50 MHZ, is used to check the resonance modes of the interferometer. The other, General Radio 1211-B Unit Oscillator, mainly serves as the signal input to the power amplifier for the transmitting transducer. This oscillator can be modulated by an external source through its power supply. We have built a SCR gate in conjunction with a General Radio Unit Pulser 1217-A to modify it as a pulsed signal generator. The transient behavior of subharmonic generation in the interferometer can be studied by such conversion.

The power amplifier was originally designed and constructed by Barger[42] for his research work on acoustic cavitation. This amplifier can be driven to 400 watts output with a 1 V rms input signal and has the half power points at 12 KHZ and 1.5 MHZ. We find it quite suitable for driving the quartz transducer of the interferometer at a high impedance level. A General Radio Variable Inductor type 107-J is used to tune out the stray capacity in its output circuit.

During preliminary studies on subharmonic generation phenomenon, we have employed a Lysco 600-S ham transmitter as a power source. The output stage of this transmitter is a beam power pentode 807 which can deliver maximum power up to 50 watts. A regulated power supply, Lamda model 71, is used as the plate voltage supply for the pentode to adjust the output level. A matched network has to be inserted between the transmitter and the quartz transducer to obtain optimal results. This arrangement was solely for qualitative studies of subharmonics when the quartz transducer is operated around its third harmonic, 4.5 MHZ.

During the experimental investigation, the frequency of the driving signal is checked by a Hewlett-Parkard 5244L Electronic Counter.

For parallelism alignment of the interferometer, the signal is provided by a Hewlett-Parkard type 161 Pulse Gener-

ator. The alignment procedure will be described later.

There are two separate channels for detecting the re-
sponse of the system. The acoustic probe is mainly for
absolute acoustic pressure measurement. It has a self con-
tained battery operated preamplifier for eliminating ground-
ing and noise problems. Fig. 4-7 shows its circuitry which
has about 50 dB gain. The output of this preamplifier can
be fed directly to the scope to display the waveform.

Another channel is provided by the quartz disc wall in
the interferometer. Since this detector has high sensitivity
to the subharmonics, its output is directly connected to a
scope, Tektronix type 565 Dual-Beam Oscillascope, and a wave
analyzer, Hewlett-Parkard model 310A. The wave analyzer
also serves as a filter for picking up the particular subhar-
monic component. The frequency of this subharmonic is then
measured by an another electronic counter, Hewlett-Parkard
model 523B.

Voltage and current probes, both manufactured by
Tektronix, are employed to monitor the output waveform of
the power amplifier so that we can be sure that no distorted
signal drives the transmitting transducer during experimental
investigations.

3. Experimental Procedure

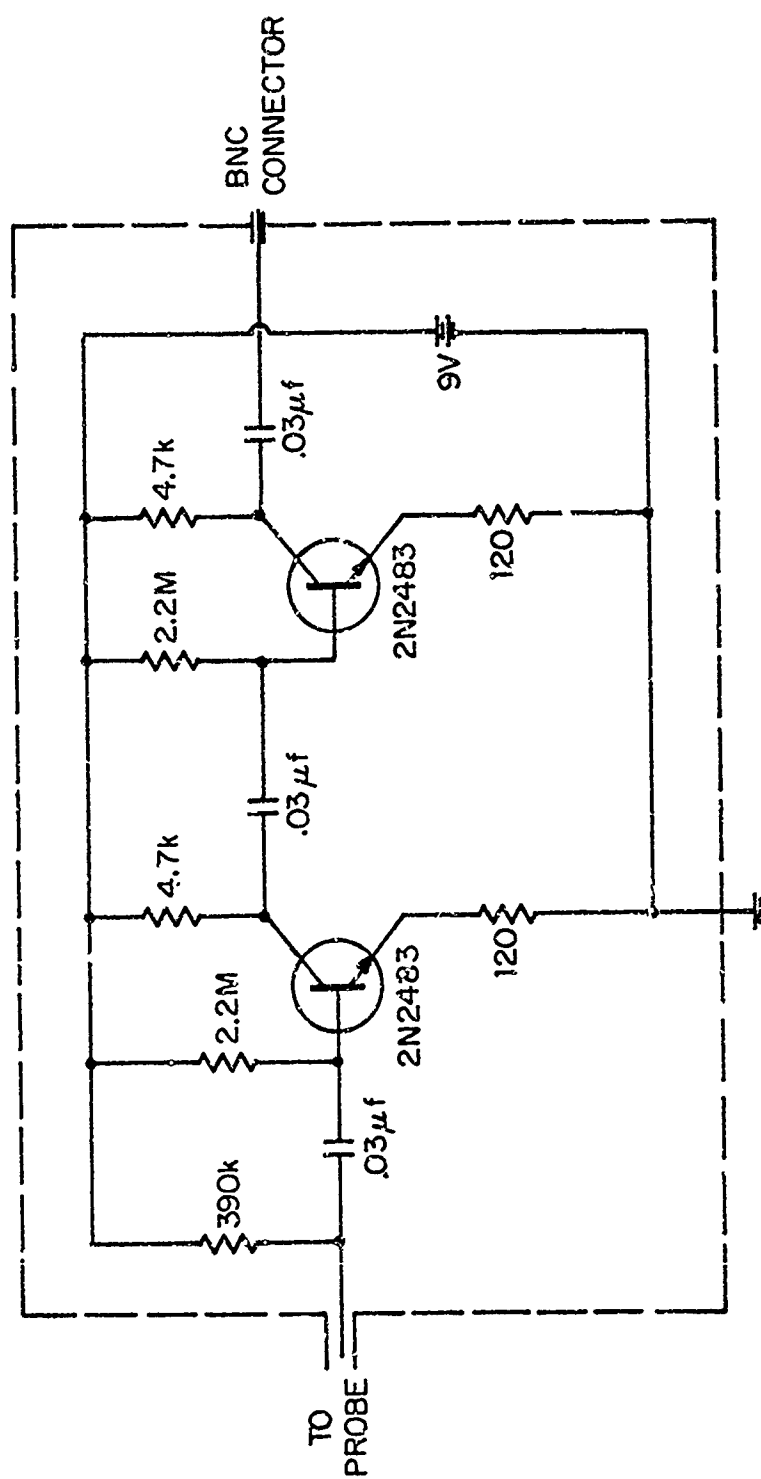In investigating the subharmonic generation phenomenon,

FIG. 4-7 PROBE PREAMPLIFIER

quantitative measurements can be made of two important pa-
rameters: the driving signal threshold for exciting the sub-
harmonics and the frequency components of the excited sub-
harmonics. These parameters depend on the physical property
of the medium as we have concluded in the previous analysis.
However, in the actual experimental situation, the results
are also effected by the way the system is set up. We will
mention some of our experiences during preliminary test
in the early experimental stage before describing the actual
procedure we finally adopted for data collection.

Without any treatment of the water used in the reso-
nator, we found it was almost impossible to excite subhar-
monics with some air bubbles attached to the face of the
boundary walls of the interferometer. However, even after
those bubbles are removed, either externally or by self
dissolution, the excited subharmonics appear to be very un-
stable. Further increases in the driving signal intensity
only seem to extinguish the existence of subharmonics. This
peculiar phenomenon was finally explained when we discovered
that gaseous cavitation was occurring along the path of the
acoustic standing wave in the interferometer. Tiny gas
bubbles, which can be observed by shining collimated light
on them, are dancing around. Sometimes they aggregate to-
gether to become a larger bubble and then move away by
buoyancy forces. Such activities, we believe, will absorb

more acoustic energy and interfere with the resonance modes
of the interferometer so that the threshold of exciting sub-
harmonics is increased, makes the sustenance of subharmonics
more difficult. In the low frequency range, the threshold
for acoustic cavitation is lower than the subharmonic thresh-
old and therefore the observation of subharmonics becomes
more difficult. Hence we reached the conclusion that we
should control the water used in the experiment to avoid the
interfering effects of gaseous cavitation.

Because the energy of the intense acoustic wave is
absorbed in the resonator, we have observed that subharmonics
become unstable due to temperature changes during a long
period of operation. A $2^{o}C$ change in temperature has be re-
corded after about 5 hours continual operation. We have
overcome this problem by using pulsed signals to reduce the
heat generated in the water.

Our initial experience with the instruments has re-
vealed some misleading data from the quantitative measure-
ments. One of them is that the quartz disc serving as the
boundary wall of the interferometer can only be used as a
detector for the system's response. This is a very conven-
ient way to monitor subharmonic phenomena but, as the re-
sponse of the particular quartz disc is frequency dependent,
it is not a proper way to take quantitative data. A
similar situation also applies to the transmitting trans-

ducer. The acoustic intensity inside the interferometer is not necessarily proportional to the voltage across the quartz plate but depends on other factors such as alignment and tuning of the interferometer, separation of two boundary walls, the natural resonance frequency of the quartz disc, the condition of radiative beam spreading, and losses due to the viscosity of the liquid, etc. This is true even when different quartz crystal discs are used with the different driving signal frequencies, since their thickness and condition for mounting are changed. The mounting loss plays an important role in the final intensity of an acoustic wave in the resonator. It becomes totally improper to relate a set of applied voltages on the quartz discs to the true acoustic intensity in the interferometer. For this reason, we developed a small acoustic probe for absolute pressure measurement.

Alignment of the two boundary walls of the interferometer is very critical for investigating the subharmonic phenomenon. The threshold for exciting subharmonics and the frequency components of the excited subharmonics will be altered greatly just by manipulating the parallelism of two boundary walls. In order to obtain consistent experimental results, we set up a standard alignment procedure, which will be described later, before collecting the data.

The following is a detailed description of the experi-

mental procedure we have adopted:

(a) Calibration of The Acoustic Probe

The acoustic probe is primarily designed for use at high frequencies. Since measurements of input current to the transducer at this frequency range is not very accurate, the reciprocity method for calibration becomes unsuitable under present conditions. A simple method is adopted from the current literature[41].

In studying the propagation of a finite-amplitude wave in a liquid, one of the established results is that a sinusoidal wave at the source of radiation will become a sawtooth at some distance away from the source. This distance can be expressed in terms of wave parameters and properties of the medium by the relation:

$$l = \frac{\lambda \rho c^3}{\pi(\gamma + 1)p} , \qquad (4\text{-}1)$$

where λ is the wavelength, ρ is the density of the liquid, c is the sound speed, p is the pressure amplitude of the acoustic wave, and γ is the nonlinear parameter of the liquid (about 6.5 for water). In the case of spherical wave divergence in the far field region, the variation of the amplitude of the formed sawtooth wave with the distance from the source is determined by the equation:

$$p_x = \frac{p_o}{1 + \frac{x_o(\gamma+1)p_o f}{\rho c^3} \ln \frac{x}{x_o}} \frac{x_o}{x} \quad , \qquad (4\text{-}2)$$

where f is the frequency, and p_o and p_x are the amplitudes of the sawtooth at distances x_o and x from the source respectively. This relation can be rewritten in the form of ratios p_o/p_x, and x_o/x to obtain the absolute pressure amplitude p_o as:

$$p_o = (\frac{p_o x_o}{p_x x} - 1) \frac{\rho c^3}{(\gamma+1)f x_o \ln \frac{x}{x_o}} \quad . \qquad (4\text{-}3)$$

Once the pressure is known, we can easily compute the sensitivity of the acoustic probe from its electrical output signal.

The calibration of the probe used in this experiment is carried out in an anechoic tank which has the dimensions 75 cm wide, 125 cm long, and 75 cm in depth. A 0.254 cm thick PZT-4 disc of 2 cm in diameter (manufactured by Clevite Co.) is used for the transmitting transducer. The resonance frequency of this disc is about 760 KHZ. For calibrating the probe at high frequencies, we used the second harmonic component of the distorted wave as the reference. With the preamplifier, the sensitivity of the probe around 1.534 MHZ is 23 mv/bar.

(b) Treatment of Water

The arrangement and equipment for the treatment of water used for the experimental investigation is shown in Fig. 4-6. The container is first evacuated partially by the Airejector so that the water can be sucked in through the inlet filter. After the water has completely filled up the system, we then shut off the inlet and at same time close the system by proper turning of a three way valve. The water can be continually filtered through the in-line filter by the forced circulation due to the micro-bellows pump.

The degassing process is done after the water has gone through the filter several times. A 30 mm Hg is generally reached during the final stage of degassing. Then we open up the relief valve for the system and the hydrostatic pressure in the container returns to atmospheric.

This process is repeated at the beginning of each measurement and at the beginning of each day so we can be sure that no further contamination, possibly caused by corrosion and leakage of the components, will deteriorate the system.

During the experiment, we stop the circulating pump to avoid possible interference from vibration. A focused beam of light from a 100-watt projector lamp is used to aid in

the visual detection of possible gas bubbles in the inter-
ferometer. With this arrangement, we are able to ob-
serve subharmonics at 1.5 MHZ without the occurrence of cavi-
tation.

(c) Alignment of The Interferometer

The arrangement for alignment of the interferometer is
shown in Fig. 4-8a. The transmitting transducer is ener-
gized by a 10 microsecond, 50 volts DC pulse. This pulse
will excite the quartz disc in the transducer and an acoustic
wave will radiate out into the water inside the interfero-
meter. The pulsed wave will be picked up again by the trans-
mitting transducer after it has reflected back from the
other boundary wall of the interferometer. This reflected
signal can be detected with a tuned tank connected to the
transmitting transducer and displayed on the oscilloscope.
If the repetition rate of the DC pulse is slow compared to
the time required for wave traversal across the interfero-
meter, the successive reflected pulsed signals will also be
detected by the scope. By monitoring the amplitudes of those
reflected pulses, we can align the reflected wall of the
interferometer with its adjusting screws. The best alignment
for the parallelism of the boundary walls is obtained when
the amplitudes of pulsed signals become a maximum and de-
crease exponentially according to the time sequence of their
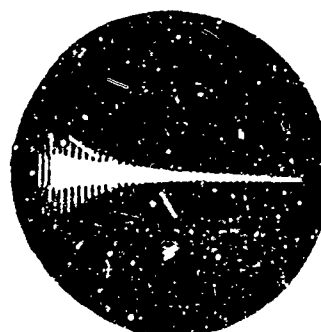arrival. This alignment proceduce is not affected by the
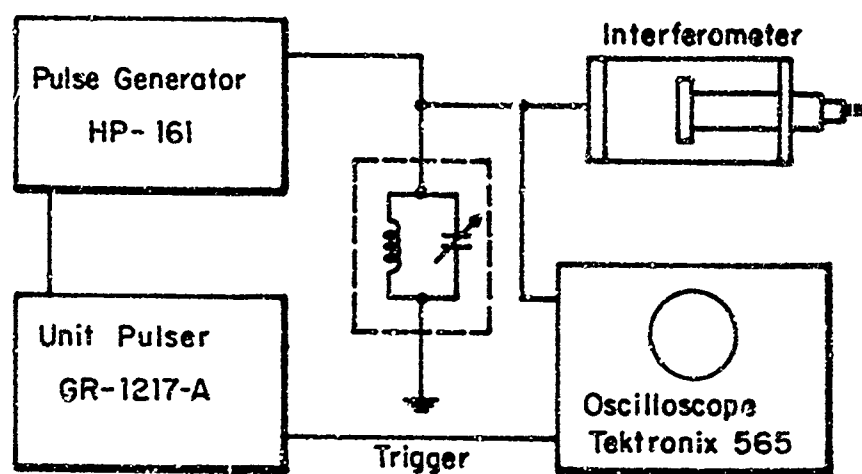
(a) ALIGNMENT SET-UP
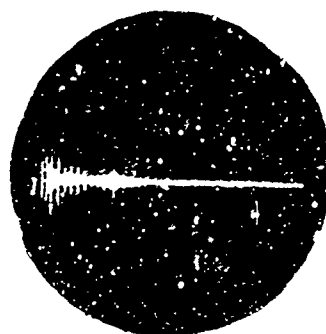
Misalignment   Alignment

(b) OSCILLOSCOPE DISPLAY

FIG. 4-8   ALIGNMENT OF THE INTERFEROMETER

length of the interferometer. A typical picture of the response signal on the oscilloscope is shown by Fig. 4-8b after the interferometer has been aligned. The decrease in the amplitudes of the successive pulses also gives the information about the quality factor (Q) of the resonator at the given resonance frequency.

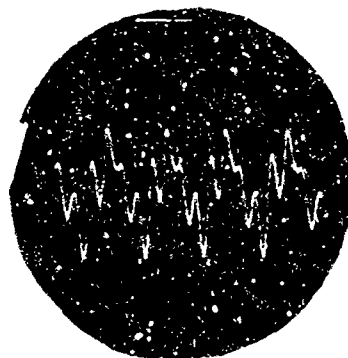(d) Excitation of Subharmonics

A strong standing wave can be established when we drive the interferometer at one of its resonance modes. This is accomplished by adjusting the length of the interferometer with the micrometer for a given input signal or changing the signal frequency for a fixed length interferometer. By increasing the signal input to the transmitting transducer of the interferometer, subharmonics may be observed from the response of the detecting quartz disc after the intensity of the acoustic wave inside the interferometer exceeds a certain level. A typical response of such subharmonic generation in the time domain is displayed in Fig. 4-9a from the picture taken on the oscilloscope. The frequency components of such signals can be further analyzed through the wave analyzer; the exact frequency is read from the electronic counter. The meter on the wave analyzer also records the relative intensity of the particular subharmonic component.

The frequency range of the wave analyzer covers from
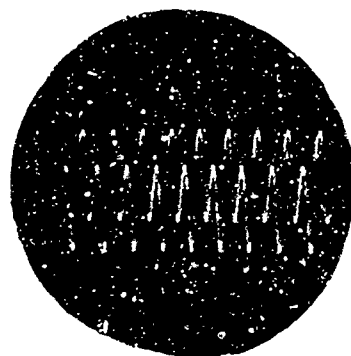
NOT REPRODUCIBLE

f_{input} = 1599.2 kHz

f_{sub} = 799.6 kHz

(.2v/cm, 1μs/cm)

f_{input} = 1544.8 kHz

f_{sub} = 1154.5 kHz

390.3 kHz

(.2v/cm, 1μs/cm)

(a) SUBHARMONIC RESPONSES

f_{input} = 1599.2 kHz

f_{sub} = 799.6 kHz

(.2 v/cm, 5ms/cm)
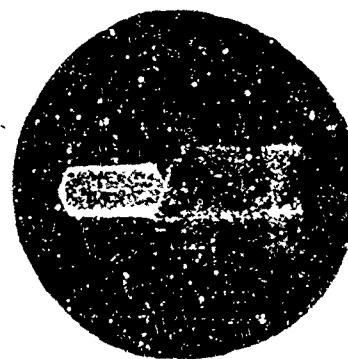
f_{input} = 1544.8 kHz

f_{sub} = 1154.5 kHz

= 390.3 kHz

(.2 v/cm, 5 ms/cm)

(b) GROWTH OF SUBHARMONICS

FIG. 4-9 OBSERVATION OF SUBHARMONICS

1 KHZ to 1.5 MHZ. Sometimes, at high driving signal levels, more than one subharmonic pair can be observed.

For gathering information about the threshold for subharmonic generation, we used long pulse train of the driving signal applied to the interferometer. The actual growth of the subharmonic acoustic wave can be displayed on the oscilloscope, such as the one shown on Fig 4-9b. From that picture, the point where the wave starts to break and subharmonics begin to appear can be easily determined. If this response is measured using the output of the acoustic probe, the level at the break point is the threshold for subharmonic excitation.

(e) Measurement of the System Parameters of the Interferometer

For comparing the experimental data and the theoretical analysis, information concerning the actual condition of the interferometer is examined to explore its relation with the mathematical model of the ideal resonator. Two parameters have been recorded as the quantitative measurement of the physical condition of the interferometer. The first parameter is the actual resonance modes of the interferometer at a given experimental condition. The other is the dissipation factor associated with each resonance mode.

A simple way has been adopted for measuring the resonance modes of the interferometer. A variable signal fre-

quency generator is directly connected to the transmitting transducer of the interferometer. By changing the frequency of the input signal, we observe the amplitude response from the detector at one of the boundary walls. The frequency at which the response amplitude is maximum is the resonance mode frequency.

For determining the dissipation factor at each mode, we just measure bandwidth of the half-power points of the response amplitude from the detector at that particular mode. A nondimensional quantity, quality factor Q, can also be computed from knowledge of the bandwith by the relation:

$$Q = \frac{\omega}{BW} \qquad . \qquad (4-4)$$

4. Experimental Data

In order to verify some of the theoretical predictions, we have kept two things in mind: the experimental condition under investigation and the physical parameters for subharmonics to be excited. The experimental data are recorded for the purpose of clarifying how good the theoretical analysis is for a real physical situation. Those data are obtained from a typical interferometer which has 1.5 MHZ and 360 KHZ X-cut quartz discs for its boundary walls.

(a) The Resonance Modes of the Interferometer

Table 4-1 lists resonance modes of an interferometer

TABLE 4-1.

The Resonance Modes of The Interferometer

Mode No.	Frequency (MHz) Cal.	Meas.	Amp.	Mode No.	Frequency (MHz) Cal.	Meas.	Amp.
1	15.3	22.1	58	43	840.2	832.0	1900
2	30.0	26.7	190	44	861.1	855.5	1400
3	48.5	48.7	170	45	981.9	879.2	1600
4	67.9	58.4	100	46	902.5	902.6	2400
5	87.9	95.0	210	47	923.6	926.2	2100
6	108.1	107.4	200	48	944.5	949.8	1500
7	128.6	124.3	160	49	965.3	973.1	2500
8	149.1	149.2	210	50	986.0	986.6	100
9	169.8	161.5	240	51	1006.7	996.5	1800
10	190.5	200.7	130	52	1027.3	1020.4	1700
11	211.2	212.2	150	53	1047.4	1043.2	1700
12	231.9	240.9	320	54	1065.0	1064.5	2000
13	252.6	255.0	260	55	1080.6	1082.9	240
14	273.3	264.4	270	56	1095.6	1096.6	1300
15	293.9	287.7	250	57	1114.1	1118.0	2800
16	314.3	310.2	260	58	1134.6	1140.9	3100
17	334.1	333.2	160	59	1155.1	1164.1	3400
18	351.6	352.3	220	60	1175.8	1187.5	2600
19	365.2	365.0	190	61	1196.5	1192.7	170
20	381.8	383.6	260	62	1217.5	1211.0	3500
21	401.3	408.0	370	63	1238.1	1234.5	3100
22	421.6	430.7	660	64	1258.8	1257.8	2500
23	442.2	453.8	300	65	1279.6	1281.3	2700
24	463.0	477.9	320	66	1300.3	1304.5	1900
25	483.5	489.7	300	67	1321.0	1327.6	3000
26	504.6	500.8	280	68	1346.1	1339.6	800
27	525.4	524.5	440	69	1362.4	1351.5	2000
28	546.3	548.1	1400	70	1382.4	1374.4	200
29	567.1	571.5	900	71	1402.2	1397.2	2400
30	587.9	594.8	640	72	1421.0	1418.7	1700
31	608.8	618.2	540	73	1436.4	1436.3	2000
32	629.5	629.4	500	74	1449.7	1458.2	1800
33	650.2	641.7	450	75	1466.3	58.4	2100
34	670.7	664.7	360	76	1484.3	1489.0	2500
35	690.7	687.5	390	77	1502.2	1509.0	2500
36	705.8	703.1	330	78	1520.5	1529.5	6200
37	722.9	723.2	180	79	1539.3	1533.1	460
38	725.6	741.1	570	80	1555.5	1550.1	
39	757.8	762.4	930	81	1578.8	1572.8	1700
40	778.1	785.0	1500	82	1599.0	1595.3	1700
41	798.7	806.8	2400	83	1619.5	1618.2	1700
42	819.5	809.6	180	84	1640.3	1640.7	

for a spacing of 3.58 cm at 26°C. The calculated modes are
based on model described in Chapter III, section 6, and com-
puted from a computer. The constants for the characteristic
equation of Eq. (3-63) used during computer programming are:

$$R = 10.2702$$
$$f_d = 1500.0$$
$$f_s = 360.0$$
$$f_h = 21.0$$

The measured values are obtained experimentally from the
interferometer used in subharmonic observation. The proce-
dure of such data taking has been already described in the
previous section.

The quality factor, Q, associated with the resonance
modes is also recorded as a reference to indicate the sig-
nification of such a particular mode.

(b) Threshold for Subharmonic Excitation

There are two parameters for setting up the experiment
for observing subharmonics: one is the length of the inter-
ferometer and the other is the driving signal frequency.
The dots in Fig. 4-10a are the data for the subharmonic
threshold with different lengths of the interferometer; Fig.
4-10b is a record showing a general tendency of the subhar-
monic threshold to change as a function of the driving signal
frequencies. Those data are taken without adjusting other
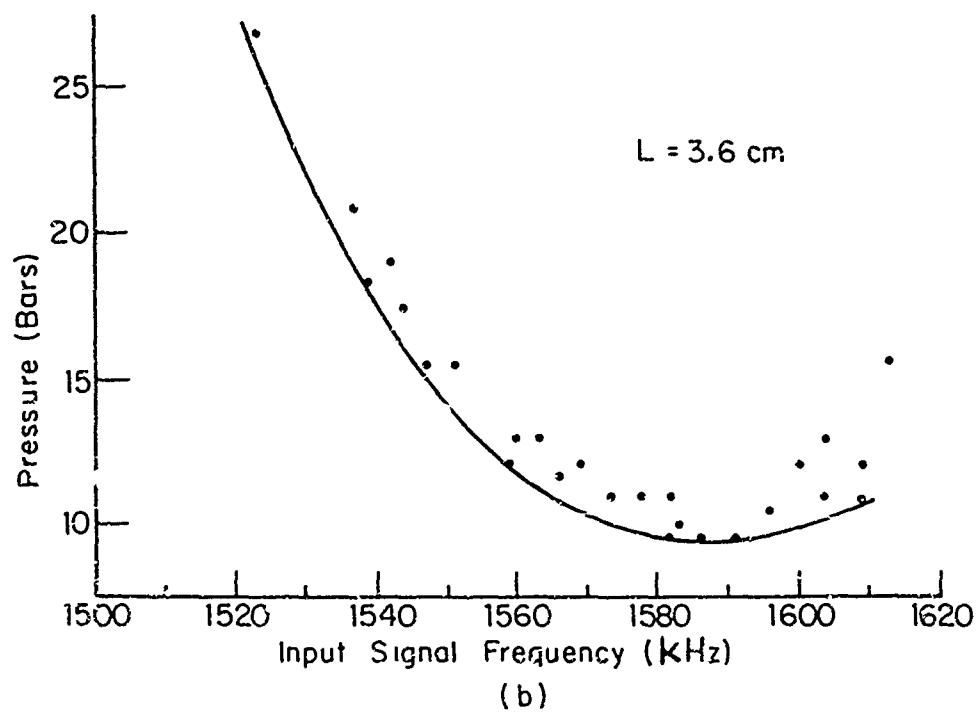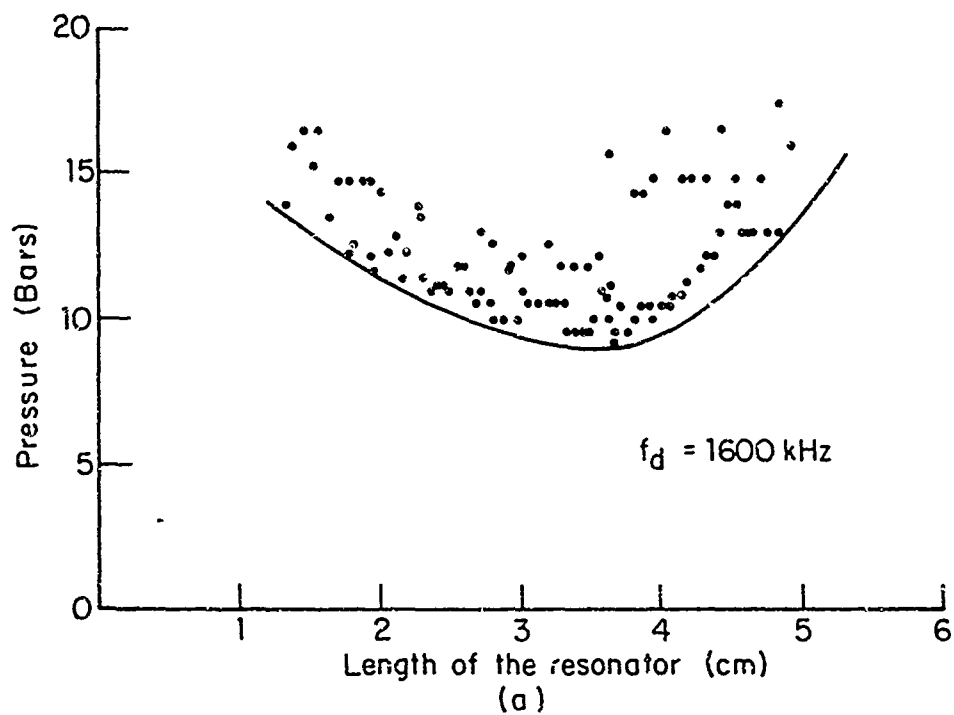references of the whole experimental system. Since the

FIG. 4-10 THRESHOLD FOR SUBHARMONIC EXCITATION

subharmonic frequency components change with interferometer
length and driving signal frequency, those experimental
points do not have the same frequency components. However,
the general tendency of the minimum threshold for exciting
the subharmonics can be indicated by the solid lines in
those figures.

(c) Amplitude and Frequency Components of Subharmonics

Two sets of experimental conditions have been carried
out in a detailed study of the amplitude and frequency com-
ponents of the observed subharmonics. Fig. 4-11a shows, for
a case of subharmonic of one-half, that the change in sub-
harmonic amplitude measured from the wave analyzer as the
driving signal intensity increases. Sometimes. under dif-
ferent conditions, more than one pair of subharmonics
appear. Fig. 4-11b is an example of such a circumstance.
The frequencies are measured by an electronic counter whose
accuracy is about $\pm$ 5 HZ in our present measuring range.
Precision of the data on the reading of subharmonic fre-
quencies is dominated by the stability of the signal gen-
erator which, for our equipment, is about $\pm$ 10 HZ. Hence,
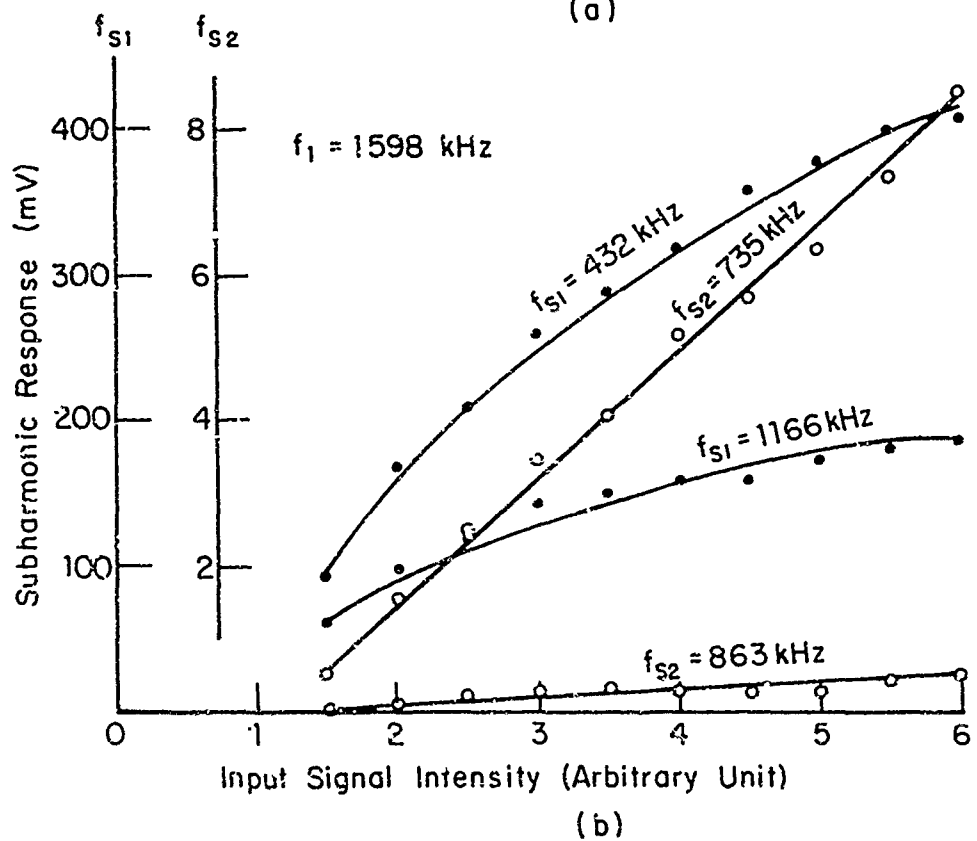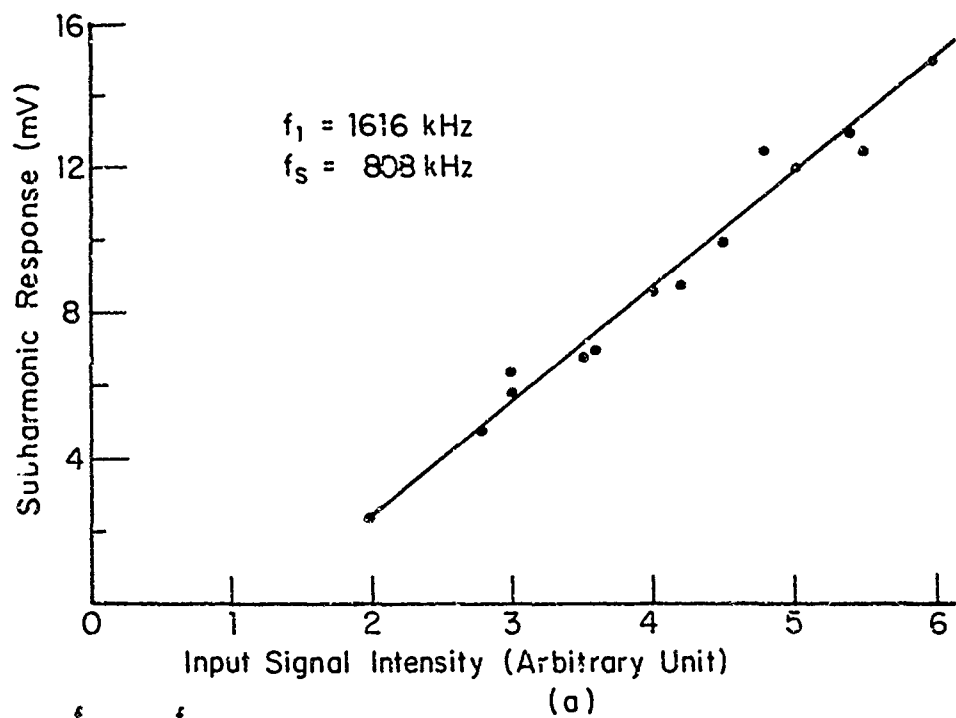the frequency data can be valid up to $\pm$ 15 HZ.

FIG. 4-11 INTENSITY OF SUBHARMONIC RESPONSE

5. Discussion of the Experimental Results

Some physical explanations of the threshold of sub-
harmonic generation are gleaned from the data concerning
changes in the threshold as a function of length of the
interferometer as shown in Fig. 4-10a. When the distance
between the boundary walls of the interferometer is small,
the loss is dominated by the transducer mounting loss which
is independent of the interferometer's length. However,
the amount of medium, which provides the nonlinear coupling
mechanism, is proportional to the space between the boundary
walls of the interferometer. These two factors make the
threshold for exciting the subharmonics decrease with the
length of the interferometer, as is clearly indicated from
the experimental data. When the length of the interfero-
meter becomes very large, the experimental results show
that the subharmonic generation threshold increases with
the length of the interferometer. This is due to the in-
fluence of the other losses such as the viscosity of the
medium, beam spreading, etc., which are a function of length.
The fact that subharmonics becomes so difficult to excite
for short spacings is evidence that the vibration of the
boundary walls does not provide an important contribution
to the nonlinear coupling responsible for subharmonic genera-
tion.

In Appendix A, we have carried out a detailed analysis

comparing the order of magnitude of the nonlinear coupling due to the boundary and to the nonlinear property of the medium.

The change in threshold for subharmonic generation with driving signal frequency, as indicated in Fig. 4-10b, covers a quite large range and does not follow a simple relation. This is due to the reason that other factors, such as dissipation and detuning parameters, should also be taken into consideration.

Information about the quality factor, Q, of the interferometer associated with resonance modes can be used to calculate the threshold for subharmonic generation according to the analysis in Chapter III. From Eq. (3-73), the simplified result for water without detuning is:

$$P_{TH} = \frac{15 \times 10^3}{\sqrt{Q_1 Q_2}} \qquad (4-5)$$

where P_{TH} is the acoustic pressure in bars, Q_1, and Q_2 are the quality factors associated with subharmonic modes 1 and 2 respectively. Based on the data of Table 4-1, the calculated minimum threshold is 5.8 bars which is close to what we have measured in Fig. 4-10.

Though the interferometer possesses many resonance modes, in general only a few pair of subharmonics are generated during experiments. This can be explained by noting

that, in addition to the threshold, those modes also have
to meet a matching condition; that is, the sum of their fre-
quencies should also equal to the frequency of the driving
signal. We use the data set of the resonance modes from Table
4-1 to check such a situation. Fig. 4-12 is dotted with
points corresponding to the sum of frequencies for a pair
of subharmonic modes in the range from 1575 KHZ to 1635 KHZ.
Two horizontal lines are drawn for the resonance modes at
1595.3 and 1618.2 KHZ. A highly intense wave can be estab-
lished if we drive the interferometer at these frequencies.
We see that there are actually only few points near these
two lines; in another words, not many subharmonic pairs
will be excited. The vertical distance between those points to
the line gives magnitude of the resultant detuning and numbers in pa-
renthesis are the geometric means of the quality factors associated
with those particular subharmonic pairs. Points far from
the line may be excited only if a much stronger signal is pro-
vided. However, the final amplitude of the excited subhar-
monic will depend, not only on the quality factor for that
particular mode, but also on its detuning from the actual
resonance. When more than one subharmonic pair is excited,
their amplitudes will be inversely proportional to the loss
and the detuning. The experimental results shown in Fig.
4-11b give such evidence. (Because of ambient temperature
changes due to the different times for data collection, there
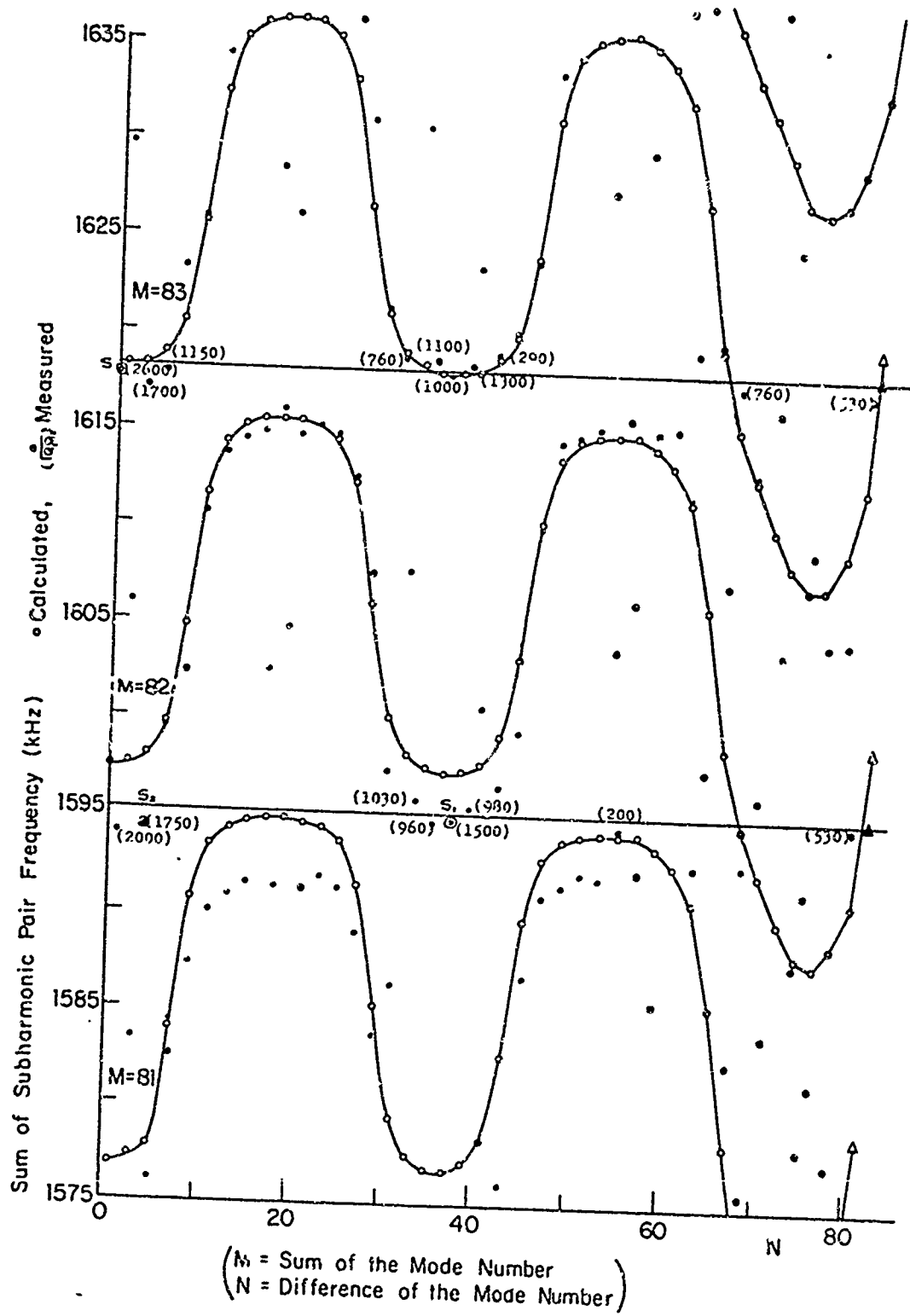
FIG. 4-12   SUBHARMONIC PAIR FREQUENCY

are frequency shifts for the resonance modes in Fig. 4-10 from the original modes recorded in Table 4-1. However, we can still identify them by the general direction of the shift. The corresponding subharmonic pairs for Fig. 4-11 are labeled with s, s_1, s_2, in Fig. 4-12. We can see that, as s_1, s_2 both have high Q's and are close to the driving signal frequency, they can appear at the same time. Since the condition for measuring the resonance frequencies is not the same, we do not attempt to use these data to calculate the threshold and subharmonic intensity for the fact of detuning).

The change in subharmonic amplitude with driving signal intensity illustrates a surprising discrepancy from results reported by Bamberg[16]. According to his observations, once the subharmonic is excited, its amplitude will level off regardless of how intense the driving signal is and finally it will disappear altogether after a further increase in driving signal intensity. We feel that our results differ from his because we have avoided cavitation during our experiments. Since gas bubbles consume energy through the cavitation process, their presence will certainly prevent further increase in the amplitude of subharmonics. This character may be a way to differentiate between subharmonic generation with cavitation and without cavitation.

Chapter V

SUMMARY

1. Conclusions

The work reported here has been an attempt to develop a mathematical analysis of subharmonic generation in acoustic systems and to check experimentally the adequacy of the theoretical description of such a phenomenon.

The principal conclusions of this thesis are the following:

(a) Subharmonic oscillation is a manifestation of system instability. The analysis of its behavior can be obtained by first assuming its existence and then determining the conditions under which i⁺ occurs. The two-variable (two-timing) perturbation method has been a very useful mathematical tool in carrying out this study.

(b) In a conservative system of three oscillators with a single nonlinear element whose energy function is $V=X_1X_2X_3$, if the sum frequency of two oscillators is close to the third one, there exist three integral constraints. By using these constraints in the relevant four-dimensional phase space we can obtain a single trajectory to describe the system's motion, and the time variable can be found by an integral along that trajectory.

(c) For a dissipative system, subharmonics can be

excited by a sufficiently strong external source, since the
nonlinearity of the system provides the coupling mechanism
for energy conversion to the lower frequencies. The losses
in the system and detuning from the exact frequency matching
condition play comparable roles in determining the threshold
required for subharmonic excitation.

(d) Subharmonics always appear in pairs except in the
degenerate case of the subharmonic mode one-half. In a dis-
tributed system, such as the acoustic interferometer, more
than one pair of subharmonics may be excited provided they
meet the frequency sum rule and the driving source is in-
tense enough. According to the theory, for a medium with
frequency independent losses, the subharmonic of one-half
has the lowest threshold for excitation for a given detuning.

(e) Subharmonic generation has been observed experi-
mentally in an acoustic interferometer. Because cavitation
was carefully avoided during the investigation, the experi-
mental results, such as the threshold level, and the specific
subharmonic modes excited, are consistent with the theoreti-
cal predictions.

2. Future Work

The theoretical study of subharmonic generation can
be further studied for nonlinear element with other form
of energy functions. For example, if the three oscillator

model possesses a second energy function, then there will be an additional phase variable and one of the three original constraints does not hold anymore. Therefore, the problem can not be reduced to quadrature. The existence of other types of constraints remains to be determined.

The one-dimensional model for the distributed system should be extended to three-dimensions. This will permit a more realistic comparision of theory and experiment. Such an approach will also allow decomposition of the wave number vectors to cover the more general case when the properties of the medium becomes dispersive.

On the experimental front, it seems that temperature control of the container will be necessary if more precise quantitative measurements are desired. A 0.2° Centigrade change will cause 0.6 KHZ shift in frequency for modes around 1.5 MHZ with the present set-up.

Liquids other than water can also be used for observing subharmonic generation. The experimental data will supply the information on the nonlinearity associated with different liquids. However, purification and possible cavitation deserves investigation before considering the meaning of the experimental measurements.

It may be interesting to extend the investigation to subharmonic generation in a solid medium resonator. Without the complications of cavitation, such nonlinear phe-

nomena may provide a different practical method of energy conversion.

Acknowledgments

Appendix A

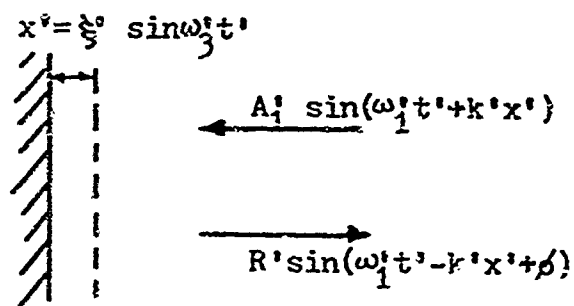REFLECTION FROM A VIBRATIONAL BOUNDARY

Fig. A-1

When waves reflected from a vibrational boundary, their amplitudes and phases will change according to the boundary conditions. Here we are discussing such effects and make a comparision with the interaction due to the nonlinearity of medium.

Fig. A-1 shows that a wave with the particle velocity of $A_1' \sin(\omega_1' t' + k_1' x')$ is incident on a rigid boundary whose surface moves harmonically with a displacement as $\xi' \sin(\omega_3' t')$. A reflected wave can be found by matching the boundary conditions, in this case, it is:

$$R' \sin(\omega_1' t' - k_1' x' + \phi') , \qquad (A-1)$$

where $R' = -A_1'$,

$$\phi' = 2k_1' \xi' \sin\omega_3' t' .$$

As: $\sin(\beta\sin\alpha) = 2J_1(\beta)\sin\alpha - 2J_3(\beta)\sin 3\alpha + \cdots\cdots ,$

$$\cos(\beta \sin \alpha) = J_0(\beta) + 2J_2(\beta)\cos 2\alpha + 2J_4(\beta)\cos 4\alpha + \cdots,$$

and

$$J_n(\beta) = \left(\frac{\beta}{2}\right)^n \left[\frac{1}{0! \, n!} - \frac{1}{1!(n+1)!}\left(\frac{\beta}{2}\right)^2 + \cdots\cdots\right] .$$

$$(A-2)$$

we can expand the reflected wave by considering the first order term of ξ' only (ξ' is a small quantity):

$$R' \sin(\omega_j' t' - k_j' x' + \phi')$$

$$= - A_1' \sin(\omega_j' t' - k_1' x') \cos(2\xi' k_j' \sin \omega_j' t')$$

$$\quad - A_1' \cos(\omega_1' t' - k_1' x') \sin(2\xi' k_1' \sin \omega_3' t')$$

$$= - A_1' \sin(\omega_1' t' - k_1' x') \left[J_0(2k_1'\xi') + 2J_2(2k_1'\xi')\cos 2\omega_3' t' \right.$$

$$\quad \left. + \cdots\cdots \right] + A_1' \cos(\omega_1' t' - k_1' x') \left[2J_1(2k_1'\xi')\cos \omega_3' t' \right.$$

$$\quad \left. + \cdots\cdots \right]$$

$$\approx - A_1' \sin(\omega_1' t' - k_1' x') - A_1' \cos(\omega_1' t' - k_1' x')$$

$$\quad \times 2k_1'\xi' \sin \omega_3' t'$$

$$= - A_1' \sin(\omega_1' t' - k_1' x') - k_1'\xi' A' \left[\sin(\omega_3' t' - \omega_1' t' + k_1' x') \right.$$

$$\quad \left. + \sin(\omega_3' t' + \omega_1' t' - k_1' x') \right] .$$

$$(A-3)$$

The amplitudes of new frequency components $(\omega_3' - \omega_1')$ and $(\omega_3' + \omega_1')$ appear as:

$$A_2^{*\prime} = k_1'\xi' A_1' , \qquad\qquad (A-4)$$

and in the nondimensional notation defined in Chapter III, it becomes:

$$A_2^{*} = \epsilon \omega_1 \xi A_1 . \qquad\qquad (A-5)$$

However, the vibrating boundary will also radiate

an acoustic wave whose particle velocity is:

$$U_3' = \xi' \omega_3' \cos \omega_3' \tau'.$$ (A-6)

This wave will interact with the reflected wave A_1 if the medium possesses a nonlinear property. According to the analysis in Chapter III, a new frequency component of $\omega_3 + \omega_1$ or $\omega_3 - \omega_1$ will appear with a relation as:

$$\frac{dA_2}{dx} = \epsilon \frac{1}{4}(1+\Gamma)\omega_2\omega_3\xi A_1 ,$$ (A-7)

or, for one dimensional problem,

$$A_2 = \epsilon \frac{1}{4}(1+\Gamma)\omega_2\omega_3\xi A_1 L ,$$ (A-8)

where L is the distance in wavelengths travelled by the two interacting waves.

Comparing Eqs. (A-7) and (A-5), we have:

$$\frac{A_2}{A_2^*} = \frac{(1+\Gamma)}{4} \cdot \frac{\omega_2 L}{\omega_1} .$$ (A-9)

Since ω_2 and ω_1 are in same order and Γ is about 6.5 for water, Eq. (A-9) indicates that A_2 is L times larger than A_2^*. This is proof that the nonlinear effect due to medium has more influence in the generating new frequency components than a vibrational boundary.

Appendix B

DERIVATION OF THE CHARACTERISTIC EQUATION FOR THE RESONANCE MODES IN THE THREE-SECTION COMPOSITE RESONATOR

The resonance modes of a certain resonator can be determined from its boundary conditions. However, for the one dimensional resonator shown in Fig. 3-2, the transmission line theory can apply for solving such a problem.

Consider each section of the composite resonator as a part of a transmission line. Since the wall at right side is terminated at a pressure release surface ($p = 0$), the acoustic impedance it represents to the left will be:

$$Z_1 = j\varrho_w'c_w' \tan k_w'H. \qquad (B-1)$$

where all the notations are defined as before.

The middle section (medium) will transfer Z_1 to its left side with a new impedance value as:

$$Z_2 = \varrho'c' \frac{Z_1 + j\varrho'c' \tan k'S}{\varrho'c' + jZ_1 \tan k'S}. \qquad (B-2)$$

The resultant impedance appearing at the left wall will then become:

$$Z_3 = \varrho_w'c_w' \frac{Z_2 + j\varrho_w'c_w' \tan k_w'D}{\varrho_w'c_w' + jZ_2 \tan k_w'D}. \qquad (B-3)$$

As the left wall also terminates with a pressure release surface, at resonance, we should have:

$$Z_3 = 0 . \qquad\qquad (B-4)$$

With the relations of Eqs. (B-1), (B-2), (B-3), and (B-4), we get:

$$\left[R(\tan k_w'D + \tan k_w'H) + \tan k'S - R^2 \tan k_w'D \tan k_w'H \tan k'S \right]$$

$$/(R - R^2 \tan k_w'H \tan k'S - R \tan k_w'H \tan k_w'D - \tan k'S$$

$$\times \tan k_w'D)$$

$$= 0 , \qquad\qquad (B-5)$$

or simply,

$$R(\tan k_w'D + \tan k_w'H) + \tan k'S - R^2 \tan k_w'D \tan k_w'H$$

$$\times \tan k'S$$

$$= 0 , \qquad\qquad (B-5)$$

which is just the characteristic equation (3-63).

Appendix C

COMPUTER PROGRAM FOR THE NUMERICAL

SOLUTION OF THE CHARACTERISTIC EQUATION

FOR A THREE SECTION COMPOSITE RESONATOR

The resonance frequency f of a one dimensional three section resonator, according to the discussion in Chapter III, should satisfy the equation:

$$R(\tan \frac{f}{f_d} \pi + \tan \frac{f}{f_h} \pi) + \tan \frac{f}{f_s} \pi$$

$$- R^2 \tan \frac{f}{f_d} \pi \tan \frac{f}{f_h} \pi \tan \frac{f}{f_s} \pi = 0, \qquad (C-1)$$

where all notations are defined as previously.

For a given resonator, the resonance modes can be determined by finding the roots of Eq. (C-1). We adopt the Newton-Raphson formula[43] for the numerical computation.

First, we define a function as :

$$F(f) = R(\tan \frac{f}{f_d} \pi + \tan \frac{f}{f_h}) + \tan \frac{f}{f_s} \pi$$

$$- R^2 \tan \frac{f}{f_d} \pi \tan \frac{f}{f_h} \pi \tan \frac{f}{f_s} \pi , \qquad (C-2)$$

and $\;\; DERF(f) = \dfrac{dF(f)}{df} \;.$

The roots of Eq. (C-1) can then be found from Eq. (C-2) by the iterative method:

$$x_{i+1} = x_i - \frac{F(x_i)}{DERF(x_i)}. \qquad (C-3)$$

Table C-1 lists the computer program for carrying out the actual computation process of Eq. (C-3). As f_s is much smaller than f_h and f_d, the separation between two successive roots will not exceed f_s. We use $0.65f_s$ for the initial value during iteration.

In this program, the region near singular points of the tangent functions is avoided to prevent the computer from overflowing. Any missed roots are determined by interpolating from their neighboring roots.

Notations used in the program follow closely to what are defined in Fig. 3-2. The final output solution $Y(I)$ is the frequency of the resonance mode in units of KHZ, and $G(I)$ is the actual value of the function $F(f)$ when $f=Y(I)$.

Table 5-1   5-2

```
// (8443?9.3.11,SNATE MEMO,TIME=2
// EXEC FORTGCLG
//FORT.SYSIN DD *
C       MODES OF A RESONATOR
        EXTERNAL FCT
        DIMENSION Y(200),G(200)
        WRITE (6,999)
899 FORMAT (1H1)
100 READ (5,101,END=500) FD,FH,FS,R
        WRITE (6,101) FD,FH,FS,R
101 FORMAT (3F7.1,F8.4)
        D=3.1415926536/FD
        H=3.1415926536/FH
        S=3.1415926536/FS
        A=(FD+FH)/FS
        DO 110 I=1,200
        Y(I)=0
110 G(I)=0
        Y(1)=-0.65*FS
        I=2
111 Y(I-1)=Y(I-1)+0.06*FS
112 Y(I-1)=Y(I-1)+0.01*FS
        I=I-1
102 I=I+1
        XST=Y(I-1)+0.65*FS
120 U=XST+D
        V=XST+H
        DO 103 J=1,15,2
        Z=J*(3.1415926536/2)
        ZU=Z-U
        ZV=Z-V
        AZU=ABS(ZU)
        AZV=ABS(ZV)
        IF(AZU.LE.1.E-05) GO TO 112
        IF(AZV.LE.1.E-05) GO TO 112
103 CONTINUE
        A=TAN(XST+D)
        AA=ABS(A)
        IF(AA.GE.1.E+74) GO TO 112
        B=TAN(XST+H)
        AB=ABS(B)
        IF(AB.GE.1.E+74) GO TO 112
200 CALL SINI(X,D,H,S,R,F,DERF,FCT,XST,1.E-06,200,IER)
        Y(I)=X
        G(I)=F
        IF(Y(I-1)-Y(I)) 300,111,111
300 E=Y(I)-Y(I-1)
        IF(E.LT.FS) Y(I)=(Y(I)+Y(I-1))/2
        IF(I-A) 102,102,400
400 WRITE (6,401)(I,Y(I),G(I),I=2,N)
401 FORMAT (1X,I3,2X,F6.1,5X,E14.5)
402 GO TO 100
500 STOP
        END
        SUBROUTINE SINI(X,D,H,S,R,F,DERF,FCT,XST,EPS,IEND,IER)
        IER=0
        X=XST
        TOL=X
        CALL FCT(TOL,D,H,S,R,F,DERF)
        TOLF=100.*EPS

        DO 6 I=1,IEND
        IF(F)1,7,1
1 IF(DERF)2,8,2
2 DX=F/DERF
        SP=3.1415926536/(5.*S)
        ADX=ABS(DX)
        IF(ADX.GE.SP) DX=(DX*SP)/ADX
        X=X-DX
        TOL=X
        CALL FCT(TOL,D,H,S,R,F,DERF)
        TOL=EPS
        A=ABS(X)
        IF(A-1.)4,4,3
3 TOL=TOL*A
4 IF(ABS(DX)-TOL)5,5,6
5 IF(ABS(F)-TOLF)7,7,6
6 CONTINUE
        IER=1
7 RETURN
8 IER=2
        RETURN
        END
        SUBROUTINE FCT(X,D,H,S,R,F,DERF)
1. F=R*(TAN(X+D)+TAN(X+H)+TAN(X+S)-R**2*(TAN(X+D))*(TAN(X+H))*(TAN(X
        +S)))
20 DERF=R*(D/(COS(X+D))**2+H/(COS(X+H))**2+S/(COS(X+S))**2-R**2*((D/
        1(COS(X+D))**2+(TAN(X+D)))*(TAN(X+S))+(TAN(X+D))*(H/(COS(X+H))**2+
        2(TAN(X+S))+(TAN(X+D))*(TAN(X+H))*(S/(COS(X+S))**2))
        RETURN
        END
/*
//GO.SYSIN DD *
1503.0    3.5.0    21.0 16.2762
/*              END OF FILE (/*)
```

BIBLIOGRAPHY

1. N. Minorsky, Nonlinear Oscillations (D. Van Nostrand Co. Inc., New York, 1962).

2. C. Hayashi, Nonlinear Oscillations in Physical Systems (McGraw-Hill Book Co., New York, 1964).

3. T. E. Stern, Theory of Nonlinear Networks and Systems (Addison-Wesley, Reading, Mass. 1965).

4. R. E. Kronauer and S. A. Musa, "Necessary Conditions for Subharmonic and Superharmonic Synchronization in Weakly Nonlinear Systems," Quart. Appl. Math. 24, 153-160 (1966).

5. S. A. Musa and R. E. Kronauer, "Sub- and Superharmonic Synchronization in Weakly Nonlinear Systems: Integral Constraints and Duality," Quart. Appl. Math. 25, 399-414 (1968).

6. J. M. Manley and H. E. Rowe, "Some General Properties of Nonlinear Elements--Part 1, General Energy Relations," Proc. I.R.E. 44, 904-913 (1956).

7. D. G. Tucker, "The Exploitation of Non-linearity in Underwater Acoustics," J. Sound. Vib. 2, 429-434 (1965).

8. H. L. F. Helmholtz, Sensations of Tone (Dover Publications, Inc., New York, 1954).

9. Lord Rayleigh, The Theory of Sound (Dover Publications, Inc., New York, 1954).

10. R. Esche, "Untersuchung der Schwingungskavitation in Flunssikeiten," Akust. Beihefte, 4, 208 (1952).

11. P. Desantis, D. Sette, and F. Wanderlingh, "Cavitation Detection: The Use of The Subharmonics," J. Acoust. Soc. Am. 42, 514-516(L) (1967).

12. P. W. Vaughn, "Investigation of Acoustic Cavitation Thresholds by Observation of the First Subharmonic," J. Sound. Vib. 7, 236-246 (1968).

13. D. J. Dunn, M. Kuljis, and V. G. Welsby, "Nonlinear Effects in a Focused Underwater Standing Wave Acoustic System," J. Sound. Vib. 2, 471-476(1965).

14. A. Eller and H. G. Flynn, "Generation of Subharmonics of Order One-Half by Bubbles in a Sound Field," J. Acoust. Soc. Am. 46, 722-727 (1969).

15. E. A. Neppiras, "Subharmonic and Other Low-Frequency Emission from Bubbles in Sound-Irradiated Liquids," J. Acoust. Soc. Am. 46, 587-601 (1969).

16. J. A. Bamberg, "Subharmonic Generation in an Acoustic Fabry-Perot Interferometer," Technical Report No. 16, Ultrasonics Laboratory, Michigan State University (1967).

17. A. Korpel and R. Adler, "Parametric Phenomena Observed on Ultrasonic Waves in Water," Appl. Phys. Lett., 7, 106-108 (1965).

18. W. R. McCluney, "An Investigation of Subharmonic Generation in an Ultrasonic Resonant Cavity," Technical Report No. 2, Ultrasonics Laboratory, The University of Tennessee (1966).

19. Ching-Tu Chang and M. A. Breazeale, "A Study of the Ultrasonic Spectrum in a Resonant Cavity," Technical Report No. 3, Ultrasonics Laboratory, The University of Tennessee (1967).

20. B. D. Cook, "Progress in Nonlinear Acoustics," Dept. of Physic, Michigan State University (Private Communication).

21. L. Adler and M. A. Breazeale, "Generation of Fractional Harmonics in a Resonant Ultrasonic Wave System," J. Acoust. Soc. Am. 48, 1077-1083 (1970).

22. M. Luukkala, "Fine Structure of Fractional Harmonic Phonons," Phys. Letters, 25A, 76-77 (1967).

23. M. Luukkala, "Threshold and Oscillation of Fractional Phonons," Phys. Letters, 25A, 197-198 (1967).

24. M. Luukkala, "On the Instability of Phonon Breakdown," Annales Academiae Scientiarum Fennicae, Series A, VI. Physica, 306 (1969).

25. P. J. Dallos and C. O. Linnell, "Subharmonic Components in Cochlear-Microphonic Potentials," J. Acoust. Soc. Am. 40, 4-11 (1966).

26. P. J. Dallos and C. O. Linnell, "Even Order Subharmonics in the Peripheral Auditory System," J. Acoust. Soc. Am. 40, 561-564 (1966).

27. P. J. Dallos, "On the Generation of Odd-Fractional Subharmonics," J. Acoust. Soc. Am. 40, 1381-1391 (1966).

28. A. O. Gilchrist, "The Free Oscillations of Conservative Quasilinear Systems With Two Degrees of Freedoms," Int. J. Mech. Sci. 3, 286-311 (1961).

29. R. E. Kronauer and S. A. Musa, "The Exchange of Energy between Oscillations in Weakly-Nonlinear Conservative Systems," J. Appl. Mech., ASME., 33, 451-452 (1966).

30. G. F. Carrier and C. L. Pearson, Ordinary Differential Equations (Blaisdel, Waltham, Mass. 1968).

31. Y. Tsuzuki and M. Kakuishi, "Parametric Excitation of Contour Modes of Vibration in AT-Cut Quartz," Proc. I.E.E.E., 55, 463 (1967).

32. E. F. Ghiron, "Anomalies in the Propagation of Acoustic Waves of Great Amplitude," Alta Frequenze, 4, 530 (1935).

33. F. V. Hunt, "Note on the Exact Equation Governing the Propagation of Sound in Fluids," J. Acoust. Soc. Am. 27, 1019-1039 (1955).

34. N. N. Andreev, "Concerning Certain Second-Order Quanties in Acoustics," Soviet Physics-Acoustics 1, 2-11 (1957).

35. W. Keck and R. T. Beyer, "Frequency Spectrum of Finite Amplitude Ultrasonic Waves in Liquids," The Physics of Fluids, 3, 346-352 (1960).

36. R. I. Beyer, "Parameter of Nonlinearity in Fluid," J. Acoust. Soc. Am. 32, 719 (1960).

37. L. Adler and E. A. Hiedemann, "Determination of the Nonlinearity Parameter B/A for Water and m-Xylene," J. Acoust. Soc. Am. 34, 410 (1962).

38. L. Adler, "Parametric Generation of Ultrasonic Waves: Linear and Nonlinear Phenomena," Technical Report No. 7, Ultrasonics Laboratory, The University of Tessessee (1970).

39. T. F. Hueter and R. H. Bolt, _Sonics_, John Wiley and Sons, Inc., New York, (1955).

40. E. V. Romanenko, "Miniature Piezoelectric Ultrasonic Receivers," Soviet Physics-Acoustics, 3, 342 (1957).

41. L. D. Rozenberg, _Sources of High-Intensity Ultrasound_, Translated from Russian by James S. Wood, Plenum Press, New York, (1969).

42. J. Barger, "Thresholds of Acoustic Cavitation in Water," Technical Memorandum No. 57, Acoustics Research Laboratory, Harvard University (1964).

43. K. S. Kunz, _Numerical Analysis_, (McGraw-Hill Book Company, Inc., New York, 1957).